INVESTIGATION OF THE PERFORMANCE OF CONCRETE MASONRY WALLS PLASTERED BY HIGH PERFORMANCE MORTAR UNDER CYCLIC LOADING

BY

AHMED AWAD SAEED SADOON

A Thesis Presented to the
DEANSHIP OF GRADUATE STUDIES

KING FAHD UNIVERSITY OF PETROLEUM & MINERALS
DHAHRAN, SAUDI ARABIA

In Partial Fulfillment of the
Requirements for the Degree of

MASTER OF SCIENCE

In

CIVIL ENGINEERING

APRIL 2016

KING FAHD UNIVERSITY OF PETROLEUM & MINERALS

DHAHRAN- 31261, SAUDI ARABIA

DEANSHIP OF GRADUATE STUDIES

This thesis, written by **AHMED AWAD SAEED SADOON** under the direction of his thesis advisor and approved by his thesis committee, has been presented and accepted by the Dean of Graduate Studies, in partial fulfillment of the requirements for the degree of **MASTER OF SCIENCE IN CIVIL ENGINEERING.**

Dr. Ali H. Al-Gadhib
(Advisor)

Dr. Salah U. Al-Dulaijan
Department Chairman

Prof. Mohammed H. Baluch
(Co-Advisor)

Prof. Salam A. Zummo
Dean of Graduate Studies

Dr. Mohammad K. Rahman
(Member)

16/5/16
Date

Prof. Omar S. Baghabra Al-Amoudi
(Member)

Dr. Mohammed A. Al-Osta
(Member)

Dedication To

My Beloved Parents

and

My Brothers & Sisters

and

My Wife

ACKNOWLEDGMENTS

First and foremost, I thank Allah for endowing me with health, patience and knowledge to complete this work. Acknowledgement is due to King Fahd University of Petroleum & Minerals for the support given to this research through its excellent facilities and for granting me the opportunity to pursue my graduate studies with financial support.

I'm grateful to my major advisor Dr. Ali Al-Gadhib for his constructive guidance, valuable advice and cooperation. I acknowledge, with deep gratitude and appreciation, the inspiration, encouragement, valuable time and guidance given to me by Prof. Mohammed Baluch, who served as my co- advisor. Thereafter, I am deeply indebted and grateful to Dr. Mohammad K. Rahman, Principal Investigator for this research funded by Deanship of Scientific Research, for his extensive guidance and support in the development of my research work and personal involvement in all phases of experimental and numerical work carried out in this research. I am also grateful to Dr. Mohammed A. Al-Osta, and Prof. Omar S. Baghabra Al-Amoudi, committee members, for their constructive guidance, valuable advice and cooperation.

I also acknowledge the sincere and untiring efforts of Eng. Imran who assisted me during all stages of my experiments. Thanks and acknowledgments are due to the laboratory technicians, Eng. Omer and Eng. Najamuddin, for their tremendous help.

Finally, I would like to express my deepest gratitude to my mother, father, brothers, sisters, my wife, and all other relatives, for their emotional and moral support throughout my academic career and also for their love, patience, encouragement and prayers.

TABLE OF CONTENTS

LIST OF TABLES

LIST OF FIGURES

LIST OF ABBREVIATIONS

ASTM	:	American Society for Testing and Materials
LVDT	:	linear variable differential transformer
SFRHM	:	High strength mortar reinforced with steel fiber
URM	:	unreinforced masonry wall

ABSTRACT

Full Name : AHMED AWAD SAEED SADOON

Thesis Title : INVESTIGATION OF THE PERFORMANCE OF CONCRETE MASONRY WALLS PLASTERED BY HIGH PERFORMANCE MORTAR UNDER CYCLIC LOADING

Major Field : CIVIL & ENVIRONMENTAL ENGINEERING

Date of Degree : APRIL 2016

Masonry buildings are the oldest type of buildings that existed through the entire history of civilization. The masonry walls can act as a compressive element with magnificent capacity but, when it comes to resist in-plane lateral loads such as wind and earthquake, it shows bad performance. Experimental investigation and numerical simulation were carried out to assess the behavior of unreinforced concrete masonry (URM) walls using high strength mortar reinforced with steel fibers (SFRHM) in form of plaster on one side and two sides. Three walls of 800 mm in length and width and 100 mm in thickness were made using hollow concrete blocks. Three specimens were built to evaluate the effect of high strength mortar reinforced with steel fibers; one used as control specimen, two plastered by high strength mortar reinforced with steel fibers with a thickness of 10 mm on one side, the last was plastered by high strength mortar reinforced with steel fibers with a thickness of 10 mm on both sides. The walls were tested under constant vertical load with horizontal load in form of in-plane cyclic loading. The experimental results show significant increase in the shear capacity of the wall plastered with SFRHM. Finite element modeling of the walls, using ABAQUS software captured the lateral load-displacement response of the wall with good accuracy using the plastic damage model.

ملخص الرسالة

الاسم الكامل: أحمد عوض سعيد سعدون

عنوان الرسالة: التحقيقات المعملية لاداء الحوائط الحجرية الاسمنتية المطلية بمادة اسمنتية عالية القوة تحت الحمل الافقي المتكرر.

التخصص: الهندسة المدنية والبيئة

تاريخ الدرجة العلمية: أبريل 2016

تعتبر المباني الحجرية غير المسلحة من أقدم انواع المباني التي كانت موجودة عبر التاريخ الحضاري كله. هذه المباني لها قدرة عاليه على تحمل قوي الضغط الراسية، ولكن عندما يتعلق الأمر بمقاومة الأحمال الجانبية مثل الرياح والزلازل، فانها تظهر اداء سيئاً وتنهار بصورة كارثية. تم اجراء التجارب المعملية والمحاكاة الرقمية لتقييم سلوك هذه المباني الحجرية غير المسلحة باستخدام مادة اسمنتية عالية القوة معززة بألياف فولاذية (SFRHM) في شكل طلاء على جانب واحد من الحائط وايضا علي جانبي الحائط. وتم بناء ثلاثة جدران (800 مم في الطول والعرض و 100 مم في السمك) باستخدام الطوب الخرساني المجوف. بنيت ثلاث عينات لتقييم تأثير هذه المادة الاسمنتية عالية القوة المعززة بالالياف الفولاذية: العينة الاولى تم استخدامها كعينة مرجعية، العينة الثانية تم استخدام الطلاء الاسمنتي المعزز بالالياف الفولاذية على جهة واحدة من الجدار بسمك قدره 10 مم، العينة الاخيرة تم استخدام الطلاء الاسمنتي المعزز بالالياف الفولاذية على جهتي الجدار بسمك قدره 10 مم. تم اختبار هذه الجدران الحجرية تحت التحميل الرأسي المستمر والثابت مع الحمل الأفقي، الذي كان في شكل حمل افقي دوري. تم ملاحظة الضرر في عينات الجدران وطرق الانهيار لكل جدار حجري، وسجلت استجابة هذه الجدران مع الزيادة التدريجية في الحمل الجانبي في شكل منحنيات الحمل الانحرافية. أظهرت النتائج المعملية زيادة كبيرة في القدرة على زيادة قوة القص باستخدام هذه المادة الاسمنتية عالية القوة والمعززة بالالياف الفولاذية (SFRHM). تم استخدام برنامج محاكة (ABAQUS) لكي يمثل التجارب المعملية التي اجريت؛ وقد اعطي نتائج مماثلة مقارنة مع النتائج المعملية.

CHAPTER 1

INTRODUCTION

1.1 Introduction

Although the construction of buildings nowadays is mainly made of reinforcement concrete and steel, still the use of ordinary masonry buildings is very common. In general, masonry buildings can be found in regions like India, Middle East, Eastern Europe and some parts of Asia [1]. Because of easy installing, low cost and availability in different types (clay, concrete, stone…), people keep using the construction of masonry wall and it represents the majority of the residential buildings in the developing countries [2]. Masonry wall is the component of structures made from individual units laid in and bonded together by using mortar. Most commonly used materials to construct masonry walls are brick, marble, granite, stone, travertine, limestone, cast stone, tile, cob, glass block, concrete block, and stucco. The key advantages of masonry wall are the thermal mass of a building (thermal mass refers to materials such as masonry and water that can store heat energy for extended time, it prevents rapid temperature fluctuations) and protection of the building from fire has been increased. Moreover, there is no requirement of painting, resulting in reduced life-cycle costs and the useful life cycle is 500 years, which is 5 to 20 times higher than structural steel.

Most common uses of masonry wall are for partition wall, structural wall, retaining wall, and even in heritage structures. It is well-known that those structural elements are constructed mainly of unreinforced masonry wall (URM). In spite of this, URM structures behave badly when subjected to earthquakes. As a result, catastrophes take place, causing a big loss in terms of lives and economy [3].

URM is regarded as anisotropic in terms of elastic properties as well as failure criteria. Orthogonal planes of weakness are attributed to the mortar joints. Failure modes for URM components comprise of compressive crushing, diagonal tensile splitting of units, tensile cracking along head and bed joints, and the sliding shear failure of bed joints [3].

In recent years, nano-technology has engrossed significant scientific attention for the uses of the particles in nanometer scale (10^{-9} m) scale [4]. This nano size particle can modify the existing properties to significantly improved properties than previously used particle size materials with similar chemical composition. As a consequence, it will be convenient for the industries to replace many existing products with higher performance and design new structures to a unique level [5].

The nano scale particles influence the mechanical response of concrete substances that relay on structural components. Consequently, nano-technology has the ability to reshape the concrete in terms of its molecular structure. It also enhances the substance's bulk properties. Nano technology can also improve the volume stability, durability, mechanical response and durability of the concrete. The innovative influences related with nano-technology, give the development of lowering the cost as minimum as possible, improve the durability and getting high strength concrete (the development of

the ultra-high performance depends mainly of nano-technology [4]. It may guide to good utilities of concrete substances. There are 3 major virtues of using nano materials. The first major advantage is to get concrete with high-performance strength. The second virtue is to decrease cement quantity in the concrete mix resulting in getting the same value of strength and decreasing the environmental pollution because of the cement and more importantly lowering the cost. The third virtue is reducing the construction process times as they are capable of producing concrete with reduced curing time [5].

Now-a-days, because of the good mechanical, electrical, chemical and thermal properties and amazing performance of nano particles, many concrete researchers in cement and polymer-based materials are showing attention on nano materials.

Fibers had been used as reinforcement since prehistoric times. At that time, straws were used in mud bricks and horsehair were used in mortar. In the 1900s, fibers of asbestos were used in concrete. The idea of composite materials came in 1950s and fiber-reinforced concrete was one of the topics of interest. Steel fiber is one kind of fiber reinforcement system, which increases structural integrity, tensile strength and ductility. The key advantage of using steel fibers in mortar or concrete is: steel fibers are useful as multi-directional reinforcement, which helps improving the crack resistance [6].

As stated by the Saudi Geological Survey [7], Saudi Arabia is subjected to a range of earthquake activity from low to moderate. Damaging earthquakes have been recorded in Yemen (1982), Egypt (1992) and the Gulf of Aqaba (1995) where the newest event, of magnitude 6.3 on the Richter scale, was followed by over 7000 aftershocks and caused significant structural destruction in the Haql town located in the North-West of Saudi

Arabia. As any country, the Kingdom of Saudi Arabia possesses buildings with concrete masonry walls all around the area and mostly they consist of URM walls. Since most of these buildings are located in regions prone to seismic activity, there is a movement by some private and governmental sectors in the Kingdom to strengthen structural elements.

Since nano-technology in concrete is a relatively new research area in Saudi Arabia, not much study has been done yet to investigate the properties of concrete containing nano materials. In the proposed research work, a number of mortar specimens were prepared to study the uniaxial compression and tensile properties of high strength mortar modified with nano materials. Then, this high strength mortar was used as a plastered in the concrete masonry wall, further augmenting the nano-mortar with steel fiber as reinforcing additive and tested under cyclic loading. Strengthening procedure was developed for the existing concrete masonry wall and procedure of constructing a high performance wall was developed.

1.2 Needs for This Research

Most old concrete masonry constructions have not been originally designed to withstand seismic loading. The wall systems constructed in Saudi Arabia are mostly considered as a load bearing type, designed only to sustain gravity loading. Since the Kingdom of Saudi Arabia region is vulnerable to the risks of earthquake hazards, there is a need for investigation to gain knowledge about the performance of such structures subjected to seismic loading and to propose suitable strengthening methods for enhancement of their lateral resistance and verify their effectiveness in order to protect structures (new and existing).

1.3 Objectives

The primary motive of this research work was to study the behavior of masonry prisms and ordinary concrete masonry walls plastered with a high strength mortar containing nano-silica and steel fibers under axial and lateral loadings. The behavior would also be simulated using nonlinear finite element modeling. In order to achieve this, concrete masonry prisms were tested under axial load and masonry walls were tested under cyclic loading environment.

The specific objectives of this investigation were the following:

(a) Characterization of the materials used for the masonry walls and the surface treatment;

b) To comprehend the seismic response of normal concrete masonry walls based on indices of strength and the initial stiffness under cyclic loading;

c) To comprehend the seismic response of normal concrete masonry walls retrofitted using plaster of high strength mortar reinforced with steel fiber on one side and both sides based on indices of strength and the initial stiffness under cyclic loading;

d) To develop mechanistic model that can estimate the capacity of the improved masonry wall using high performance mortar; and

e) To carry out preliminary finite element modeling of the walls in the ABAQUS software that can capture the lateral load-displacement response of the masonry prisms and masonry walls using the plastic damage model.

CHAPTER 2

LITERATURE REVIEW

2.1 Introduction

In the last thirty years, the behavior of unreinforced masonry walls against cyclic loading was investigated by many researchers all over the world to improve and understand their performance. A number of conventional methods were introduced to increase the shear capacity of the walls. Conventional methods such as surface treatment (Ferrocement [8], Reinforced plaster [9], and Shotcrete [10]), Grout and epoxy injection[11], and Post-tensioning with rubber tires [12] were investigated.

Many disadvantages were discovered in these conventional techniques involving: wasting time, taking much space, discomforting the occupancy, disturbs the beauty of the façade, etc. In addition, these techniques resulted in an increase in the earthquake-induced inertia forces because of the additional mass. Owing to these drawbacks of using conventional techniques, the usage of fiber reinforced polymers (FRP) [13–17] opens an optimistic vision in the efforts to reduce the vulnerability of the masonry wall against the excitation action exerted by an earthquake. After years of using fiber reinforced polymers (FRP) types, a number of problems have shown up. Problems like high temperature, high cost and bad surface bond with the clay bricks represent some of the difficulties that were facing the use of fiber-reinforced polymers. Many researchers tried to use textile-reinforced mortar as potential solution [18].

Only few researchers used the idea of using high strength mortar with steel fiber as surface treatment to retrofit un-reinforced masonry walls [19]. The use of steel fiber facilitates the application of the mortar layer utilizing the common trowel because it holds the mortar together. In addition, steel fiber has the ability to improve the ductility behavior as well as increasing the energy dissipation of the wall [19].

2.2 High Strength Mortar Reinforced with Steel Fibers

Sevil el al. [20] developed the idea of using mortar with steel fiber in order to strengthen the infill hollow blocks in reinforced concrete frames. Trials were made to determine the optimum mortar that could be used as retrofitting material. The steel fiber content of 2% (by volume) came out to be the most convenient steel content to be used according to many tests that were carried out (compressive strength, flexural strength and adhesion strength) [20].

Three specimens were built to assess the effectiveness of using high strength mortar with steel fiber. The first specimen used as a control specimen to be compared with other two in terms of lateral strength, initial stiffness and energy dissipation. A reference mortar was used to be applied to the second specimen, while the last specimen was used to apply the intended mix, which was mortar with steel fiber, to observe the enhancements [20].

According to Sevil el al. [20], all specimens were tested under combined axial load and reversed lateral load in an attempt to simulate the seismic behavior. Displacement transducers were used to measure all deformations that took place during the test. All

cracks and mode of failures were noticed and marked during the process of conducting wall tests.

According to the test results [20], the use of high strength mortar with steel fiber proved to be effective in terms of lateral strength, initial stiffness and energy dissipation. The lateral strength was considerably increased by a factor of 1.53 and 2.02 for the specimens with reference mortar and for the specimen with high strength mortar reinforced with steel fiber, respectively. The initial stiffness was remarkably enhanced by a factor of 2.86 and 3.14 for the specimens with reference mortar and for the specimen with high strength mortar reinforced with steel fiber, respectively.

Churilov el al. [21] carried out a number of experimental tests to deeply investigate the behavior of the masonry walls under cyclic load, and also to observe important information; such as shear strength, initial stiffness and energy dissipation. This work was divided into two main categories; the first one consisted of testing four unreinforced masonry walls, the other one consisted of testing four walls strengthened with reinforced mortar on one or two sides of the walls (which was referred to as RC jacketing by the author). To construct the eight walls with the structural conditions in Macedonia, lime mortar with solid clay bricks were used. Using the idea of RC jacketing, to improve the performance of the unreinforced masonry walls, was the main objective of this study.

According to the test results [21], the walls strengthened by mortar reinforced with steel mesh proved to be effective to significantly increase the shear strength capacity of all retrofitted walls as well as initial stiffness. The increase in shear strength was in a range of 2 to 3 times the control specimen.

According to Churilov el al. [21], many mechanistic models (Eurocode 6 [22] , CSA S304.1-04 [23] , PIOVSP [24], the provisions of Tomazevic [25] and formulas developed by FEDRA [26]) were used to estimate the shear capacity of the retrofitted walls. Good agreement was found between the mechanistic models and test results. The model of Tomazevic [25] proved to be the best option available to predict the shear capacity of the strengthened walls, while the other mechanistic models were successful to predict the shear capacity of unreinforced masonry walls.

Facconi et al. [19] used mortar reinforced with nanosilica and short high strength steel fibers as surface treatment technique to improve the behavior of masonry walls. The aim of this study was to apply this reinforced mortar in the form of external overlays to enhance the performance of the solid clay masonry walls against cyclic loading in an attempt to increase the shear capacity of masonry walls.

According to Facconi et al. [19], one of the specimens was used to be retrofitted after it was subjected to destroying cyclic loading, in order to examine the effect of the strengthening method on existing buildings. Also, to improve the bond between the wall surface and coating material, two steel dowel connections were installed. A number of tests were conducted to evaluate the mechanical properties of strengthening material, many of these properties were used to estimate the shear capacity using the available mechanistic models. Four walls were tested; one as reference specimen, two and three strengthened with 25 mm thickness layer with different types of steel dowel connection, the last was the first one but after it was repaired with 25 mm thickness layer.

According to Facconi et al. [19], The results revealed the improvement in the shear capacity by 30% higher than the reference sample, also enhancement in the stiffness by 60% in the elastic level of the experiment.

2.3 Use of Nano-silica

Haruehansapong et al. [4] investigated the benefits of using nano-silica in the mortar in order to observe the compressive strength and the microstructure characteristics for the mortar containing nano-silica using different sizes of particles (40 nm, 20 nm and 12 nm). One specimen was used as the control to observe the changes in terms of compressive strength as well as microstructure. In addition, the silica fume with a size of 100 nm was utilized to make better comparison, since the silica-fume is one of the best pozzolanic materials due to its small particles. Both of the nano-silica and micro-silica were used with different percentage of the cement content (3%, 6%, 9% and 12%).

According to Haruehansapong et al. [4], the use of nanosilica proved to be effective to significantly increase the compressive strength for all specimens regardless of its particle size or its dosage. Also, the use of particle size of 40 nm came out to give the highest compressive strength, while the use of nanosilica with a percentage of 12% (by cement weight) came out to be the optimum value that could be used to give highest compressive strength.

According the test results [4], the optimum value that could be used as replacement of the cement had no correlation with the particle size of the nanosilica. Also, the

microstructure photographs for all specimens were consistent with the increase in compressive strength due to the size particles and the percentage of replacement content.

Mukharjee et al. [5] examined the influence of using nano-silica in the mortar to study how the compressive strength and water absorption could be affected by the partial replacement of the cement with nano-silica as well as the water/cement ratio. The nano-silica replacement as a percentage of cement content was 0%, 1.5% and 3%, while the water/cement ratio was maintained at 0.4, 0.45 and 0.5.

A number of 9 mixes were made to ensure that every combination would be used to study the interaction between the level of nano-silica replacement and water/cement ratio. Also, compressive strength analysis was provided to examine the combined influence of nano-silica addition and water/cement ratio [5]. Based on the tests results, the increase in the value of water/cement ratio resulted in decreasing the value of compressive strength. In addition, the increase in the value of nano-silica content, resulted in increasing the value of compressive strength.

According to Mukharjee et al. [5], the addition of nano-silica was found to be effective in reducing the water absorption of mortar, while the increase in water/cement ratio was found to be a factor in increasing the water absorption of mortar. In addition, both of nano-silica addition and water/cement ratio were proved effective to influence the compressive strength as well as water absorption.

2.4 Use of Steel Fibers

Song et al. [27] examined the use of steel fiber to improve the brittle behavior of the concrete. The influence of high strength steel fiber on concrete in terms of compressive strength, flexural strength, toughness index, and modulus of rupture was investigated in this study. The main purpose of the paper was to enhance the poor performance of the concrete against tensile stresses. The concrete in general is well-known for its low capacity for shear stresses and strain ductility. The percentage of the fiber volume was 0.5%, 1.0%, 1.5%, and 2.0% with respect to the entire volume of the mix.

According to the study results [27], the use of the high strength steel fiber with different steel fiber ratio increased the compressive strength capacity. Also, the maximum compressive strength was achieved at a steel fiber ratio of 1.5% with 15.3% higher than the control specimen, while a small drop was observed at 2.0% (volume fraction) but still higher than the other entire steel fiber ratio expect for 1.5%.

Based on the tests results [27], a range of 20% to 100% improvements were achieved in the splitting tensile test. Also, any increase in the steel fiber ratio, resulted in increasing in the splitting tensile strength. Moreover, modulus of rupture followed the same behavior with a range of 28% to 130% improvements. Analytical investigation was presented in this reference [27] to predict the compressive strength, tensile strength and modulus of rupture. A good agreement was found between the strength models and the test results.

In order to study the mechanical properties and the impact resistance of the concrete containing steel fiber as reinforcing material, Nili and Afroughsabet [28] carried out a research with two different water/cement ratio (0.45 and 0.36) including the effect of

using silica fume as a pozzolanic material. Steel fibers with a percentage of 0%, 0.5% and 1.0% were utilized to observe the effect with large range, while a percentage of 8% of the cement content was replaced by silica fume.

Based on their experimental results [28], the addition of the steel fiber improved the overall performance of the concrete. The splitting tensile strength and flexural strength were significantly increased by the incorporation of steel fibers. The mix with 0.45 water/cement ratio reached increase of 19% with 1% steel fiber ratio, while the mix with 0.36 water/cement ratio reached increase of 13.6% with 1% steel fiber ratio.

According to Nili and Afroughsabet [28], the compressive strength was more influenced by the partial replacement of the cement content with silica fume than the addition of the steel fibers. Also, it was increased by 32.5% with the addition of both 1% steel fiber ratio and 8% silica fume (replacement of cement content). Moreover, the maximum splitting strength was achieved with a 1% steel fibers and silica fume incorporation, improvement of 74% for the mix with 0.45 water/cement ratio and 62 % improvement for the mix with 0.36 water/cement ratio.

2.5 Textile-reinforced Mortar

Because of the many disadvantages that are related to the use of fiber-reinforced polymers to improve the performance of the unreinforced masonry walls, many researchers tried to use textile-reinforced mortar as potential solution [18]. Problems like high temperature, high cost and bad surface bond with the clay bricks represent some of the difficulties that are facing the use of fiber-reinforced polymers.

Papanicolaou et al. [18] tested a number of twenty two masonry walls under in-plane cyclic loading to study the effect of using textile-reinforced mortar on the behavior of unreinforced masonry walls to observe the enhancements in the shear capacity and the increasing deformability of the unreinforced masonry walls.

According to Papanicolaou et al. [18], all masonry walls were constructed to be divided into three groups; the first group was in form of shear walls (1300 mm length and 800 mm width), the second group was in form of beam-columns (1300 mm length and 400 mm width), the last group was in form of beams (400 mm length and 1300 mm width). All specimens were fabricated using perforated clay bricks. Since the application of textile-reinforced mortar is an alternative solution to fiber-reinforced polymers, the experimental setup was installed in a way that a comparison between textile-reinforced mortar (TRM) and fiber-reinforced polymers (FRP) were investigated.

According to the experimental results [18], TRM was found to be a good solution to enhance the performance of the unreinforced masonry walls. In addition, the increasing deformability of walls with TRM is better than walls with FRP, while the strength capacity of TRM walls came out to be in a range of 60-70 % of the FRP walls.

2.6 Shotcrete Layers

Shotcrete method is a system of welded steel mesh (with fixed spacing in all directions) embedded into a layer of shotcrete. Also, shear dowels are usually installed to improve the bond between the wall and the shotcrete layer.

Interesting research was carried out by Elgawady et al. [29] on half-scale brick clay masonry walls using shotcrete. Three walls were tested; one control, two plastered in one side by 40 mm, the last was plastered in two sides by 20 mm for each face. 100-mm spacing between the welded steel mesh was used in all direction, while a diameter of 4 mm was utilized for the reinforced bars.

According to Elgawady et al. [29], the results showed that the lateral capacity was increased significantly by 3.5 times compared with the control sample. Also, energy dissipation analysis was conducted to observe the amount of energy that could be dissipated through the shotcrete method (the more energy dissipation, the better for seismic resistance). According to the test results [29], the energy dissipation was notably increased by a factor of 1.5 for the one-side specimen and 4.0 for the two-side specimen, compared to the control specimen.

2.7 Effect of Mortar Reinforced with Fibers on Compressive Strength

Basaran et al. [30] constructed 24 walls with dimensions of 400 mm length, 400 mm width and 100 mm thickness. Four walls were used as reference specimens, while the others were plastered with different types of reinforced plaster mortar (2%, 3% polypropylene and 5% steel fiber). According to the tests results, the load-bearing capacity has increased significantly after using special reinforced plaster in both sides of the walls compared with the control samples. Furthermore, the stiffness of the walls has improved notably by such unique coating.

Interesting research was carried out by De Oliveira and De HanaI [31]. They tested eight models of concrete masonry prism with two samples of every model. The first model was a reference, while the second and the third were retrofitted by weak mortar and strong mortar, respectively. Strong mortar with steel welded meshes and another strong mortar with steel welded meshes using two different types of connectors were used for the fourth, fifth and sixth models, respectively. The last two models were reinforced by strong mortar with steel fibers and weak mortar with polypropylene fibers.

According to De Oliveira and De HanaI [31], the test results revealed that concrete masonry prism reinforced with strong mortar plus welded meshes increased the ultimate load capacity by a factor of about 1.44. The efficiency of strengthening with mortar overlays was affected by the failure mechanism of the prism.

CHAPTER 3

EXPERIMENTAL PROGRAM AND RESULTS

In this research, steel fiber reinforced with high strength mortar (SFRHM) was used to improve the performance of masonry walls against in-plane shear loading by constructing three walls (one as a control specimen, other by (SFRHM) plaster of 10 mm thickness on one side only, and the last by (SFRHM) plaster of 10 mm thickness on both sides).

Tests were carried out to observe improvements in shear strength capacity, and initial stiffness. In addition, numerical simulation using ABACUS was made to get a better overall understanding for the behavior of walls that were retrofitted with steel-fiber reinforced high strength mortar (SFRHM).

3.1 Experimental Program for Prism Test

Compressive strength of masonry is the most dominant parameter that is involved in every design code in masonry structures. Prism test method is one of two methods that are preferred by the researchers and designers to evaluate the compressive strength of masonry. While the other method, which is the unit strength method, depends only on block and mortar strength and it does not take into consideration the effect of workmanship and curing.

Among other factors, the mechanisms that govern the behavior of masonry wall depend on the amount of compressive strength on the wall and since the plastering technique method is used as a retrofitting material for improving the seismic response of the

unreinforced masonry wall, it's very important to assess the axial capacity of plastering technique. In addition, plastering the wall with mortar layers to close a crack or to rebuild damaged parts is used in rehabilitation of the existing building, giving additional importance to assess the axial capacity of plastering technique.

3.1.1 Specimens

Four un-reinforced concrete masonry prisms were cast with dimensions of 410 mm (height) x 410 mm (length) x 100 mm (thickness) according to ASTM C 1314 [32]. Each prism consisted of two courses (a course is a horizontal layer of bricks) and one head joint at the lower course. The hollowness represents 27% of the cross-section area of the block. Prism arrangement is shown in Figure 3.1. These prisms were fabricated with hollow concrete units having dimension of 200 x 400 x 100 mm by expert mason to reduce differences of workmanship as much as possible.

One concrete masonry prism was used as a reference specimen to compare the enhanced specimens with it. The adopted strengthening material, which comprised nano-silica and steel fiber, was utilized to retrofit three samples in the form of external overlays. Some samples were plastered only on one side with a thickness of 10 mm, others with a thickness of 10 mm on both sides and a thickness of 20 mm on both sides. Table 3-1 shows the experimental program for all samples.

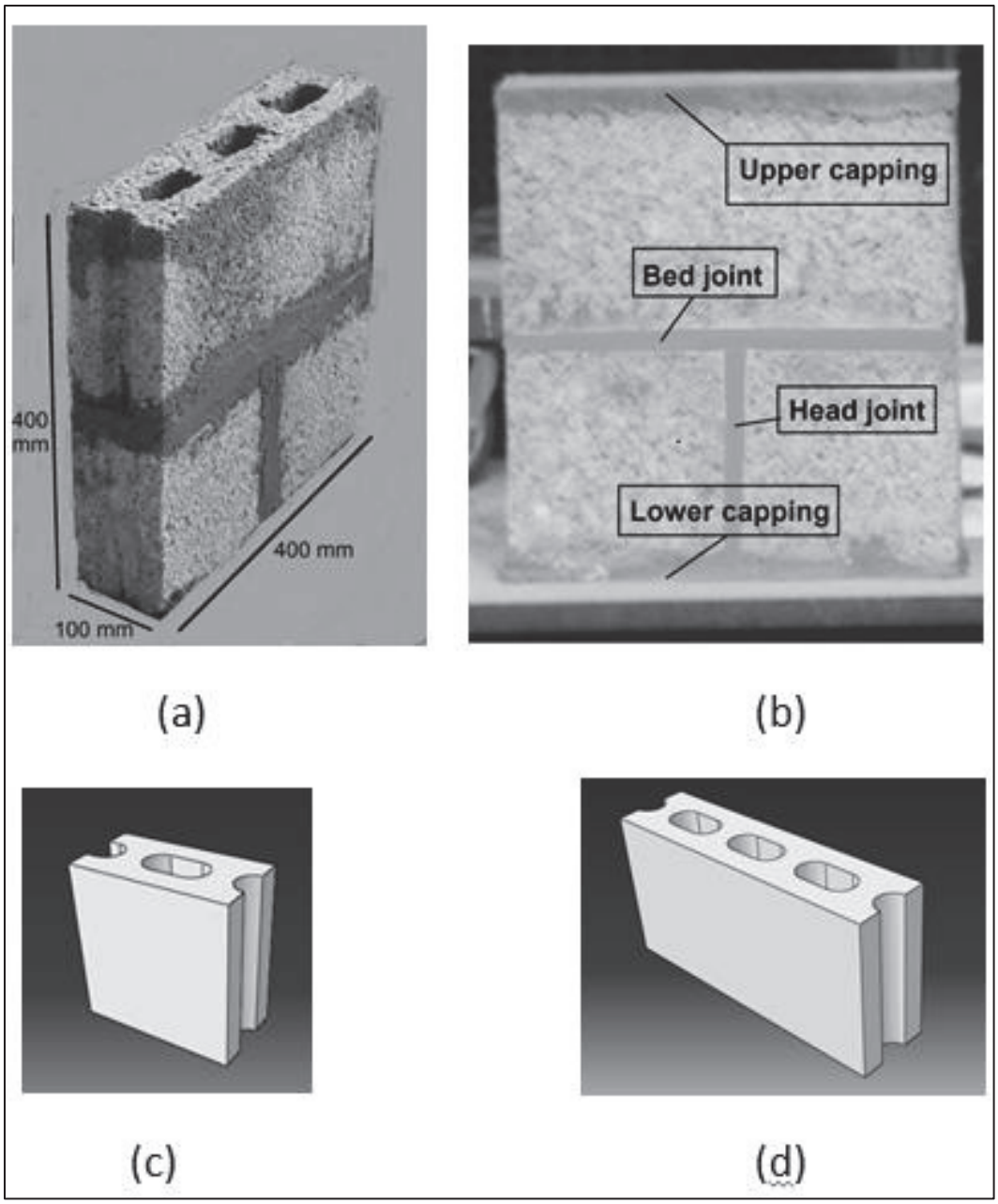

Figure 3-1: Details of the concrete masonry prism: (a) Unit block without capping; (b) Unit block with capping; (c) Half unit block; (d) Full unit block.

Table 3-1: Summary of the experimental program

Sample No.	Specimen ID	Type	Description
1	P00	CONTROL	Un-reinforced prism without strengthening
2	PN01	Plaster strengthening one side	Un-reinforced prism strengthened with SFRM plaster (10 mm one side)
3	PN11	Plaster strengthening two sides	Un-reinforced prism strengthened with SFRM plaster (10 mm two sides)
4	PN22	Plaster strengthening two sides	Un-reinforced prism strengthened with SFRM plaster (20 mm two sides)

3.1.2 Properties of Materials for Masonry Units

A number of trials were carried out to come up with strong, workable and durable mix. Portland cement (ASTM C 150 Type I), nano-silica (colloidal nano silica suspensions from Akzo Nobel Germany, Cembinder® 50), fine aggregate (natural dune sand), steel fiber (length of 12 mm, diameter of 0.15 mm and tensile strength of 2500 MPa) and super-plasticizer (Glenium 51) were used to produce the final mix (see Table 3).

The nano-silica was utilized to replace part of the cement and to enhance the compressive strength of the coating material as well as to improve the durability and microstructure of the strengthening material [4, 5]. The steel fiber was used here in the selected mix to reduce the cracks, and give more ductile behavior and increase the tensile strength [27, 28]. Table 3-2 illustrates the ingredients of the selected strengthening material.

Cubes (150×150×150 mm) and cylinders (diameter 75 mm, height 150 mm) were tested for finding out the compressive strength of the SFRHM mix according to ASTM C 39 and C 109. Furthermore, one sample was tested for the modulus of elasticity in accordance with ASTM C 469.

One specimen was tested under direct tension according to ASTM D 638 to get the tensile strength. Flow table test was conducted to evaluate the workability of the SFRHM mix according to ASTM C 1437. Table 3-3 illustrates the mechanical properties of the selected strengthening material.

Table 3-2: Mixture proportions of the selected mortar

Mixing material	Quantity
w/b (by mass)	0.45
Cement (kg/m^3)	500
Nano-silica (by cement weight)	6%
Super plasticizer (by cementitious weight)	2%
Steel fiber (by mix weight)	2%
Density (kg/m^3)	2293

Table 3-3: Mechanical properties

Mechanical properties	Value
Cylindrical compressive strength [MPa]	42
Cubic compressive strength [MPa]	52
Tensile strength [MPa]	5.5
Elastic modulus [MPa]	27000
Flow table [mm]	200

3.1.3 Experimental Program for Tests on Masonry Prisms

All the specimens were tested inside steel frame, which is closed from the top and the bottom to act as vertical reactions (Figure 3-2). A vertical hydraulic jack inside the steel frame was used to exert axial pressure to the specimen. Two steel plates were put in the steel frame to transfer the vertical load from the hydraulic jack to the specimens; one plate under the specimen, the other one above the specimen. Figures 3-2 and 3-3 show the details of the experimental setup.

One load cell was attached to the hydraulic jack to measure the vertical applied load, while three linear variables differential transducers (LVDT's) were utilized to measure displacements; one to measure horizontal displacement, the other two to measure vertical displacement. In addition, four strain gauges were placed on the top corners of the prism to check the eccentricity.

All the strain gauges, LVDT's and the load cell were connected to a data logger device to collect and monitor the data. Instrumentation setup is shown in Figure 3-4.

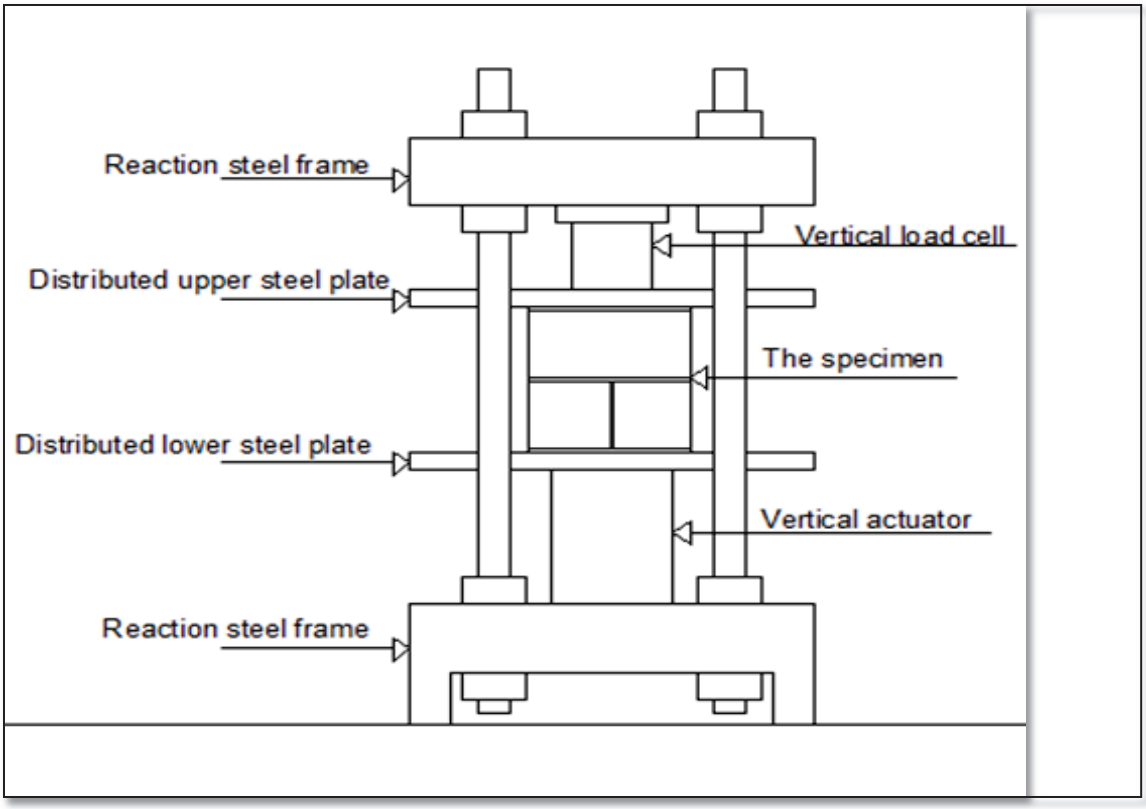

Figure 3-2: Details of the experimental setup

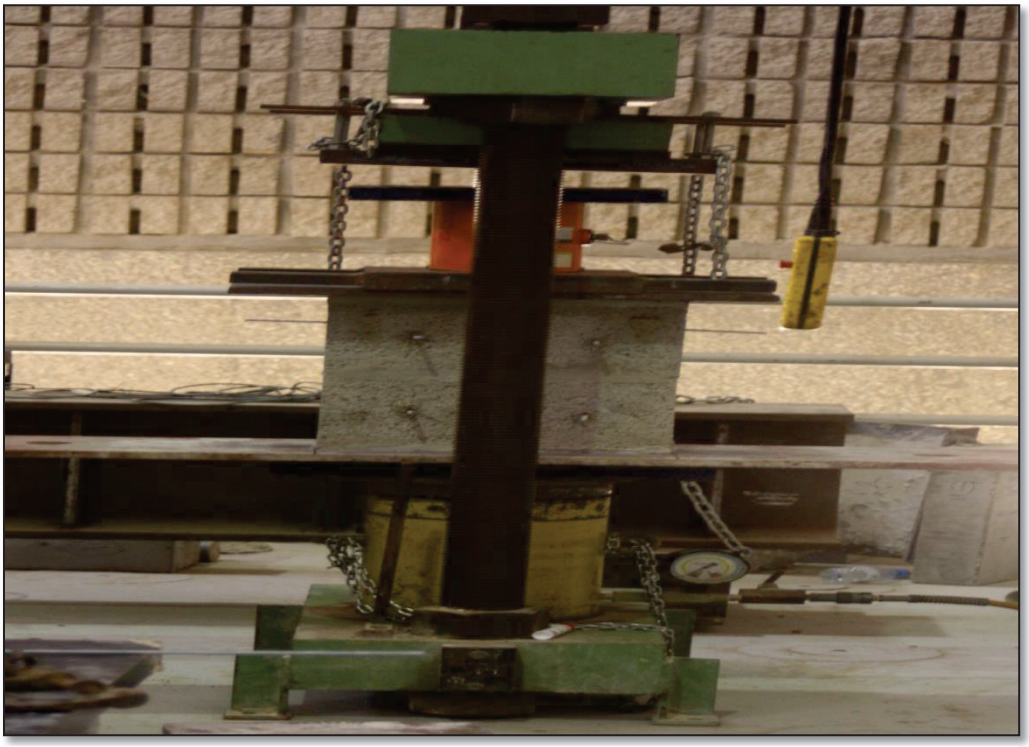

Figure 3-3: Details of the real experimental setup

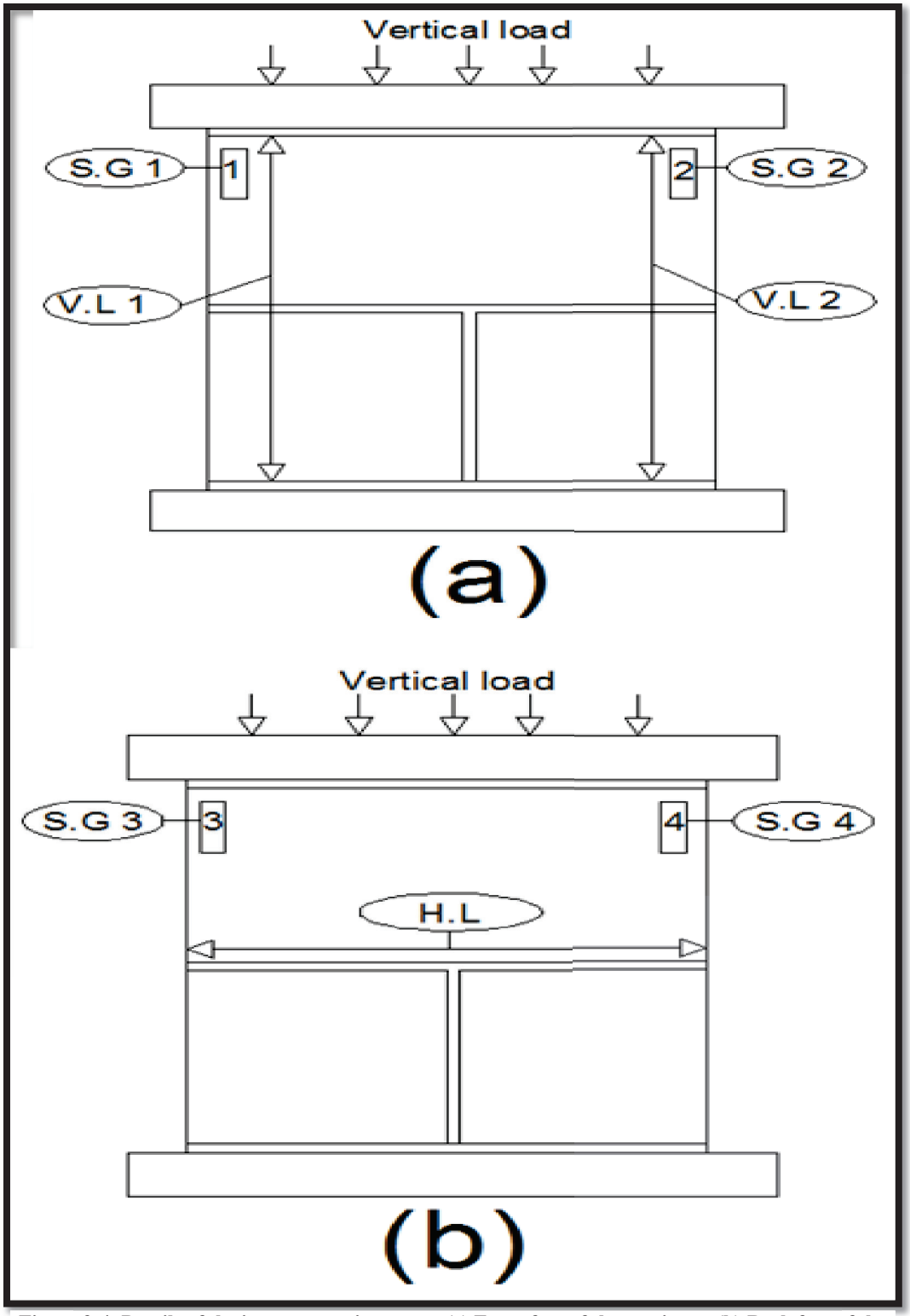

Figure 3-4: Details of the instrumentation setup: (a) Front face of the specimen; (b) Back face of the specimen

3.1.4 Experimental Results for Prism Tests

Every specimen was tested in three cycles; the first cycle was up to 50 kN, the second cycle was up to 100 kN, the last one was up to failure. The purpose of the first and second cycles was to check the eccentricity of the specimen through the means of four strain gauges installed on the top corners of each concrete masonry prism.

Regarding the control specimen, a vertical crack in the web mid-face occurred at a vertical load of 260 kN corresponding to vertical displacement of 0.25 mm. After this crack took place, the specimen developed no vertical resistance and fail immediately.

The one-side specimen (plastered only on one side) of 10 mm thickness was developed a vertical load of 310 kN corresponding to 0.54 mm vertical displacement. The first crack, which is the mid-face vertical crack, occurred at 260 kN similar to the control specimens but it developed a small strength after the first crack took place.

The two-side specimen (plastered on both sides) of 10 mm thickness was reached a vertical strength of 480 kN with a displacement of 0.55 mm. The mid-face vertical crack took place at 252 kN corresponding to 0.16 mm displacement.

The two-side specimen (plastered on both sides) of 20 mm thickness developed a vertical load of 550 KN (corresponding to 0.33 mm vertical displacement). The first crack, which is the mid-face vertical crack, was occurred at 328 kN with 0.11 mm displacement. Figure 3-5 illustrates the load vs. deflection for all strengthened prisms compared with the control specimen.

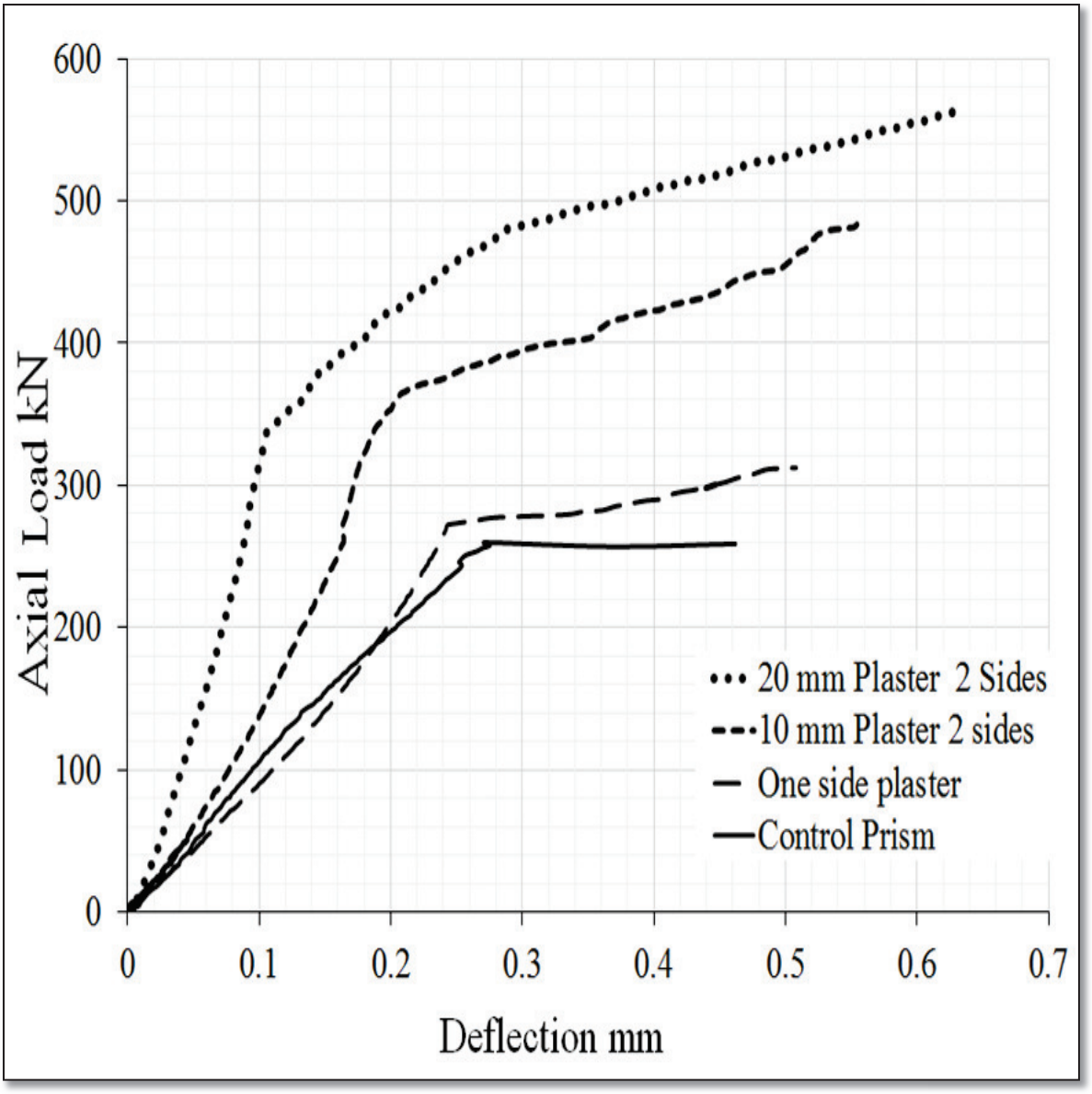

Figure 3-5: Load vs. deflection for concrete masonry prisms

3.1.5 Failure Modes and Stiffness of Prisms

Three types of failure modes dominate the behavior of the compressive strength of concrete masonry prisms. All the specimens developed a vertical crack in the mid-face of the web with an average vertical load of 300 kN, but the corresponding vertical displacement wasn't the same because of the difference in stiffness for each specimen.

The specimens without any plaster failed after the mid-face crack in the web immediately, due to the crushing of the top block. Figure [3.6a] shows the mode failure of the non-retrofitted specimen.

The specimen with only one side 10 mm thickness developed small strength after the first crack (mid-face crack in the web). Due to crushing of the un-coated part of the prism, the whole prism collapsed. Figure [3.6b] shows the mode failure of the one-side specimen.

The specimen with two sides 10 mm and 20 mm thickness developed remarkable increase in capacity after the first crack but it failed due to crushing of the top block and that led to de-bonding between the plaster and the prism. Figure [3.6c] and Figure [3.6d] show the mode failure of the two-side specimens.

The property of the stiffness for each prism is very important since it shows how the prism resists the deformation. The effect of the retrofitting material on the initial stiffness property is shown in Figure [7.3]. The initial stiffness was calculated in a range of (0-0.1) mm.

It's clear that the stiffness was increased as results of using the retrofitting material. The specimen with 20 mm thickness on both sides developed 200% increase in stiffness compared with the control specimen, while the specimen with 10 mm thickness developed only 30% increase in stiffness.

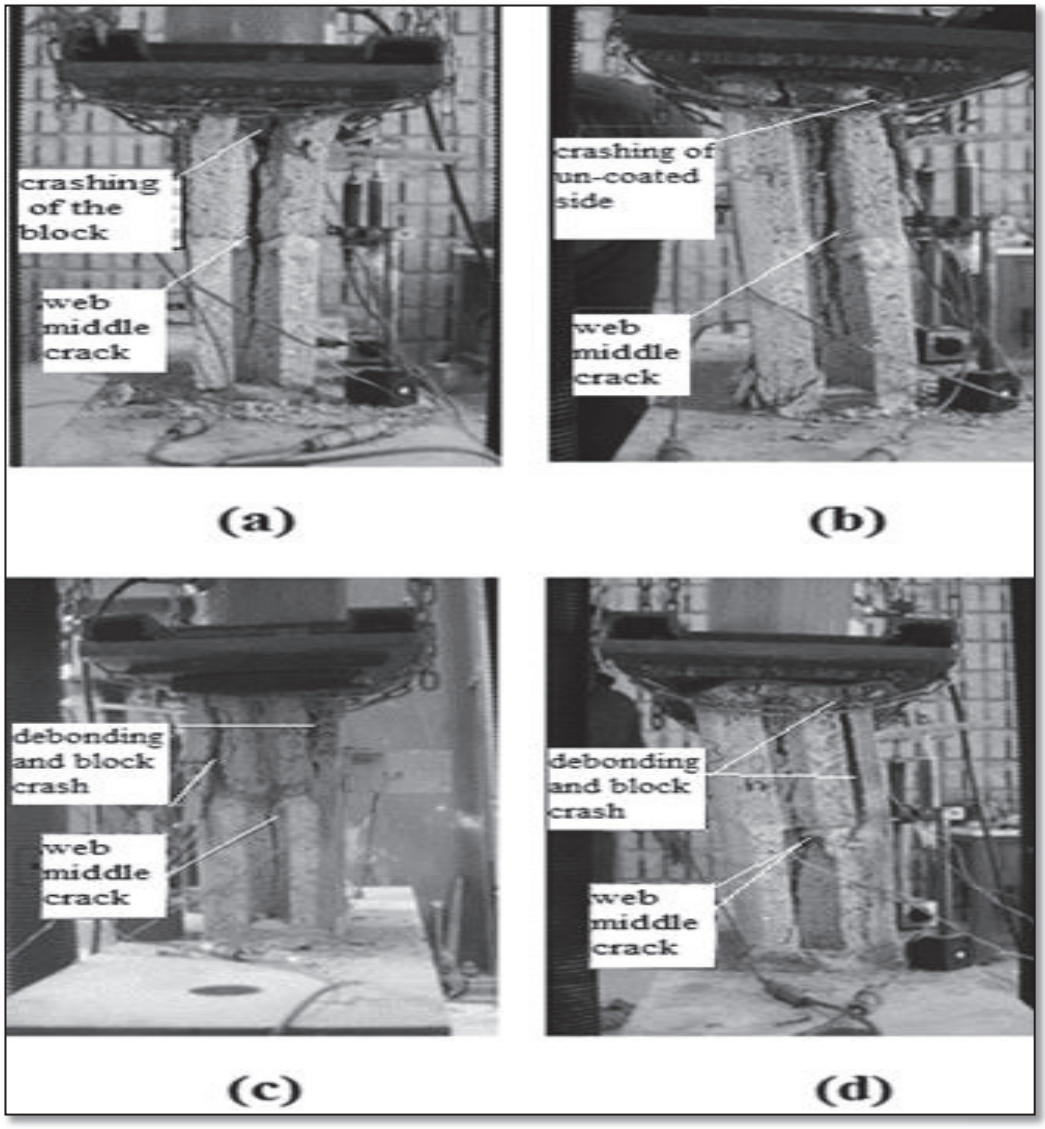

Figure 3-6: Failure modes: (a) non-retrofitting specimen; (b) one side 10 mm thickness; (c) two sides 10 mm thickness; (d) two sides 20 mm thickness.

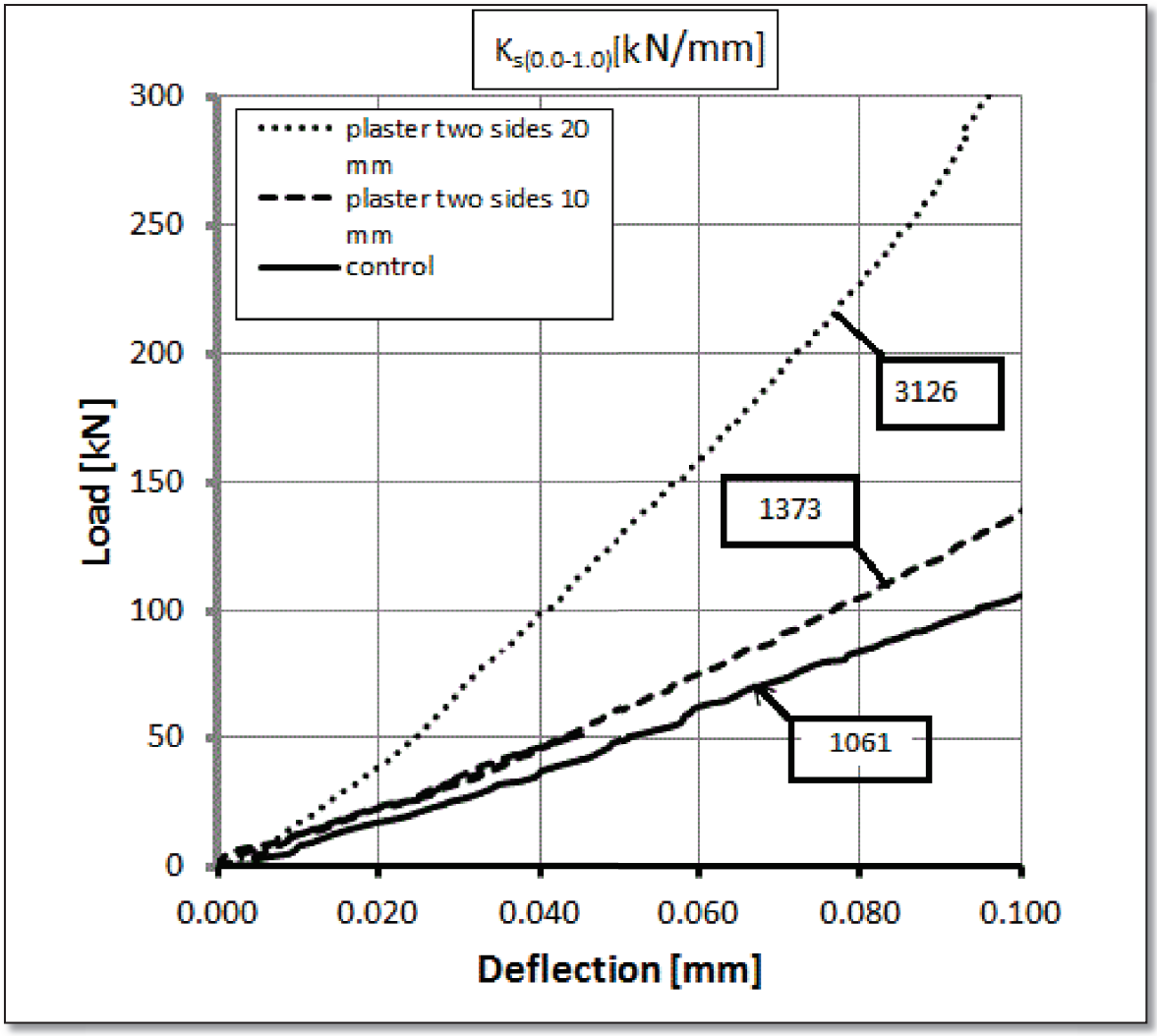

Figure 3-7: Effect of the retrofitting material on the initial stiffness

3.2 Experimental program for Tests on Masonry Walls

Wall test is the main objective of this study; each wall was subjected to constant axial load (represents the gravity load) and cyclic horizontal load (represents the earthquake load). It was made to assess the benefit of using high strength mortar reinforced with steel fiber SRFHM. This kind of test was utilized over the years by many researchers to test masonry walls against cyclic loading to evaluate the improvements in shear capacity in the strengthening specimens comparing to the control specimen.

3.2.1 Specimens

A number of three concrete masonry walls were made with dimensions of 800 mm (height) x 800 mm (length) x 100 mm (thickness). Since the shear failure is the most dominant type of failure that frequently takes place, the aspect ratio (the ratio of the width to the height of wall) was 1:1 to get shear dominant behavior under the combined axial and lateral loadings. These specimens were fabricated with hollow concrete units having dimensions of 200 mm x 400 mm x 100 mm. All the specimens were built in the reaction floor near the testing setup by expert mason to reduce workmanship differences as much as possible.

The first specimen was used as a reference sample to observe the enhancement in the retrofitting specimens in terms of ultimate shear strength and lateral stiffness. The second specimen was built with type M mortar in the head and bed joint and then plastered on one side only with 10 mm thickness of SFRHM plaster using common trowel.

The third sample was built with type M mortar in the head and bed joint and then was plastered on both sides with 10 mm thickness of SFRHM plaster using common trowel. The description of each wall is shown in Table 3-4.

Table 3-4: The description of each wall

Sample No.	Specimen ID	Type	Description
1	W00	CONTROL	Un-reinforced wall without strengthening
2	WN01	Plaster strengthening one side	Un-reinforced wall strengthened with SFRHM plaster (10 mm one side)
3	WN11	Plaster strengthening two sides	Un-reinforced wall strengthened with SFRHM plaster (10 mm two sides)

3.2.2 Material Properties for the Components of Masonry Units

A thickness of 10 mm was put between the bricks using type M mortar to construct all the walls and the plaster was put for the second and third specimens after the construction of walls. The mortar was prepared within two stages: first the cement was mixed with sand at a ratio of 1:3, and then the water was added to the dry mix of cement and sand with water-cement ratio of 0.6. The compressive strength of type M mortar was obtained by testing three cubes (cured into water tank for 28 days) according to ASTM C 109. An average of 22 MPa was provided according to these tests.

In this study, nano-silica high strength mortar reinforced with steel fiber was used to act as thin plaster layer which has the ability of resisting the in-plane shear forces and it is referred to as SFRHM. The mix design and the mechanical properties of SFRHM were mentioned in clause 3.1.3.

After the cast of all walls, they were subjected to curing process for about 28 days with continuous water curing (water hose was used to saturate the walls with water and then all walls were covered with a plastic sheets to keep the water inside the walls, this process was done for 28 days).

3.2.3 Experimental Setup for Test on Masonry Walls

All walls were built directly on top of a steel U channel in the reaction floor near the testing setup so that transporting the wall from one place to another was achieved without damaging the wall samples. Each wall was placed in the proper position within a steel frame fabricated for testing the wall under cyclic loading (Figure 3-8).

Each wall was loaded horizontally and vertically through reinforced beam of 300 mm wide and 400 mm high. This reinforced beam was put over each wall to transfer the loads from two hydraulic jacks (one was vertical and the other was horizontal). Figures 3-8 to 3-10 illustrate the schematic laboratory set-up.

Two load cells were attached with each hydraulic jack to measure the applied loads, while three linear variables differential transducers (LVDT'S) were utilized to measure displacements; one to control and measure horizontal displacement, the other two to measure vertical displacement. In addition, two strain gauges were placed on the walls to measure the stresses and strains in the wall's blocks resulting from diagonal cracks.

All of the load cells, LVDT'S and strain gauges were connected to a data logger device through which the data were monitored and collected. Instrumentation setup is shown in Figure 3-11.V.L, H.L and S.G referred to vertical LVDT, horizontal LVDT and strain gauges, respectively.

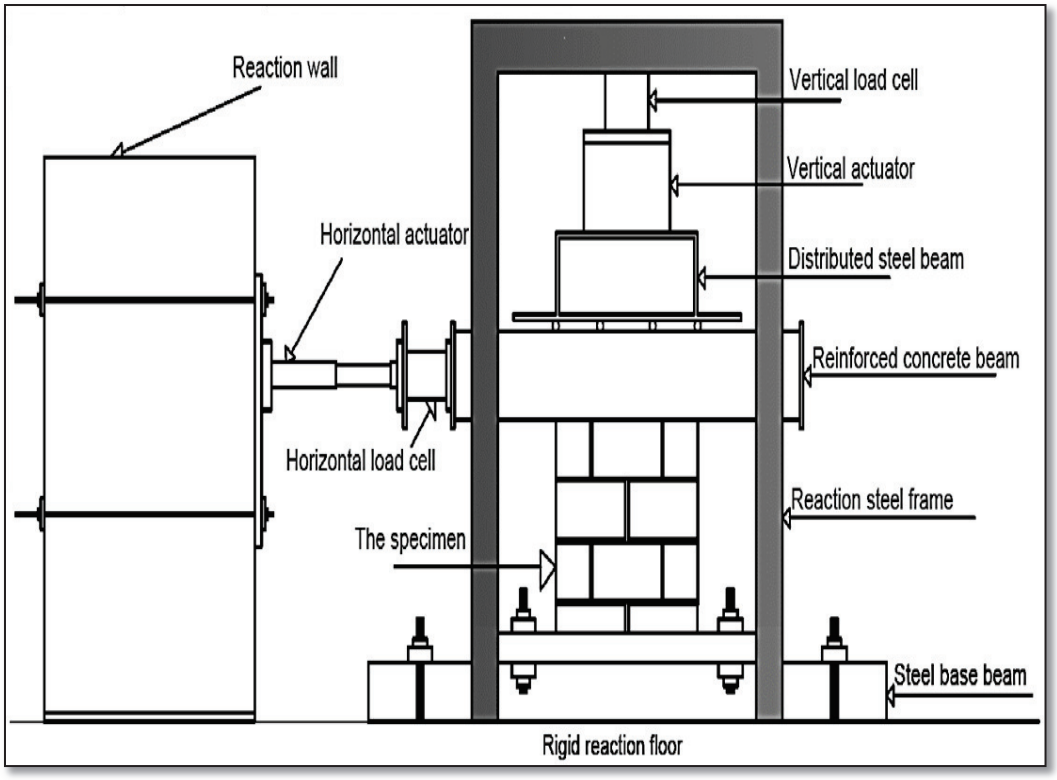

Figure 3-8: Schematic laboratory set-up in 2D

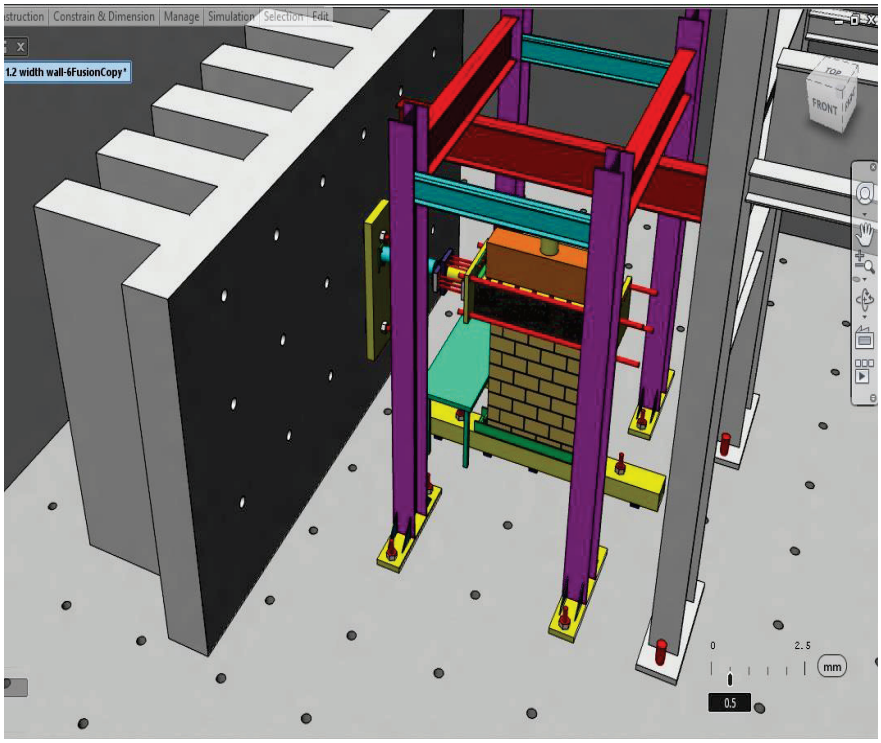

Figure 3-9: Schematic laboratory set-up in 3D

Figure 3-10: Real Laboratory set-up

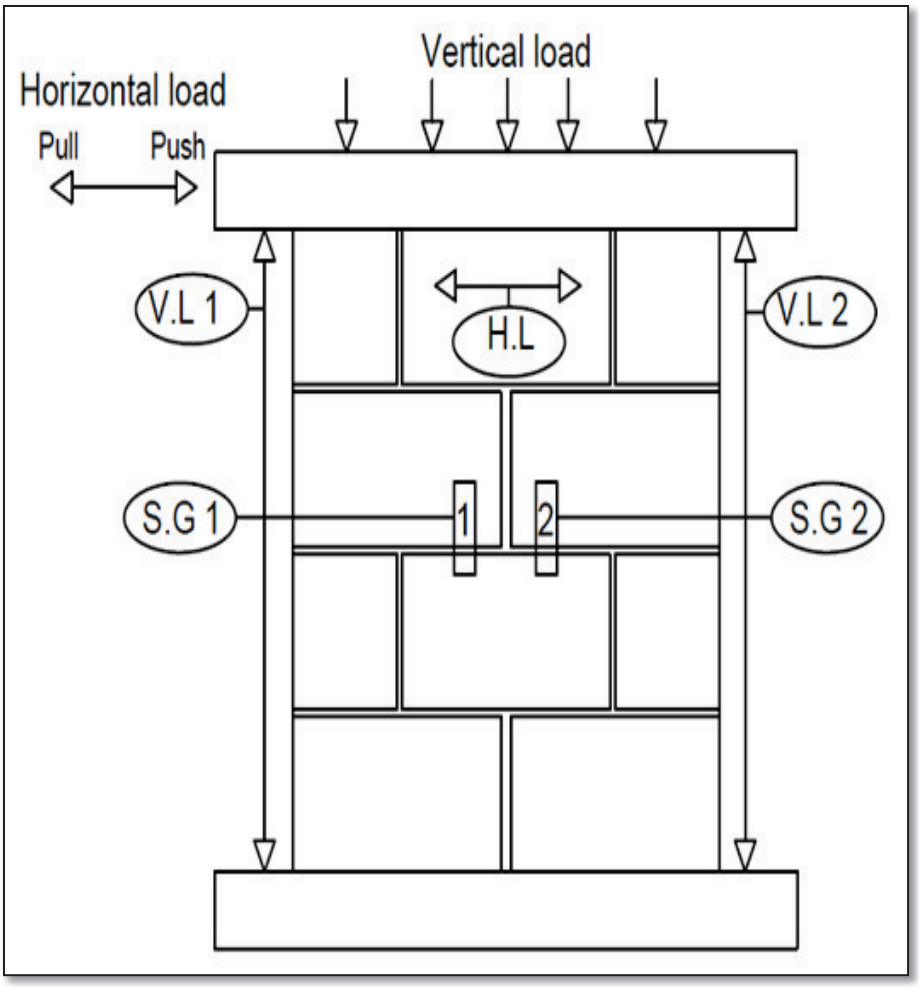

Figure 3-11: Instrumentation setup of the wall

3.2.4 Loading Scheme for Lateral Load Test

Firstly, a vertical stress of 50% of the maximum stress capacity of the prism was applied to the walls through the vertical hydraulic jack and kept constant. Secondly, the horizontal load was applied through the horizontal hydraulic jack, controlled by displacement-control system in the form of cyclic loading. The displacement-regime, which is adopted in this experiment, is shown in Table 3-5 (the drift ratio is defined as the ratio of maximum lateral drift to total height of the specimen, while the push-pull displacement represents the cyclic movements). Each wall followed this system of displacement-regime until it failed.

Table 3-5: The displacement-regime

Number	Drift ratio	Push displacement (mm)	Pull displacement (mm)
1	0.05 %	+0.5	-0.5
2	0.10 %	+1.0	-1.0
3	0.25 %	+2.0	-2.0
4	0.5 %	+4.0	-4.0
5	0.75 %	+6.0	-6.0
6	1.00 %	+8.0	-8.0
7	1.25 %	+10	-10

3.2.5 Experimental Results for the Reference Wall

The wall was tested under cyclic loading to evaluate the tensile capacity and use it as a reference to observe the increase in the retrofitting specimens. An axial load of 4.0 MPa was applied, corresponding approximately to 50% of the ultimate compressive strength of the prism of the control specimen.

A splitting crack through the blocks from the top middle part of the wall towards the bottom-compressed corner occurred during the third cycle in the positive (push) direction at 82 kN lateral force and 1.63 mm lateral displacement (i.e. crack ‘‘1’’ in Figure 3-12).

A lateral Load of 75 KN and lateral displacement of 1.9 mm , during the third cycle in the negative direction (pull), caused the same crack that was occurred in the positive direction (i.e. crack ‘‘2’’ in Figure 12).

Finally, a diagonal crack through the top corner to bottom-compressed corner took place at 85 kN lateral force and 2.9 mm horizontal displacement (i.e. crack ‘‘3’’ in Figure 3-12).

The ultimate lateral load was at 82 kN in the push direction (corresponding to 1.7 mm lateral displacement) and at 85 kN in the pull direction (corresponding to 2.9 mm lateral displacement).

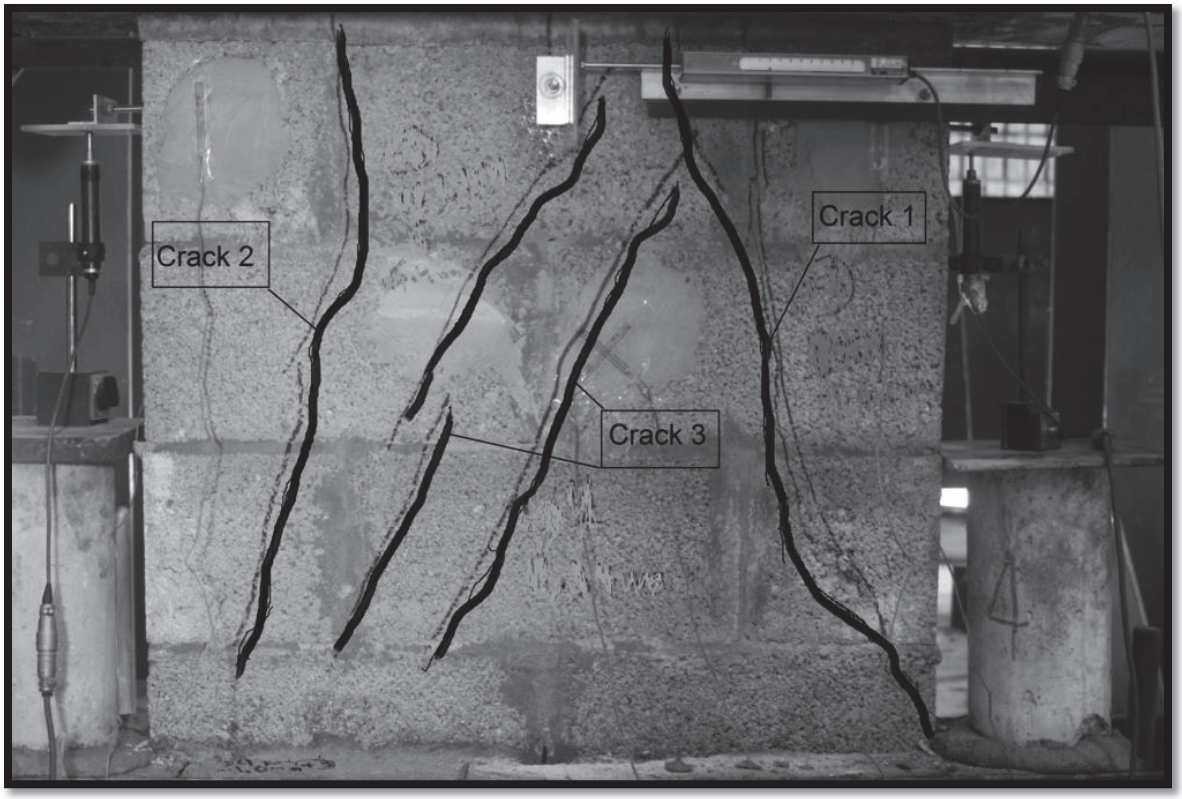

Figure 3-12: Crack pattern in the control specimen

3.2.6 Experimental results for One-side Plastered Wall

An axial load of 4.5 MPa was applied in this test, which is corresponding to 50% of the ultimate compressive strength of the prism. The wall was tested under cyclic load to observe the increase in shear capacity using one side plaster SFRHM of 10 mm.

The first crack occurred at 108 kN lateral force and 1.84 mm horizontal displacement during the fourth cycle in the positive direction (push) and remained constant (i.e. crack 1 in Figure 13). The second crack took place at 112 kN lateral force and 3.2 mm horizontal displacement during the fourth cycle in the negative direction (pull) and remained constant (i.e. crack 2 in Figure 14).

The ultimate lateral load was at 113 kN in the push direction (corresponding to 2.1 mm lateral displacement) and at 112 kN in the pull direction (corresponding to 3.2 mm lateral displacement).

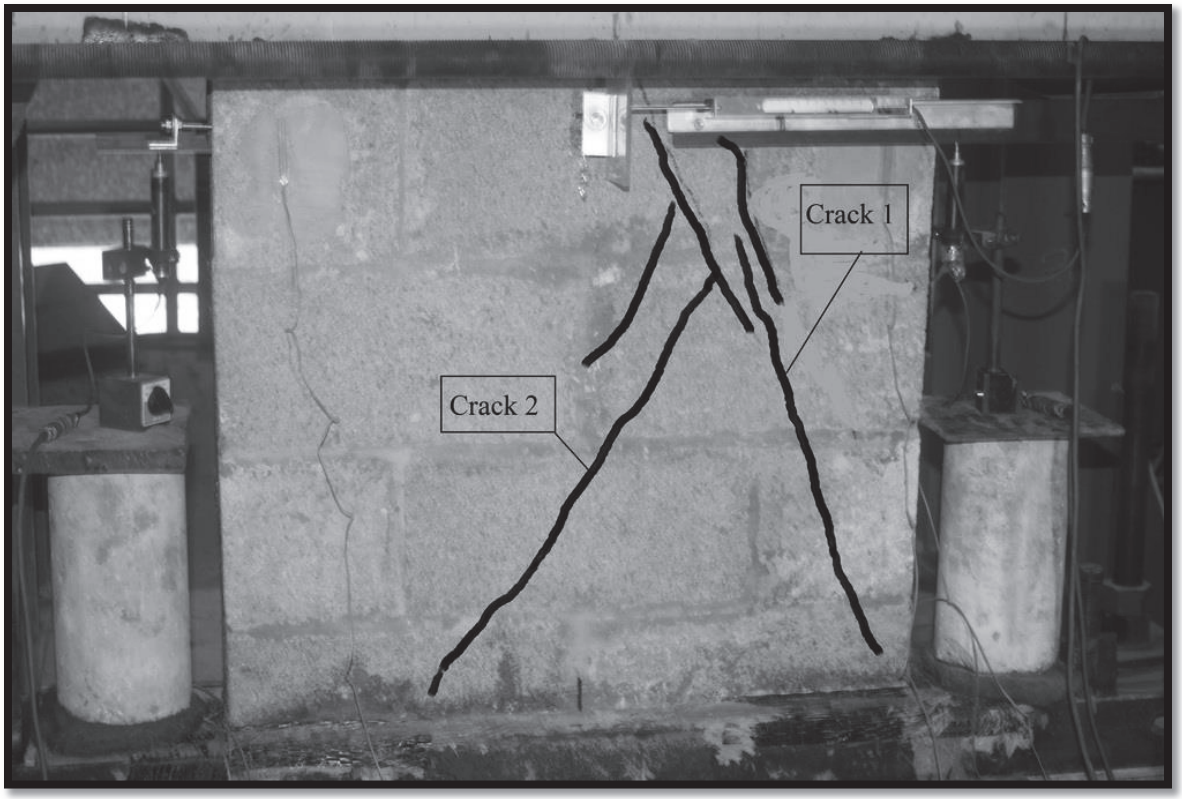

Figure 3-13: Crack pattern in the one-side plastered specimen (front face)

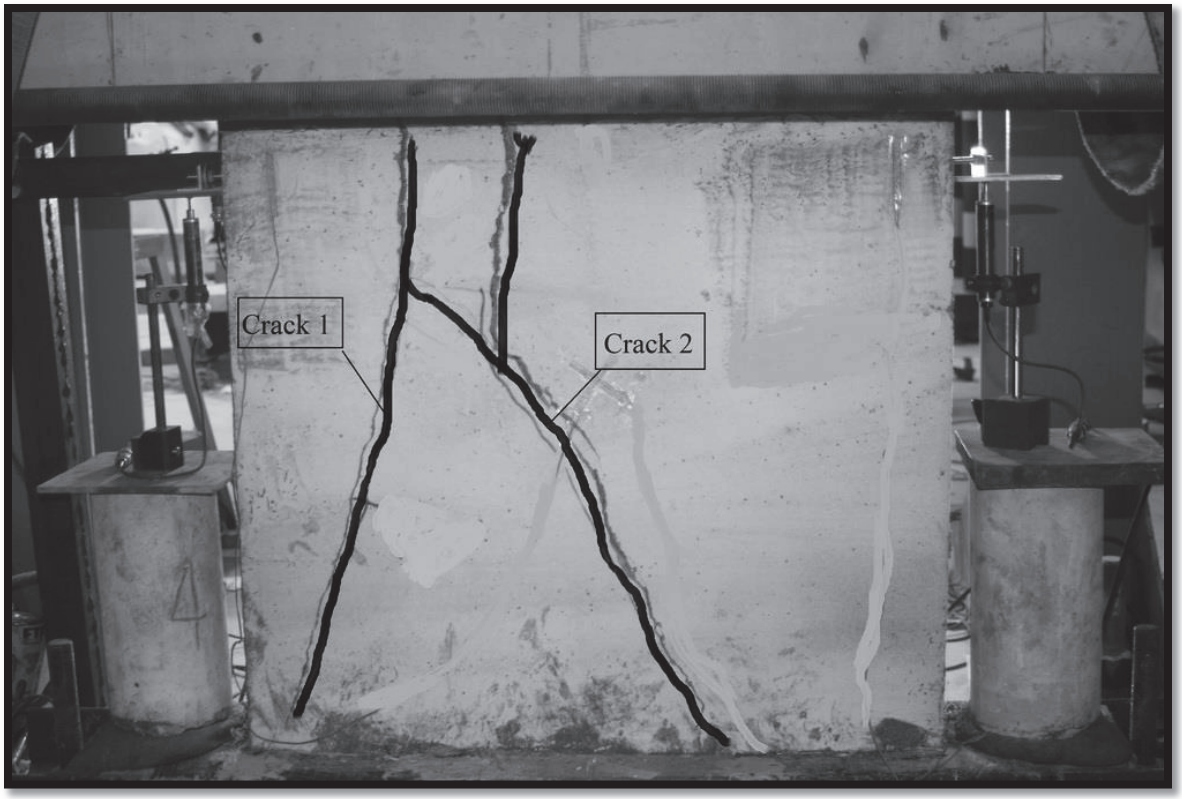

Figure 3-14: Crack pattern in the one-side plastered specimen (back face)

3.2.7 Experimental Results for Two-side Plastered Wall

Like the control specimen and one-side plaster of SFRHM specimen, this wall was also dominated by shear failure. At 150 kN lateral forces during the fourth cycle in the push direction (push), a hair crack through the blocks from the top corner of the wall towards the bottom-compressed corner took place.

In the pull direction, the capacity of the horizontal hydraulic jack ran out, resulting in no cracks and reached maximum of 140 kN lateral forces (corresponding to 2.1 mm lateral displacement).

The relationship between lateral force and lateral displacement was almost linear up to 100 kN horizontal force and then the stiffness began to deteriorate because of the shear mode failure. Figure 3-15 shows the cracks. The ultimate lateral load was 187 kN associated with 3.96 mm lateral displacement. The SFRHM layer on both sides did not prevent the diagonal crack to take place.

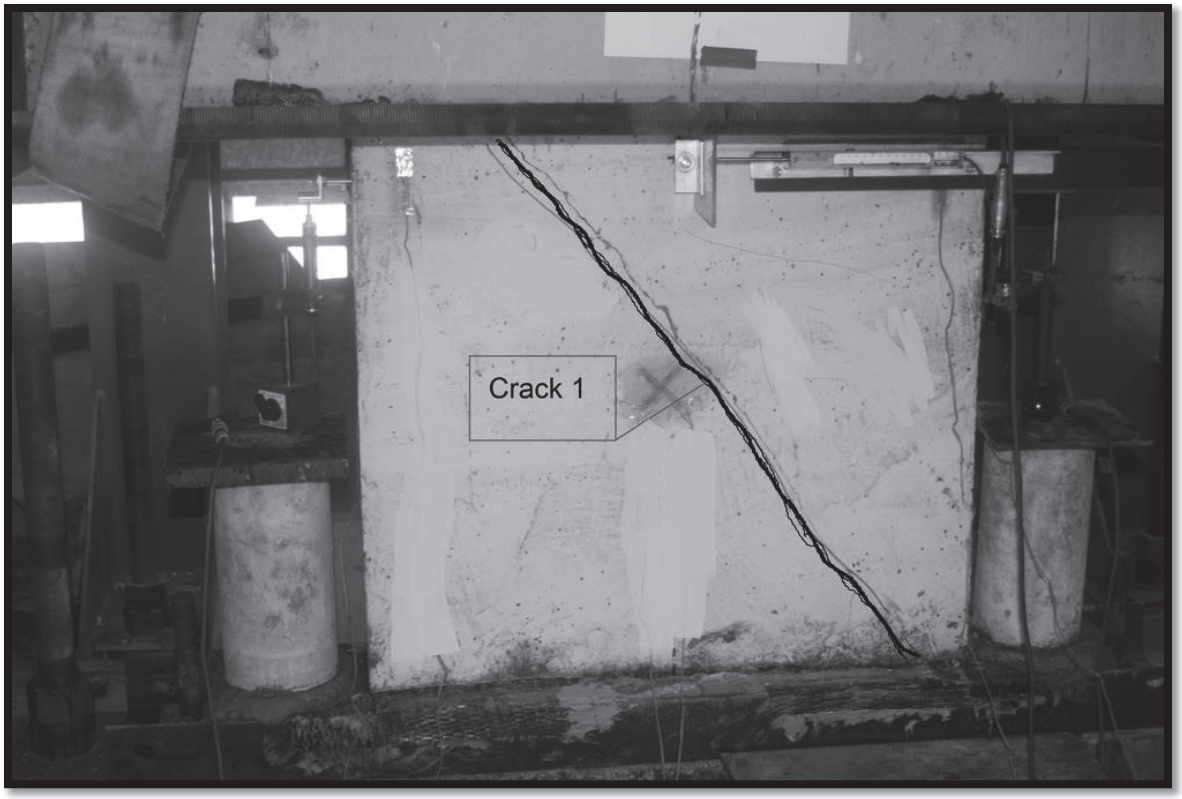

Figure 3-15: Crack pattern in the two-side plastered specimen

3.2.8 Discussion of Results from Wall Tests

The hysteretic response of all walls in terms of lateral load vs. lateral displacement is shown in Figures 3-16 to 3-18. The relationship between the lateral load and the lateral displacement is almost linear for all walls and the linearity started to change after the walls began to crack and fail, as in Figures 3-16 to 3-18.

The first specimen showed brittle behavior because it failed immediately after reaching its full capacity without showing any sign of non-linear behavior (see Figure 3-16), while the second and third specimens showed non-linear behavior once they reached their full capacity (Figures 3-17 to 3-18).

The envelope curve for every wall, which defines the extreme values of lateral capacity, is shown in Figure 3-19. It was plotted to get better understanding for behavior of retrofitted walls. As shows in Figure 3-19, compared with the reference wall, the two-side plastered wall significantly increased the shear capacity by 133 %, while the one-side plastered wall increased the shear capacity by 40%.

One of the things that were observed about using high strength mortar is the ability to improve the stiffness of the wall. Figure 3-20 illustrates how the stiffness was improved. The initial stiffness was calculated in a range of (0.0-1.0) mm to clearly observe the improvement in the initial stiffness. It's clear that the initial stiffness of the third specimen (two-side plaster) was improved by 50% higher than the reference specimen. The stiffness of the second specimen (one-side plaster) was improved by 25% higher than the reference specimen.

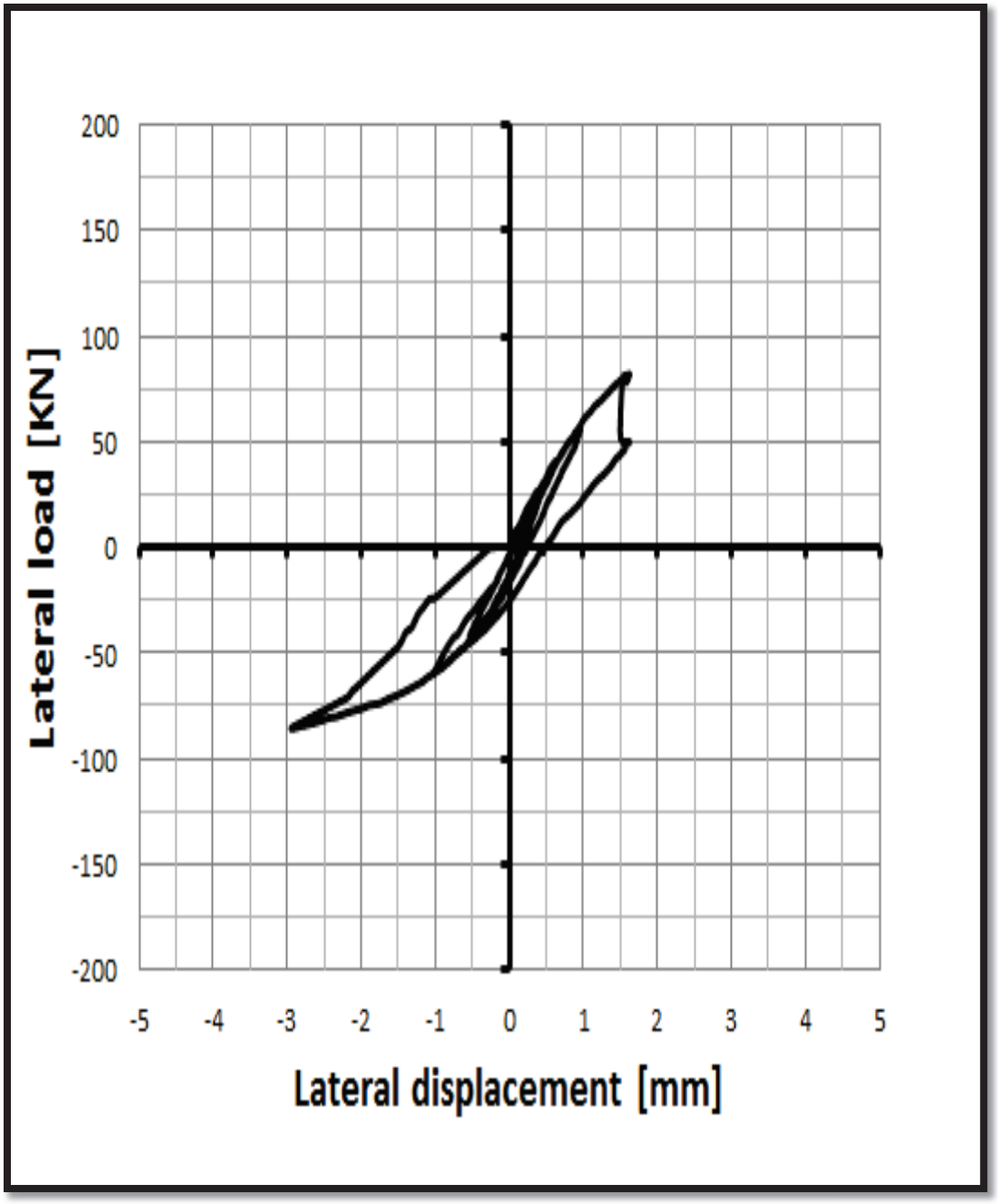

Figure 3-16: Hysteretic response of the reference wall

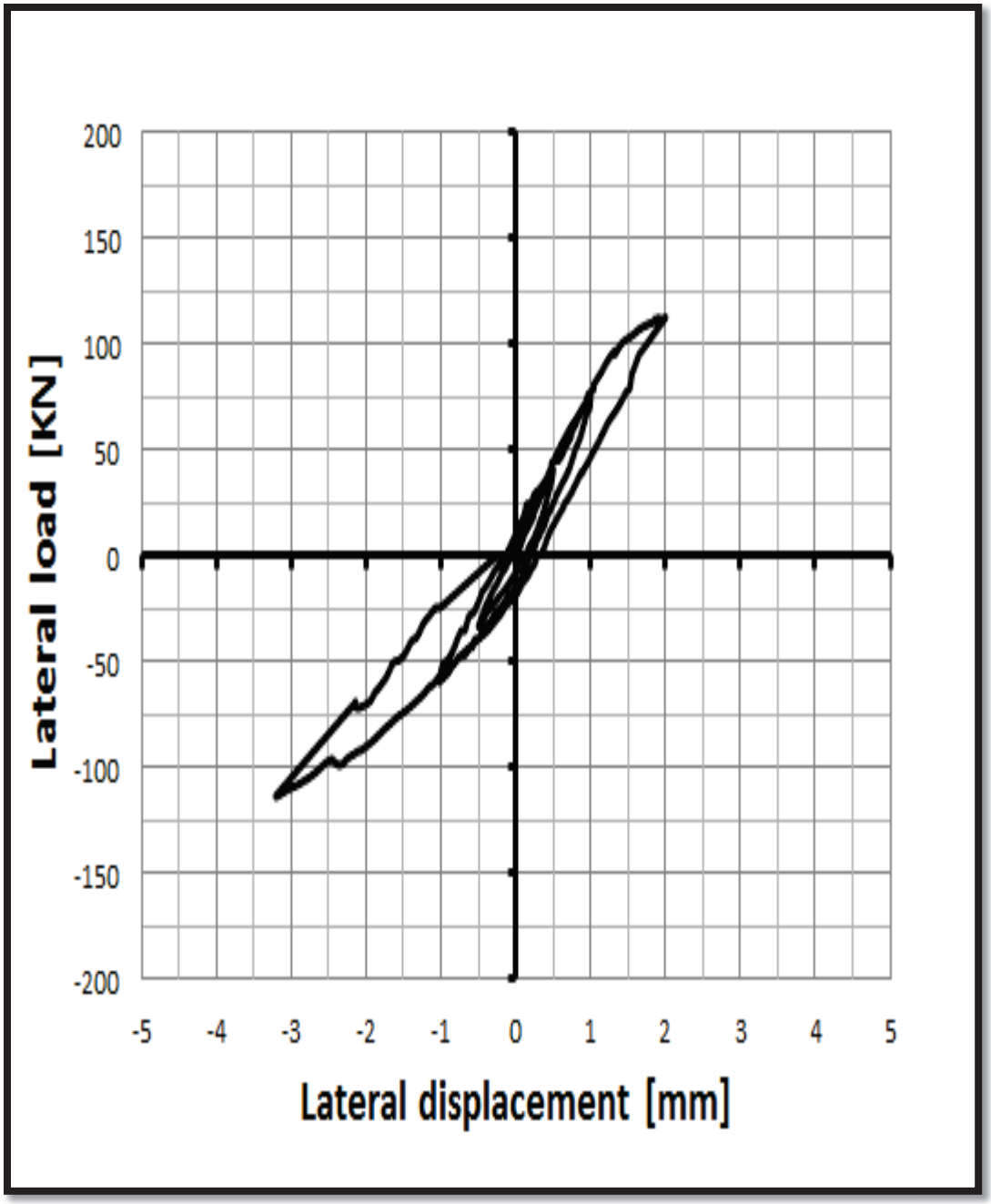

Figure 3-17: Hysteretic response of the one-side plastered wall

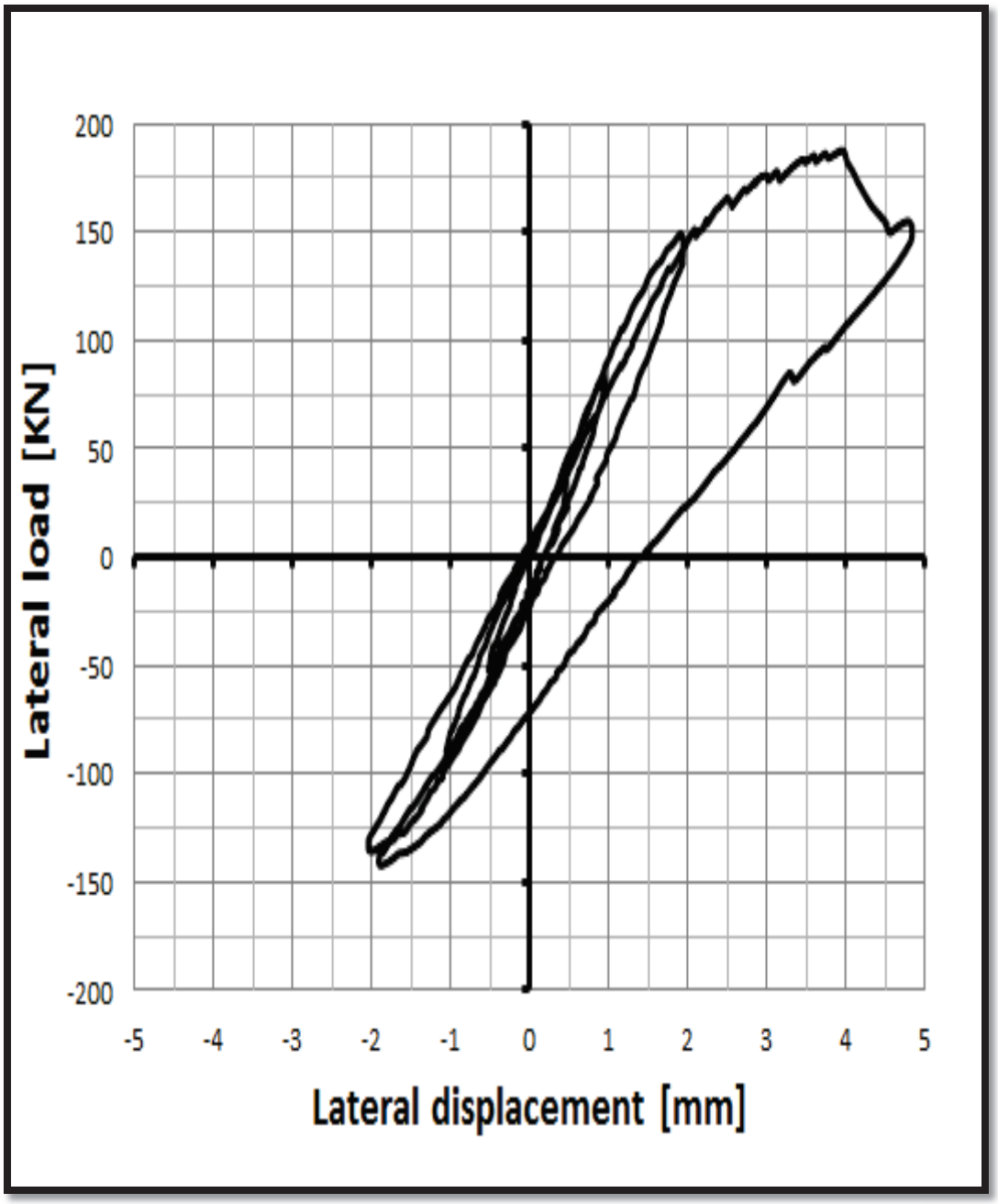

Figure 3-18: Hysteretic response of the two-side plastered wall

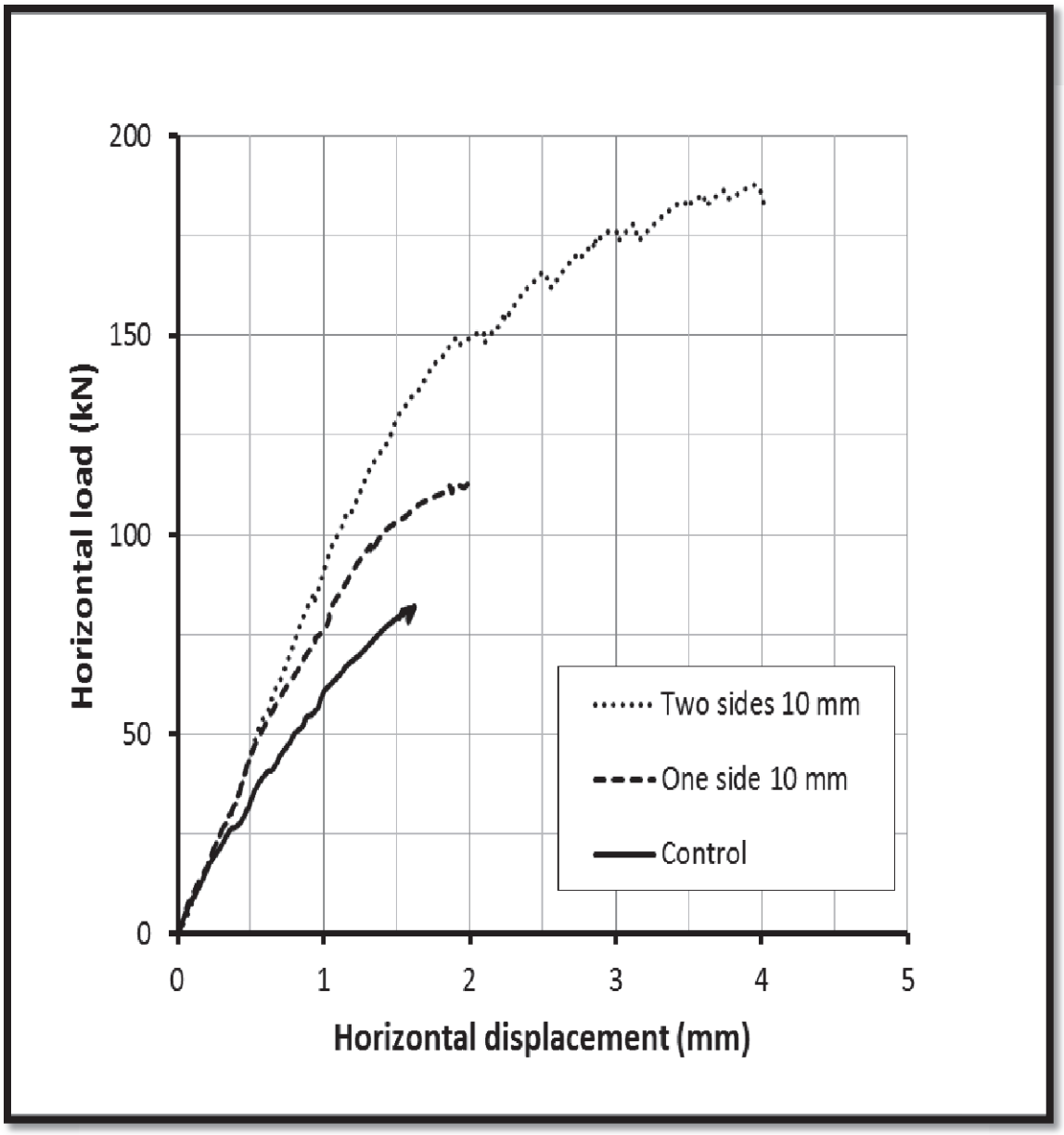

Figure 3-19: Envelope diagram for all walls

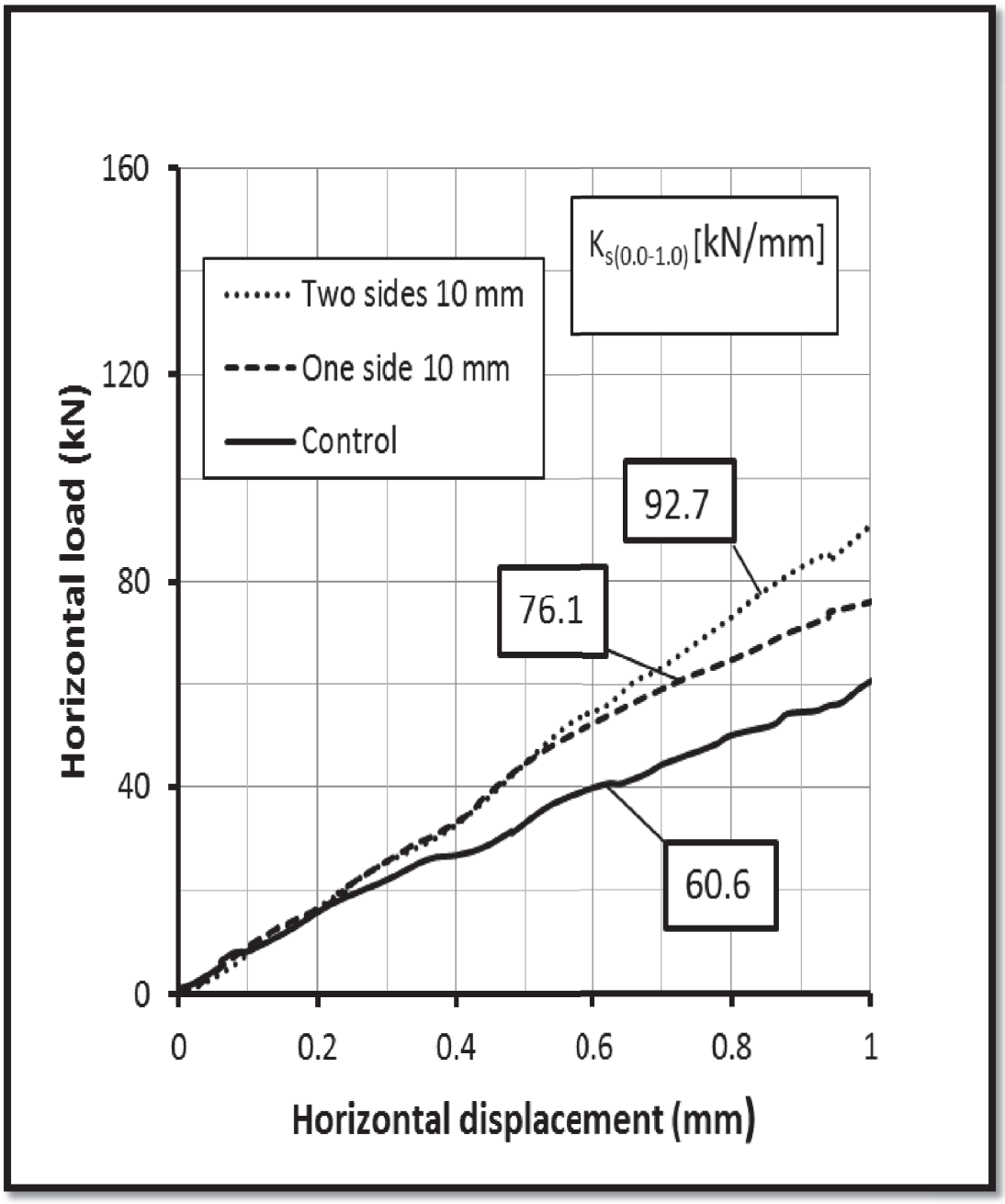

Figure 3-20: Initial stiffness for all walls

3.3 Tests on Materials Properties for Numerical Simulation

In order to carry out numerical simulation using concrete damaged plasticity model, which is incorporated in ABAQUS, stress–strain behavior of concrete block, mortar and SFRHM plaster need to be employed as well as damage factor (the damage factor aims to quantitatively represent the accrual of mechanical deterioration of a material component subjected to certain loading) and contact element (the contact element is the process of identifying the areas on the surfaces that are in contact).

Stress–strain behavior of concrete block, mortar and SFRHM plaster can be found by conducting the following tests:

- Uniaxial Compression and Tension Tests of SFRHM
- Uniaxial Compression and Tension Tests of Ordinary Mortar
- Uniaxial Compression and Tension Tests of Concrete Masonry Block

A flow chart is drawn to explain the detailed tests that were carried out to be employed in the ABAQUS.

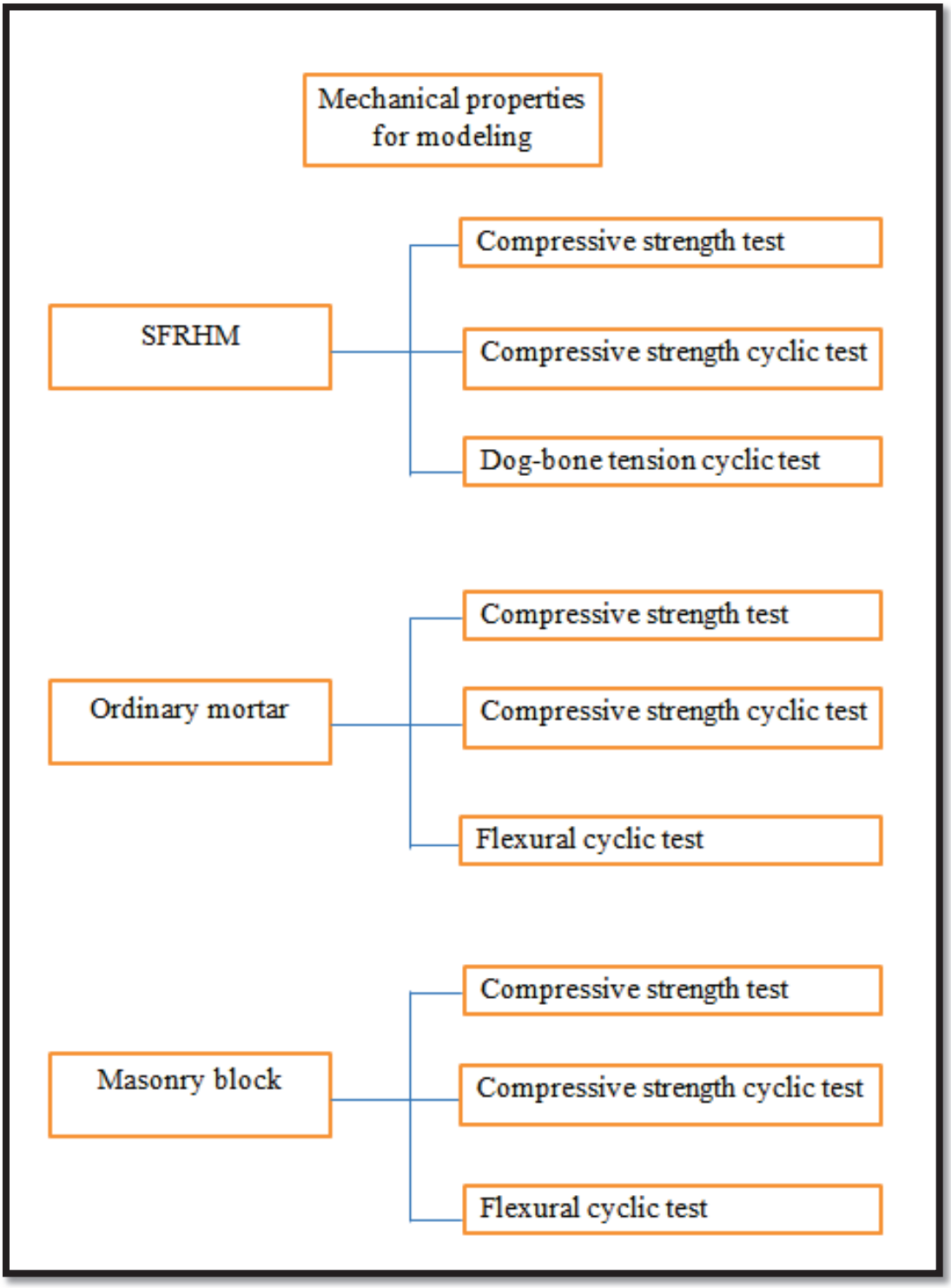

Figure 3-21: Flow chart for simulation properties

3.3.1 Compressive Strength Test of SFRHM

Cubes (50×50×50 mm) and cylinders (diameter 75 mm, height 150 mm) were tested for determining the ultimate capacity of the SFRHM mix according to ASTM C 39 and C 109. The test results are given below in Table 3-6 and Table 3-7.

Table 3-6: Compressive strength test of SFRHM (cylinder)

Specimen	Ultimate Load (kN)	Ultimate Stress (MPa)	Average Ultimate Stress (MPa)
1	112.75	45.1	42.1
2	99.00	39.6	
3	103.75	41.5	

Table 3-7: Compressive strength test of SFRHM (cube)

Specimen	Ultimate Load (kN)	Ultimate Stress (MPa)	Average Ultimate Stress (MPa)
1	233.65	52.9	52.8
2	221.29	50.1	
3	244.26	55.3	

3.3.2 Compressive Strength Test of SFRHM

According to ASTM C 109, a cylindrical specimen (diameter 75 mm and height 150 mm) of SFRHM was tested under compression. SFRHM cylinder was cast and cured in oven for 48 hours at 90ºC. Two LVDT's were placed in opposite sides of the cylinder for recording the strain development due to compressive stress. The load was applied with the percentage of compressive strength of SFRHM in progressive manner. The experimental setup is shown in Figure 3-22. The stress-strain diagram of SFRHM under compression is shown in Figure 3-23.

Figure 3-22: Loading-unloading test for SFRHM under compression

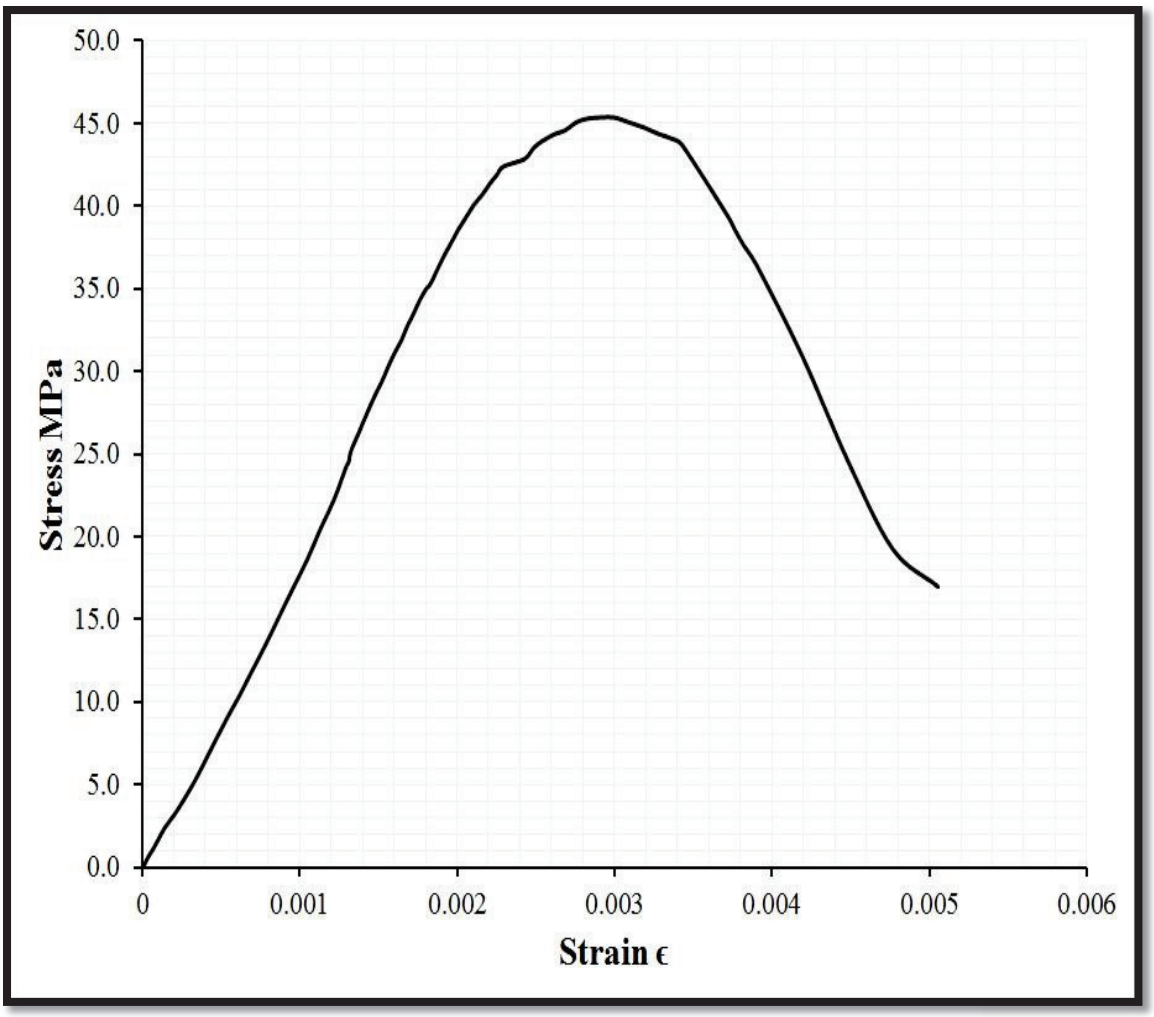

Figure 3-23: Stress-strain diagram of SFRHM under compression

3.3.3 Dog-bone Tension Test of SFRHM

In this test, a specimen was tested under direct tension according to ASTM D 638. The specimen was first cast with SFRHM and cured for 48 hours in oven at 90ºC. This test was executed under direct tension and in cyclic manner to catch the strain-softening (strain-softening is the reduction in stress beyond the peak value with an increase in the deformation). In order to catch the crack and ensure that it will take place in the center of the specimen, the sample was covered with CFRP sheets except for the center part of the sample, where the crack is expected. The experimental setup is shown in Figure 3-24.

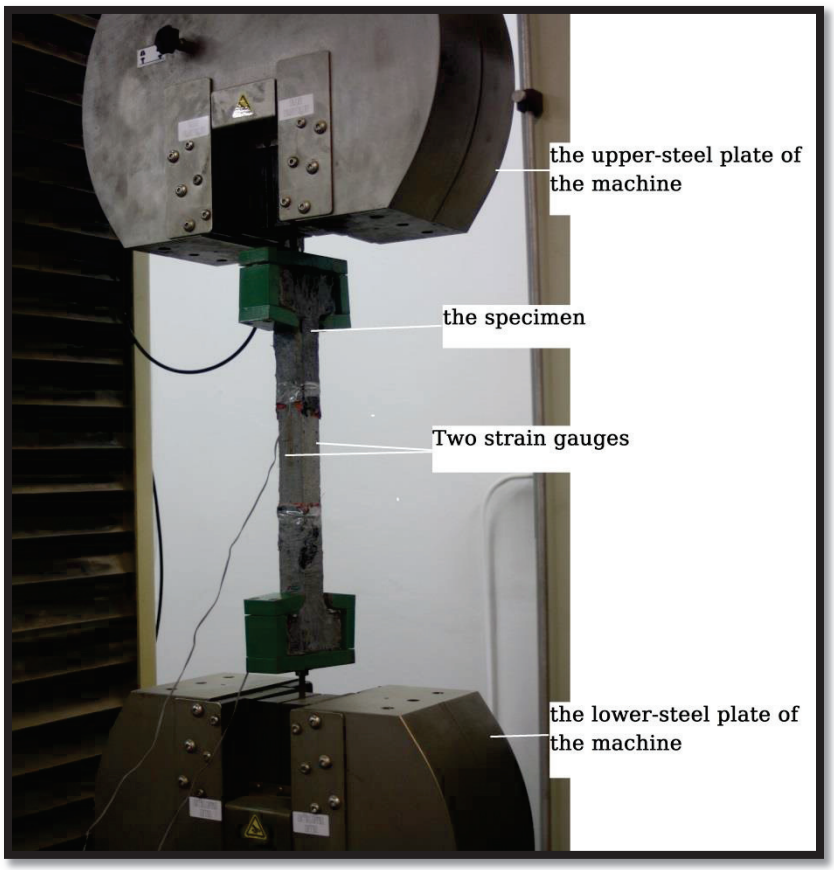

Figure 3-24: Experimental setup for SFRHM under tension

The stress-strain diagram for SFRHM under tension was drawn according to the test result and it is shown in Figure 3-25.

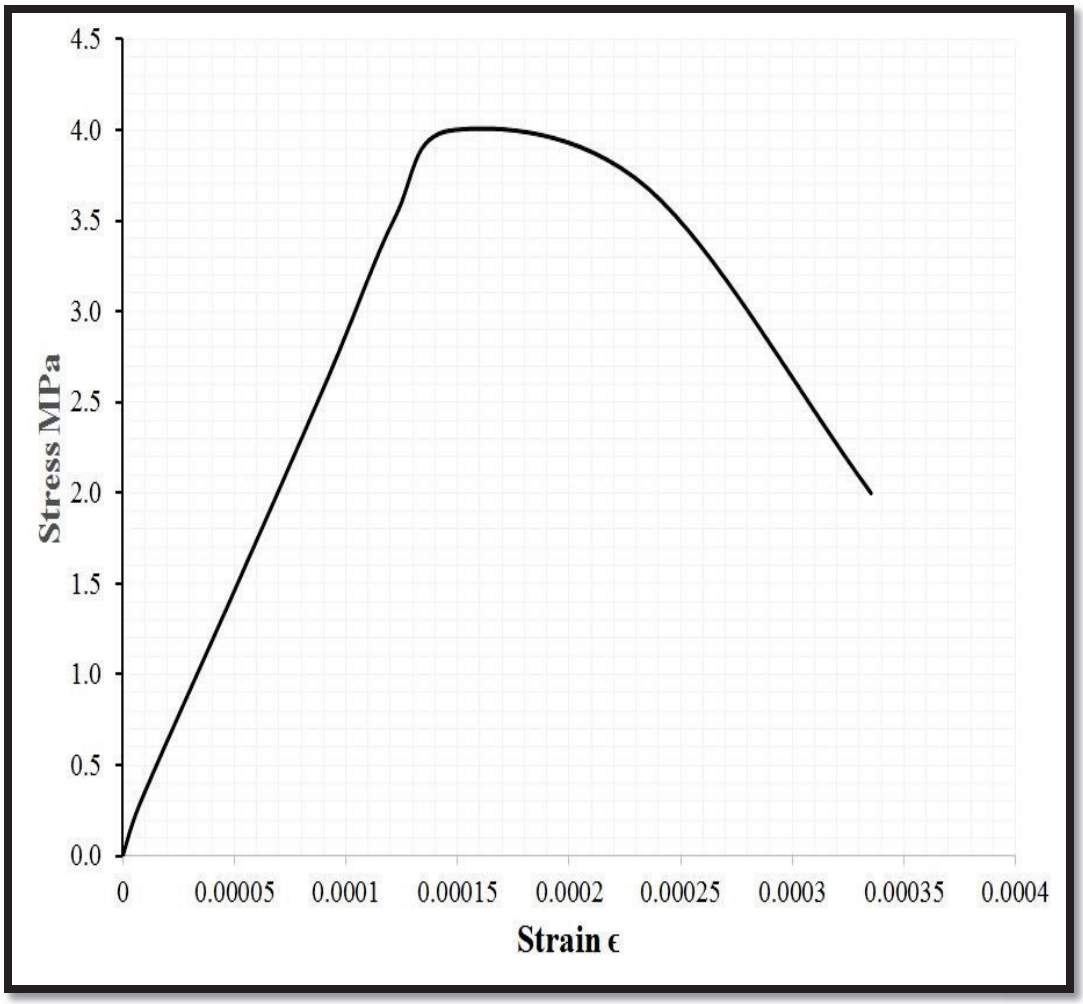

Figure 3-25: The stress-strain diagram for SFRHM under tension

3.3.4 Compressive Strength Test of Mortar

Mortar is one of the constituent that composes the masonry wall. It is well known that mortar affects the behavior of the masonry structures. In this study, Portland cement mortar was used as head and bed joint of the concrete masonry walls. To prepare the mortar, first cement was mixed with sand at a ratio of 1:3 (the most common type). Then, water was added to the dry mix of cement and sand. Water-cement ratio was maintained at 0.56 (practical in the field). After mixing, the mortar was poured into the molds to cast three specimens (50×50×50 mm). The specimens were de-molded and placed in a curing water tank for 28 days.

After curing time has been completed, the cubes were tested, according to ASTM C 39 and ASTM C 109, for finding out the compressive strength of the mortar. The compressive strength was found to be 24.6 MPa. The test results are shown below in Table 3-8.

Table 3-8: Compressive strength test of mortar (cube)

Specimen	Ultimate Load (KN)	Compressive stress (MPa)	Average compressive stress (MPa)
1	57.25	22.9	24.6
2	66.25	26.5	
3	60.75	24.3	

3.3.5 Compressive Strength Test of Mortar

To accomplish the compressive strength test of the mortar in cyclic manner, a cylindrical specimen was used, according to ASTM C 109. The specimen was cast into a plastic mold (diameter 75 mm and height 150 mm) and cured into water tank for 28 days. Then, sulfur capping was used so that the compressive stress could be applied uniformly on the specimen. Two cross strain gages were used to find out strains, developed during the test. The test setup is shown below in Figure 3-26.

During the test, load was applied in a progressive manner with a percentage of the ultimate capacity. The stress-strain diagram was drawn with the data of the test. Figure 3-27 shows the stress-strain relationship diagram.

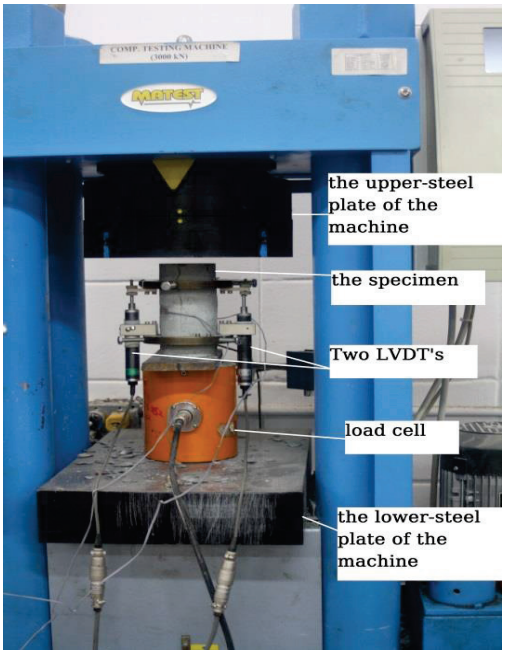

Figure 3-26: Loading-unloading test for mortar under compression

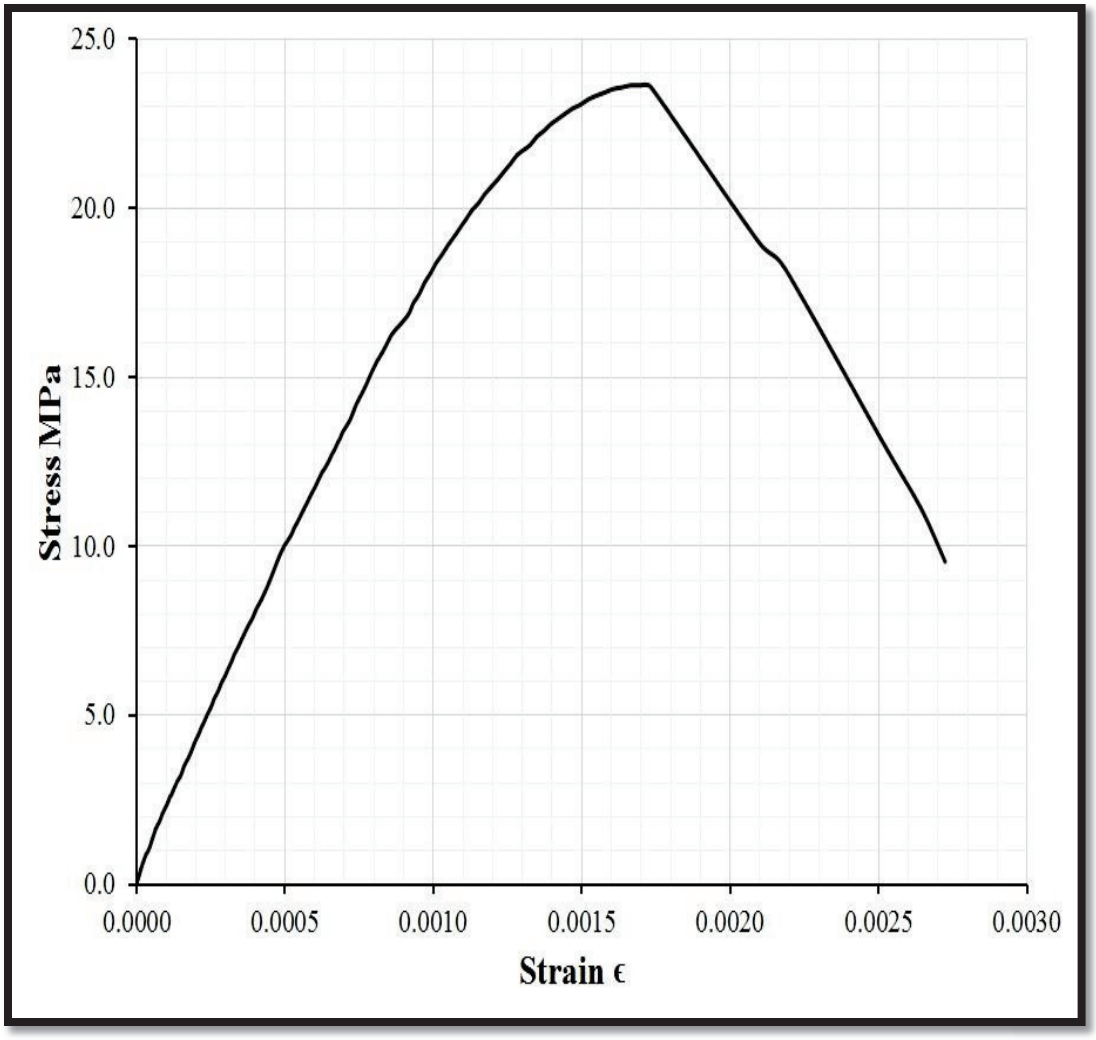

Figure 3-27: The Stress-strain diagram for mortar under compression

3.3.6 Flexural Test of Mortar

A notch beam (750×75×150 mm) was tested under four point loading flexural test. The beam was cast and cured into water tank for 28 days. After curing, a 2.5 cm notch was created in the middle of the beam along the width (75 mm side, as shown in Figure 3-28) for localizing the failure. Four strain gages were placed, two in each sides, in maximum moment region, to store the data of strains. Two metal bars were placed in L/3 distance of the span. Load was applied in cyclic manner to catch the elastic portion, strain hardening portion and softening portion. The test setup is shown in Figure 3-28.

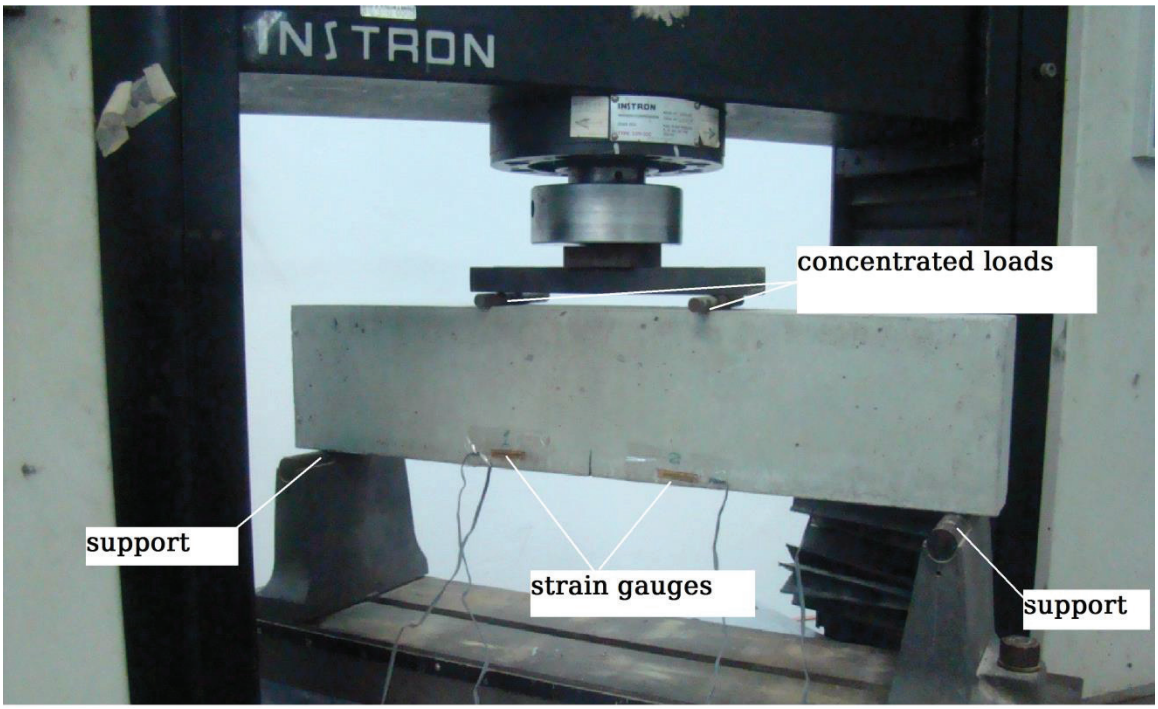

Figure 3-28: Experimental setup for flexural test of mortar

The stress-strain diagram for mortar under tension was drawn according to the test result and it is shown in Figure 3-29.

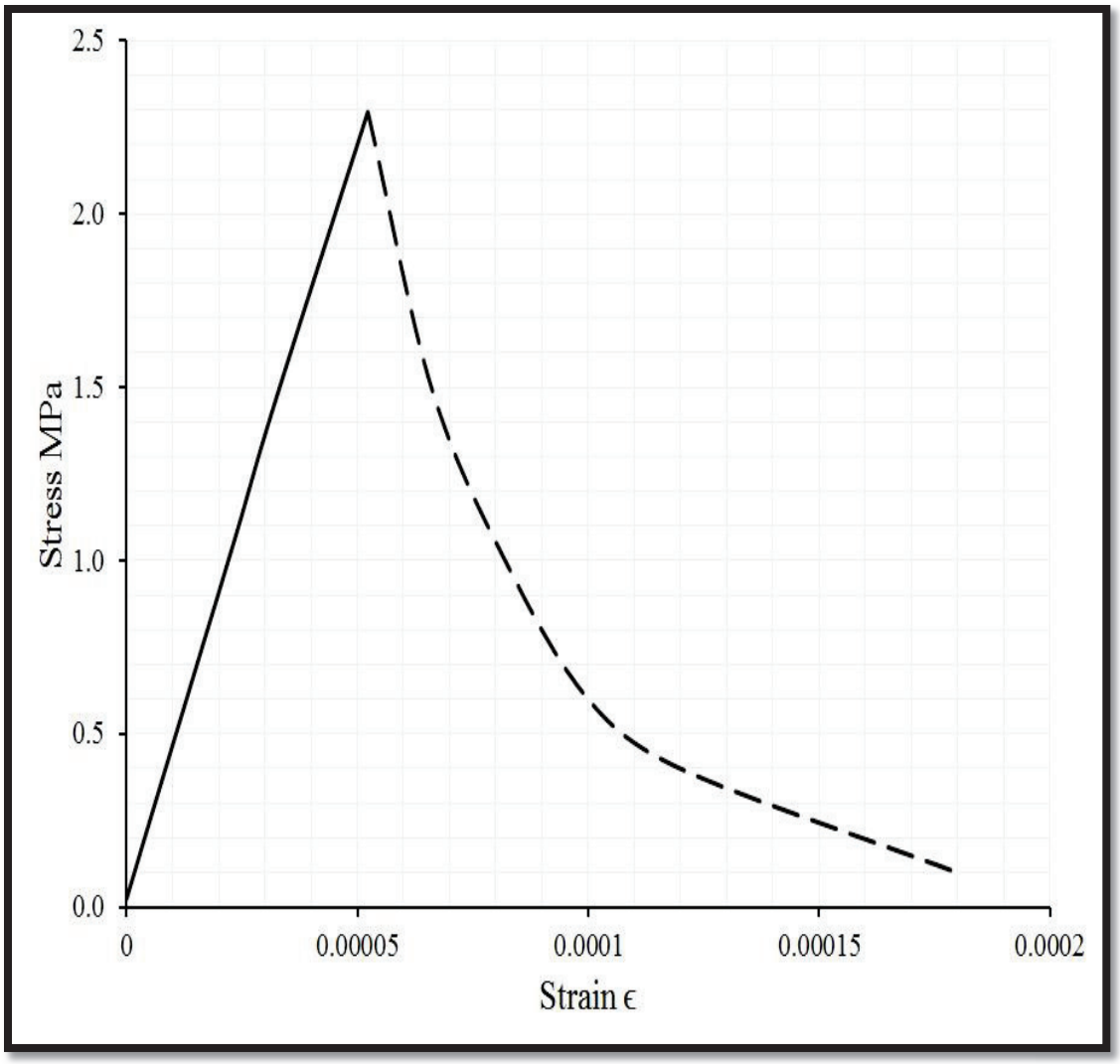

Figure 3-29: The stress-strain diagram for mortar under tension

3.3.7 Compressive Strength Test of Concrete Masonry Block

According to EN 772-1 (European Standard 2000), three blocks was tested under compression. Nominal dimensions of the block are 400×200×100 mm (L×H×W). A uniform compressive pressure was applied on the top surface of the block according to EN 772-1 (European Standard 2000).

In this type of test, the target was to find out the ultimate capacity of the block under compression. The average compressive strength was found to be 21.1 MPa. The result is shown in Table 3-9.

Table 3-9: Compressive Strength Test Result of Concrete Masonry Block

Specimen	Capacity (KN)	Capacity (MPa)	Average Compressive Strength (MPa)
1	530.7	19.12	21.1
2	543.7	19.59	
3	693.3	24.98	

3.3.8 Compressive Strength Test of Concrete Masonry Block

In this test, a uniform compressive force was applied to the concrete masonry block, in a cyclic manner (with percentage of ultimate capacity).

The surface of the block was not smooth for placing strain gage. Therefore, epoxy was used to make the surface smooth before placing the strain gages. Two cross strain gages were used in each face of the concrete masonry block. The experimental setup is shown in Figure 3-30.

After that, compressive pressure was applied in cyclic manner to catch the strain-hardening (strain-hardening is the increase in stress beyond the peak value with an increase in the deformation) and strain-softening (strain-softening is the reduction in stress beyond the peak value with an increase in the deformation).

The stress-strain diagram for concrete masonry block under compression was drawn according to test result and it is shown in Fig 3-31.

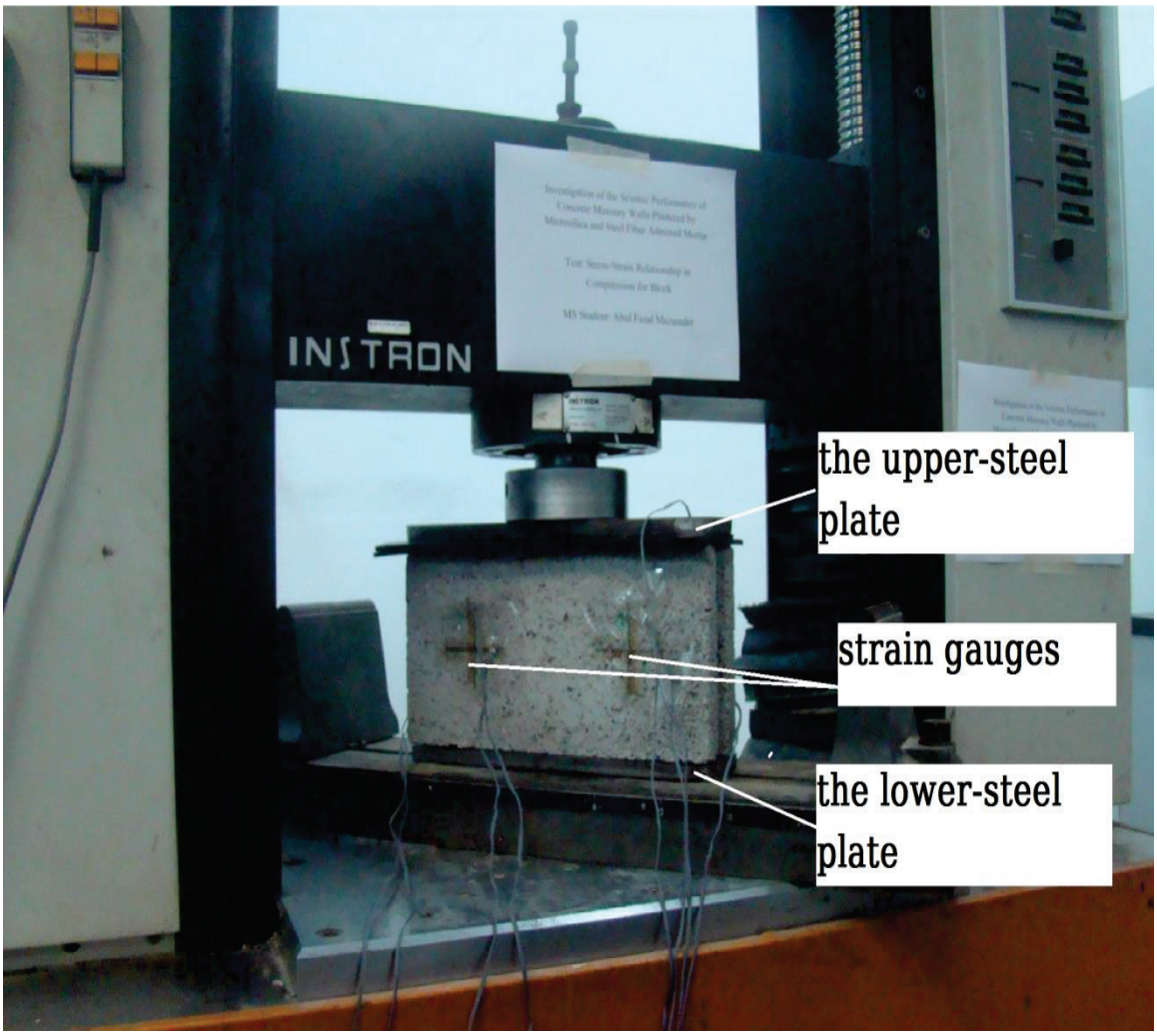

Figure 3-30: Loading-unloading test for concrete masonry block under compression

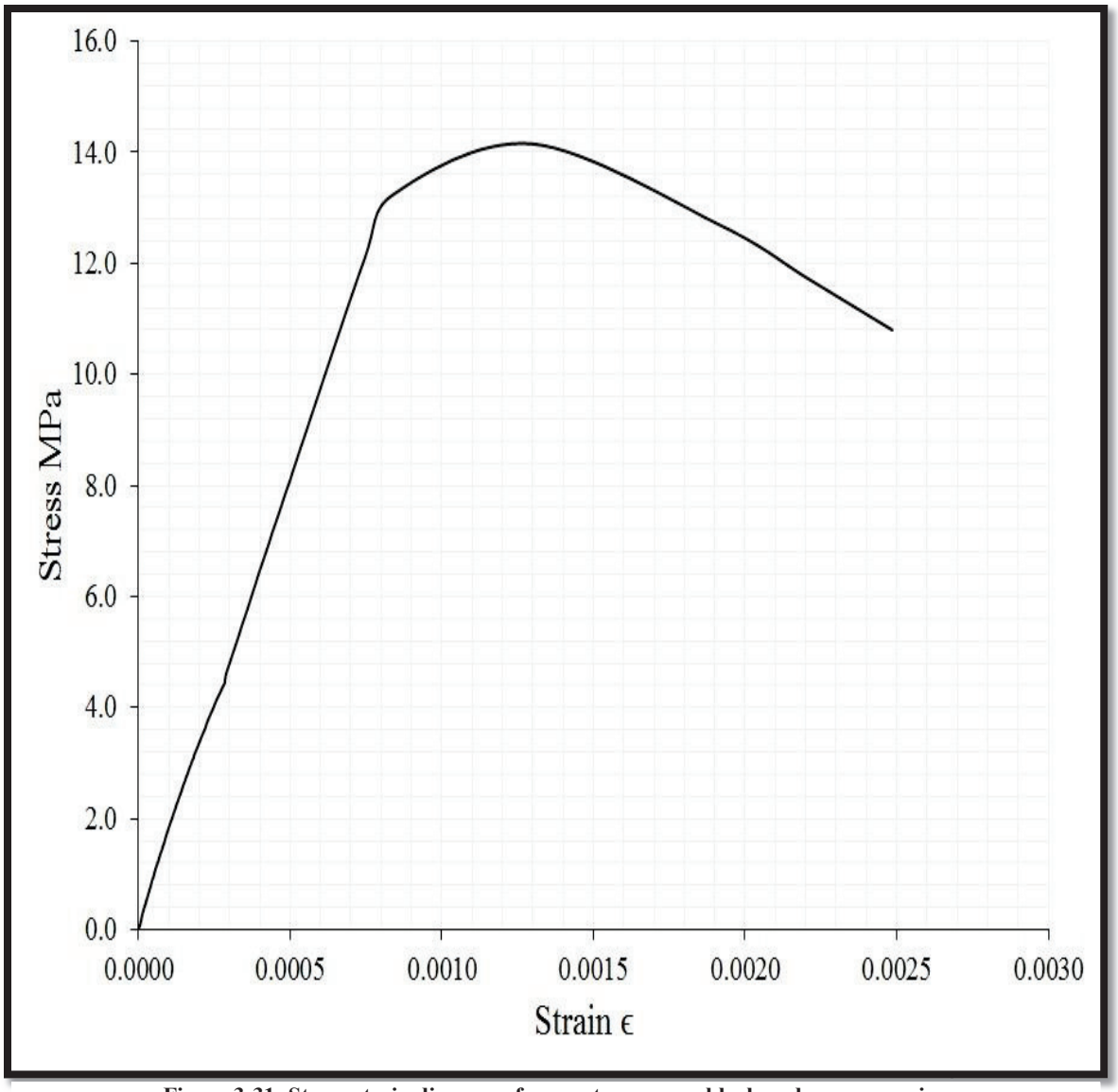

Figure 3-31: Stress-strain diagram of concrete masonry block under compression

3.3.9 Flexural Test of Concrete Masonry Block

This test was conducted under flexural load in cyclic manner. Four point bending test was conducted to find out the tension behavior of concrete masonry block. In this test, support was placed at a distance of 3 cm from each edge and two metal bars were placed on the top of the block at a distance of 8 cm from support so that the maximum moment region was 20 cm long. Failure was expected.

In the maximum moment region, the load was applied in a cyclic manner and in some percentage of the ultimate capacity. To record the strains, four strain gages were placed; in each face two gages were placed. The experimental setup is shown below in Figure 3-32.

The stress-strain diagram for concrete masonry block under compression was drawn according to the test result. The stress-strain diagram is shown in Fig 3-33.

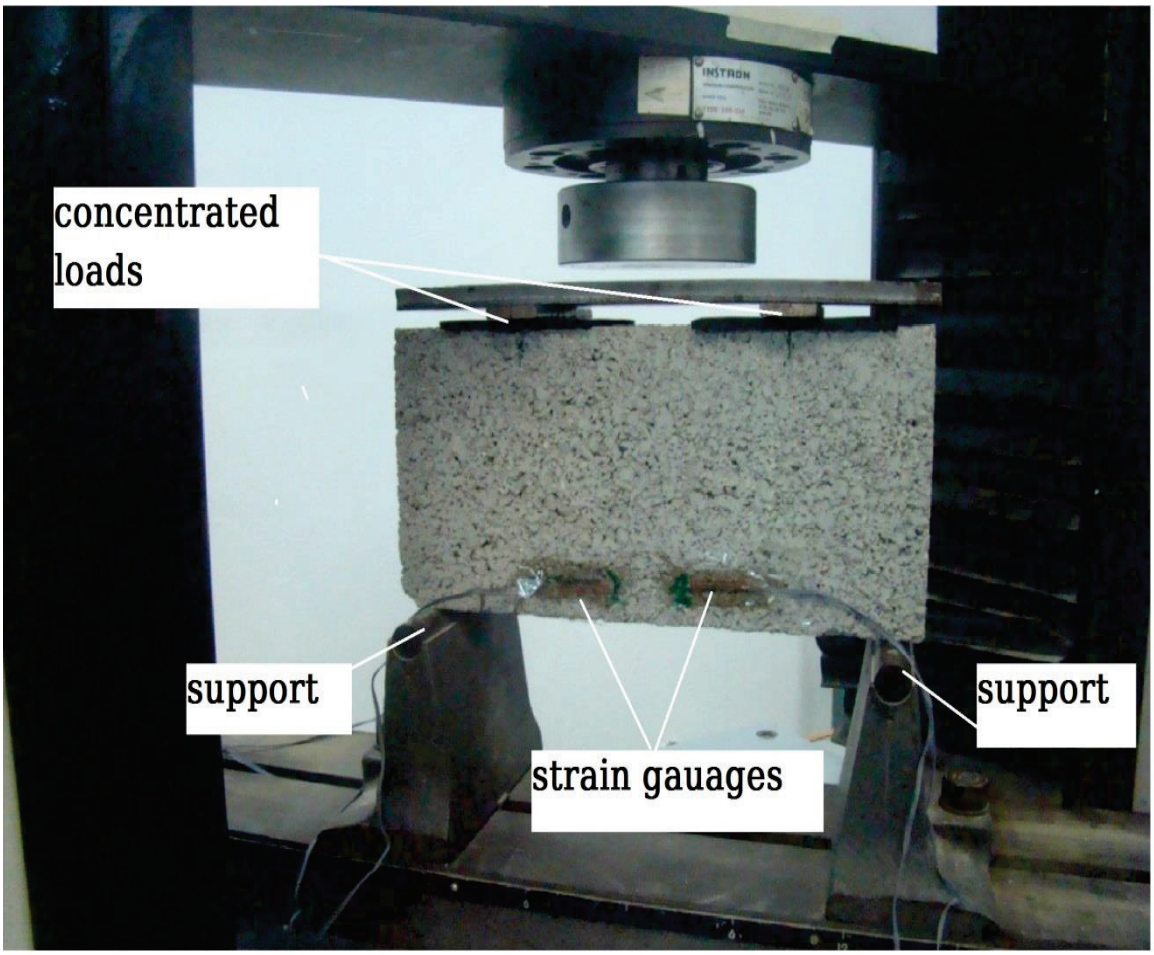

Figure 3-32: Loading-unloading test for concrete masonry block under tension

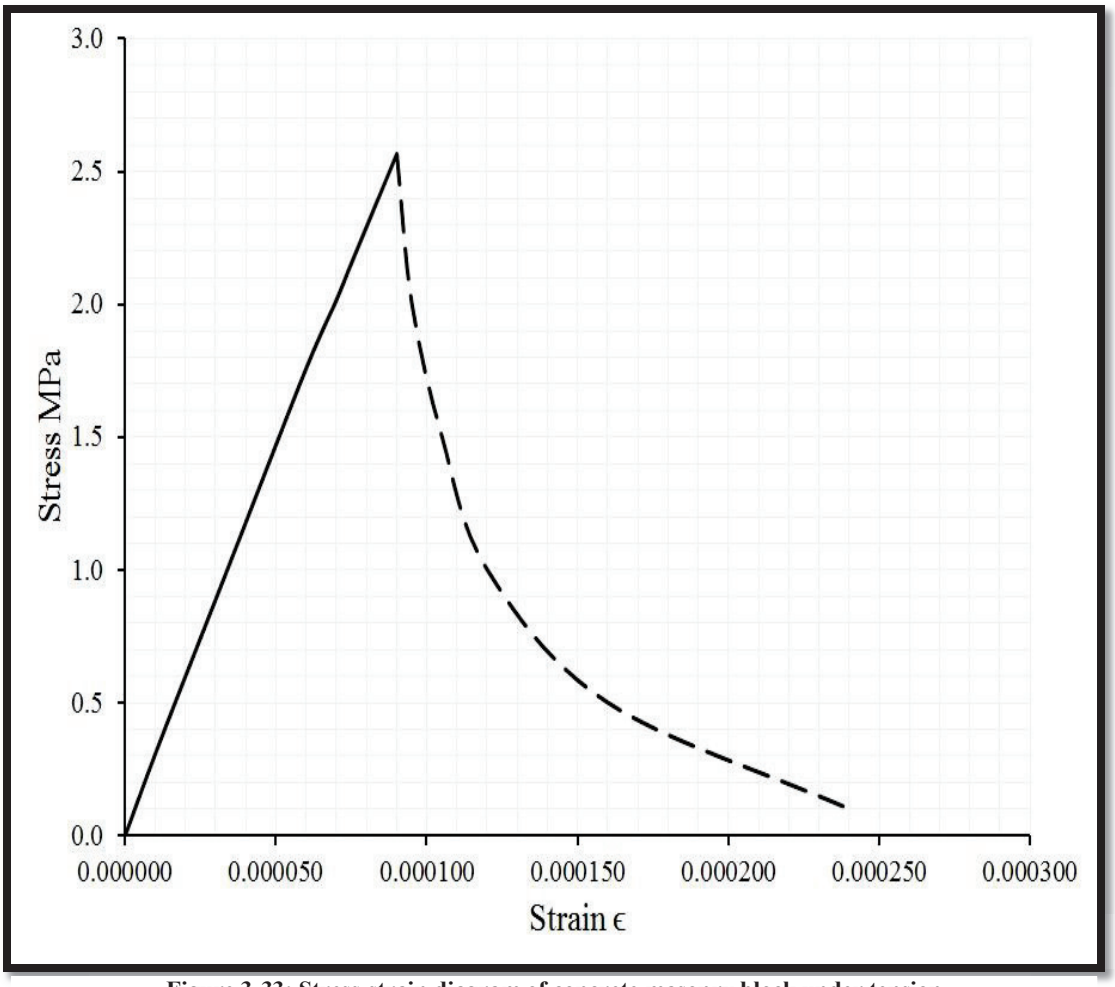

Figure 3-33: Stress-strain diagram of concrete masonry block under tension

CHAPTER 4

Analytical Investigation

4.1 Introduction

Masonry walls subjected to in-plane loading exhibit different mechanistic response based on the intensity of axial loading applied and wall aspect ratio [33]. Also, failure patterns and load deformation response of the walls are also highly influenced by the axial pre-compression and material properties.

According to Magenes and Calvi (1997), the different modes of failure (as a function of axial load) include; (i) sliding, (ii) rocking, (iii) staggered head/bed joint failure, (iv) cracks through wall blocks, and (v) crushing of wall blocks or bricks.

As reported in ACI guidelines (ACI 50 Committee 440), Li et al (2005) proposed that, the shear strength of the reinforced wall can be expressed as:

$$V = V_m + V_r \qquad (1)$$

where V_m and V_r are the shear resistance of the masonry and the contribution of any provided reinforcement to the shear strength of the wall, respectively.

Several attempts have been conducted toward understanding and predicting the behavior of masonry walls using mechanistic framework of analysis [33]. Each failure mode is characterized by different failure pattern, sequences, and gives different levels of lateral resistance. These modes of failures can be summarized as follows:

4.1.1 Sliding Failure

For walls subject to low levels of axial compression loading and/or having a low friction coefficient (μ) due to poor mortar, horizontal cracks in bed joints may form a sliding plane extending along the bed joints through the length of the wall. This results in the upper part of the wall sliding relative to the lower part (Figure 4-1).

For in-plane loading of URM, failure is usually due to debonding at the mortar-block interface and shear sliding along the bed joints with cracks developing in a stepped manner. Using a Mohr-Coulomb failure criterion, the shear strength can be modeled as

$$\tau = \tau_0 + \mu\sigma_n \qquad (2)$$

where τ is the shear bond strength, μ is the coefficient of internal friction, and σ_n is the normal compressive stress on the wall. Paulay and Priestley (1992) recommend approximating the cohesion τ_0 by 3% of the masonry gross area compressive strength (f_m) and internal friction (μ) in the range of 0.3 to 1.2. With the walls tested by Li et al (2005) being subjected to diagonal compression, the shear capacity for sliding shear along the wall bed joints can be shown to be:

$$V_{m,1} = A_n * \tau = A_n(\tau_0 + \mu\sigma_n) \qquad (3)$$

where:
$V_{m,1}$ is the sliding shear area, kN.
τ_0 is the shear bond strength, MPa.
μ is the coefficient of internal friction.
σ_n is the normal stress, Mpa.

The lateral resistance of the wall ($V_{m,1}$) is generally low in this mode of failure.

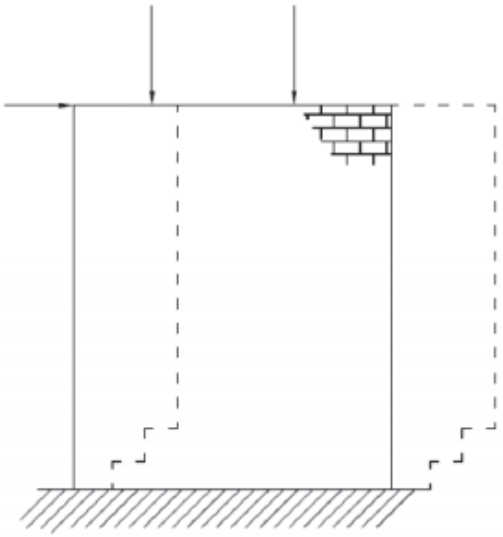

Figure 4-1: Sliding failure mode

Crisafulli et al. (1995) have suggested a more realistic distribution of normal and shear stresses acting on a block. Assuming that the variation of the normal stresses is linear with a zero value at the center of the block and maximum at the edges and that failure occurs in the joints for low levels of axial stress, it results that

$$V_{m,1} = A_n * \tau = A_n(\tau_0{}^* + \mu^* \sigma_n) \qquad (4)$$

Where:

$$\tau_0{}^* = \frac{\tau_0}{1+1.5\,\mu\frac{b}{d}} \quad (5)$$

$$\mu^* = \frac{\mu}{1+1.5\,\mu\,b/d} \quad (6)$$

where: b is the block length and d is the block depth.

4.1.2 Rocking and Toe Crushing Failure

According to Magenes and Calvi (1997), walls with a higher axial loading and stronger mortar type may be set into a rocking motion. Due to the mechanism of this type of response, toe of the wall is generally subjected to high compression force because the entire force is transferred to the base through the toe contact area. This generally results into a local crushing at the toe of the wall, followed by general collapse of the wall (Figure 4-2).

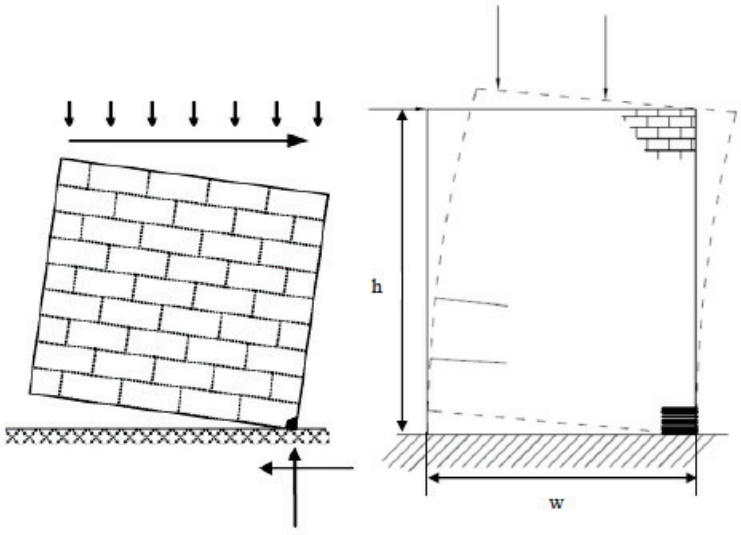

Figure 4-2: Rocking and toe crushing failure mode

4.1.3 Staggered Head/Bed Joint Failure

According to Magenes and Calvi (1997), this mode of failure is generally accompanied with higher axial force on the walls. In this case, the wall is not able to slide along a bed joint nor to rotate due to the high confinement. This results in redistribution of the force within the wall and the energy is dissipated trough staggered cracking of the head and bed joints of the wall. The lateral resistance of the wall in this case is higher than the previous modes. This type of failure is very common in dry contact masonry walls or walls with weak mortar relative to bricks (Figure 4-3).

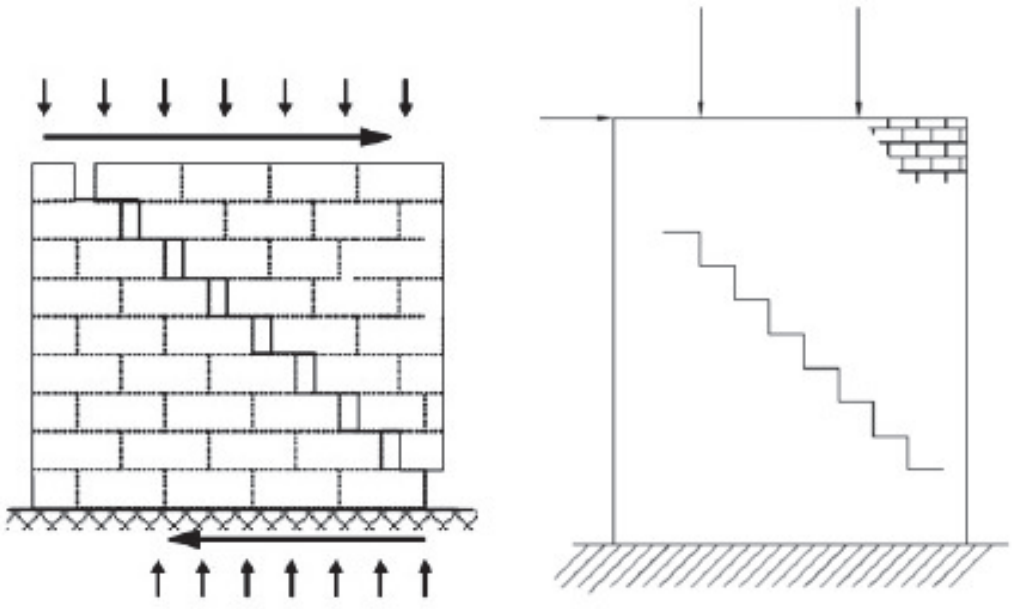

Figure 4-3: Staggered head/bed joint failure mode

4.1.4 Cracks through Wall Blocks

According to Magenes and Calvi (1997), in this failure mode, the degree of confinement is higher than in the previous modes. This prevents the wall from sliding in a staggered pattern. In this failure mode, the combination of axial and lateral forces results in an initiation of the cracks through the wall bricks due to principal diagonal tensile stress exceeding the tensile strength of the brick (Figure 4-4).

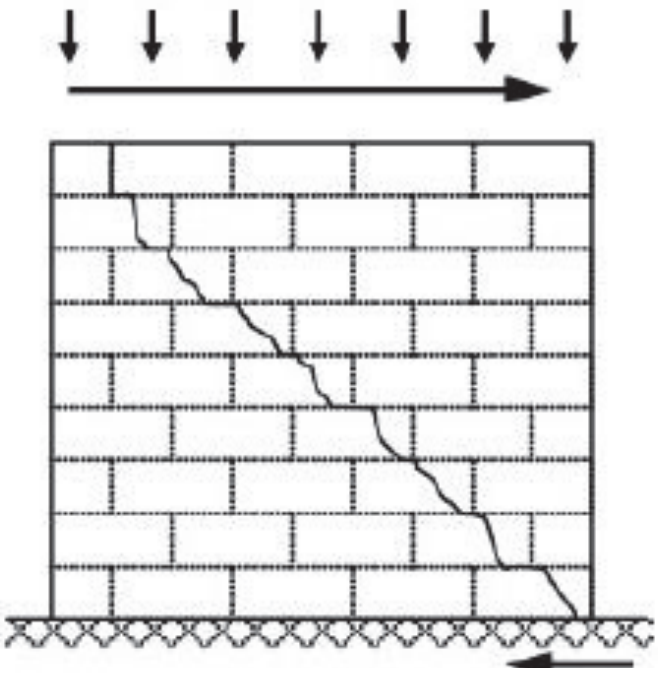

Figure 4-4: Cracks through wall blocks

Assuming that this failure occurs when the maximum tensile stress becomes equal to the tensile strength of the masonry (f_{bt}). According to Li et al. (2005) and Paulay et al. (1992), Shear capacity may be found by the following:

$$V_{m,3} = A_n * \frac{f_{bt}}{2.3} \sqrt{1 + \frac{\sigma_n}{f_{bt}}} \qquad (7)$$

where:

σ_n is the axial pre-compression, MPa.

Generally, the level of axial force is around 40-60% of the wall axial capacity. The lateral resistance of the wall in this case is the highest of all the failure modes.

4.1.5 Crushing of Bricks of the Wall

In this failure mode, the wall is subjected to extremely high axial force. Major damage to the wall results due to the high axial force (before the application of lateral force) in terms of high compression induced cracks in the wall bricks. The level of axial force in this case is generally 70-90 % of the wall axial capacity. In this case, the wall is weak in lateral resistance and the level of lateral resistance is low compared to the case when the axial force is less (Figure 4-5).

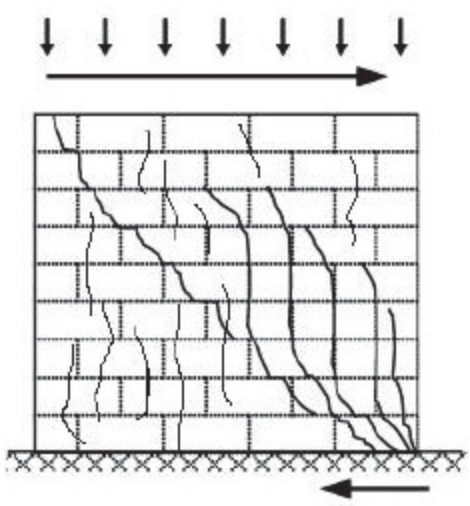

Figure 4-5: Crushing of Wall Blocks or Bricks

For this case, according to Li et al (2005), when the compressive stress approaches the wall axial capacity, the shear force to cause failure may be found by:

$$V_{m,4} = A_n * \frac{2\,d}{3\,b} * (\int_m - \sigma_n) \qquad (8)$$

where:

$\int_m$ is the compressive strength of the masonry wall, MPa.

d is the block length, mm.

b is the block depth, mm.

4.2 Contribution of the Unreinforced Wall

According to the test results (experimental results for the reference wall 3.2.5), the dominant mode of failure was cracking through the blocks. Therefore, the equation of Mann and Muller (1981) would be used to determine the shear capacity of the reference wall. The proposed equation by Mann and Muller mainly depends on the tensile strength of the bricks. The shear capacity of the unreinforced wall is calculated as follows:

$$V_m = d * t * \frac{f_{bt}}{2.3} \sqrt{1 + \frac{\sigma_n}{f_{bt}}} \qquad (9)$$

$$f_{bt} = 0.4 * \sqrt{f_m}$$

where

V_m is the shear capacity, kN.

σ_n is the axial pre-compression, MPa.

d is the width of the wall, mm.

t is effective thickness of the wall, mm.

f_{bt} is the tensile strength of the brick, MPa.

f_m is the compressive strength of the masonry wall, MPa.

4.3 Contribution of the Plastered Wall

The approach of Turnšek (1971) was adopted here. It basically depends on the value of the tensile strength of the plaster instead of the tensile strength of the wall. Until the

failure takes place, the plaster is assumed to be homogenous, elastic, and isotropic. The maximum principal tensile stress, which will be equal to the tensile strength of the plaster, is assumed to be the governing stress that causes the diagonal cracks, and the equation will be:

$$f_{pt} = \sigma_t = \sqrt{\left(\frac{\sigma_0}{2}\right)^2 + (b\,\tau_{max})^2} - \frac{\sigma_0}{2} \qquad (10)$$

where

σ_t is the axial pre-compression, MPa.

σ_0 is the axial pre-compression, MPa.

f_{pt} is the tensile strength of the plaster SFRHM, MPa.

τ_{max} is the average shear stress in the horizontal section of the wall at the maximum horizontal load, MPa.

Following this approach, the shear resistance (V_m) of reinforced masonry wall can be evaluated using

$$V_p = d_p * t_p * f_{pt}\sqrt{1 + \frac{\sigma_n}{f_{pt}}} \qquad (12)$$

where

V_p is the shear capacity of plaster, kN.

σ_{np} is the axial pre-compression on the plaster, MPa.

d_p is the width of the plaster, mm.

t_p is effective thickness of the plaster, mm.

f_{pt} is the tensile strength of the plaster, MPa.

4.4 Shear Capacity of the Reference Wall

Since the reference wall has no strengthening material, equation (9) which is associated with the contribution of the unreinforced wall was used to estimate the value of the shear capacity for the control wall. Table 4-1 shows the numerical values that are associated with the reference wall.

Table 4-1: The numerical values associated with the control wall

The name of the parameter	value
Brick tensile strength (experimental property)	f_{bt}=1.5 MPa
width of the wall (geometric property)	d =810 mm
Effective thickness of the wall (geometric property)	t =72 mm
The axial pre-compression on wall (experimental property)	σ_n =4 MPa

According to equation (9), the shear capacity of the reference wall is calculated as follows:

$$V_m = 810 * 72 * \frac{1.5}{2.3} \sqrt{1 + \frac{4}{1.5}} = 73\ KN$$

4.5 Shear Capacity of the One-side Plastered Wall

Since the one-side plastered wall has strengthening material, equation (9) (which is associated with the contribution of the unreinforced wall) plus equation (12) (which is associated with the contribution of the plastered wall) were used to estimate the value of the shear capacity for the one-side plastered wall. Table 4-2 shows the numerical values that are associated with the one-side plastered wall. The final equation will be as follows:

$$V = V_m + V_p = d * t \ * \ \frac{f_{bt}}{2.3} \sqrt{1 + \frac{\sigma_n}{f_{bt}}} + \ d_p * t_p * \ f_{pt} \sqrt{1 + \frac{\sigma_{np}}{f_{pt}}} \quad (13)$$

where

V is the total shear capacity, kN.

V_m is the shear capacity of unreinforced wall, kN

V_p is the shear capacity of plaster, kN

σ_n is the axial pre-compression on the wall, MPa.

d is the width of the wall, mm.

t is effective thickness of the wall, mm.

f_{bt} is the tensile strength of the brick, MPa.

σ_{np} is the axial pre-compression on the plaster, MPa.

d_p is the width of the plaster, mm.

t_p is effective thickness of the plaster, mm.

f_{pt} is the tensile strength of the plaster, MPa.

Table 4-2: The numerical values for the one-side wall

Name of the parameter	value
Brick tensile strength (experimental property)	f_{bt}=1.5 MPa
SFRHM tensile strength (experimental property)	f_{pt}=4.0 MPa
width of the wall (geometric property)	d =810 mm
Effective thickness of the wall (geometric property)	t =72 mm
Effective thickness of the SFRHM (geometric property)	t =10 mm
The axial pre-compression on wall (experimental property)	σ_n =4.5 MPa

According to equation (13), the shear capacity of the one-side plastered wall is calculated as follows:

$$V = V_m + V_p = 810 * 72 \ * \ \frac{1.5}{2.3} \sqrt{1 + \frac{4.5}{1.5}} + 810 * 10 * 4 \sqrt{1 + \frac{4.5}{4}} = 122$$

4.6 Shear Capacity of the Two-side Plastered Wall

Like the one-side plastered wall, equation (13) was also used to estimate the value of the shear capacity for the two-side plastered wall. Table 4-3 shows the numerical values that associated with the two-side plastered wall. Equation (13) is as follows:

$$V = V_m + V_p = d * t \ * \ \frac{f_{bt}}{2.3} \sqrt{1 + \frac{\sigma_n}{f_{bt}}} + \ d_p * t_p * \ f_{pt} \sqrt{1 + \frac{\sigma_{np}}{f_{pt}}} \qquad (13)$$

where

V is the shear capacity, kN

V_m is the shear capacity of unreinforced wall, kN

V_p is the shear capacity of plaster, kN

σ_n is the axial pre-compression on the wall, MPa.

d is the width of the wall, mm.

t is effective thickness of the wall, mm.

f_{bt} is the tensile strength of the brick, MPa.

σ_{np} is the axial pre-compression on the plaster, MPa.

d_p is the width of the plaster, mm.

t_p is effective thickness of the plaster, mm.

f_{pt} is the tensile strength of the plaster, MPa.

Table 4-3: The numerical values for the two-side wall

Name of the parameter	value
Brick tensile strength (experimental property)	f_{bt} =1.5 MPa
Plaster tensile strength (experimental property)	f_{pt} =4.0 MPa
Width of the wall and the plaster (geometric property)	d $= d_p$ =810 mm
Effective thickness of the wall (geometric property)	t =72 mm
Effective thickness of the plaster (geometric property)	t_p =20 mm
The axial pre-compression on wall and the plaster (experimental property)	$\sigma_n = \sigma_{np}$ =5.4 MPa

According to equation (3), the shear capacity of the plastered two-side is calculated as follows:

$$V = V_m + V_p = 810 * 72 \ * \ \frac{1.5}{2.3} \sqrt{1 + \frac{5.4}{1.5}} + \ 810 * 20 * \ 4 \sqrt{1 + \frac{5.4}{4}} = \ 182 \ KN$$

4.7 Discussion of the Analytical Results

Equation (9), which was used to estimate the shear capacity of the reference wall, proved to be effective to evaluate the shear capacity comparing to its experimental counterpart (the difference is 8.8%, according to Table 14).

Equation (12), which was used to estimate the effect of the plaster, found to be convenient to produce good values compared to its experimental counterpart (the difference is 7.9% for the one-side plastered wall and 2.6% for the two-side plastered wall, according to Table 14). Table 4-4 shows the comparison between the experimental and analytical results.

Table 4-4: Comparison between the experimental and analytical results

Type	**Experimental shear force (kN)**	**Analytical shear force (kN)**	**Difference**	**Mode of failure**
Reference	80.0	73.0	-8.8 %	Diagonal through the block and joints
Plastered one-side	113	122	+7.9%	Diagonal through the block and the plaster
Plastered two-side	187	182	-2.6%	Diagonal through the block and the plaster

CHAPTER 5

NUMERICAL SIMULATION OF PRISMS AND WALLS

5.1 Introduction

Finite element model (FEM) is a convenience technique that is often used to understand and predict the non-linear behavior of masonry structures [34]. Therefore, the reference and retrofitted samples were modeled in ABAQUS environment using Concrete Damage Plasticity (a constitutive model based on the combination of damage mechanics and plasticity to analyze the failure of structures) which is available in ABAQUS library. Because of its ability to capture the cracks and failure modes [34], Concrete Damage Plasticity model was adopted in this study in order to simulate the behavior of concrete masonry wall. Concrete Damage Plasticity model was used to model both concrete masonry blocks and mortar.

Some of the needed parameters were found form the experimental tests and some others were assumed using the default values. The interactions between the concrete masonry blocks and mortar were assumed to be full bond in which no relative movement (separations) in either direction (normal and tangential) was allowed. In this study, the dynamic explicit analysis (is done using an explicit solver) was adopted because the explicit analysis is much more stable and gives good results compared to standard static analysis (static analysis is done using an implicit solver), according to Al-Gohi (2013).

5.2 General Modeling Approach

The following four parts were created to be used to assemble either the prism or the wall for modeling: full block, half block, mortar and steel plate. For the plastered specimens, a plaster layer was created additional to those four parts. The steel material was created to be used as a platform for applying the axial force. All parts were modeled as 3D space, deformable materials, solid shapes and they were converted to 3D using extrusion (extrusion is a process used to create objects of a fixed cross-sectional profile).

All parts were assembled together by using a command called “create instant” and then the command “translate” to move each part to its specific location.

Regarding the materials properties, four materials were created; block material, mortar material, plaster material and steel material.

The value of the density was specified for each material as well as the elastic properties such as Young’s modulus and Poisson’s ration (obtained experimentally). Table 5-1 shows the density, Young’s modulus and Poisson’s ratio that were specified.

Since the Concrete Damaged Plasticity model was adopted in this study, three main properties were deployed (plasticity, compressive behavior and tensile behavior), according to Al-Gohi (2013). Table 5-2 shows the plasticity parameters used in the model, while Figure 35 and Figure 36 show uniaxial compression stress vs. inelastic strain and tensile stress vs. inelastic strain, respectively, all the parameters in Figure 5-1 and -5-2 were obtained from the experimental results (see chapter 3, clause 3.3).

Table 5-1: Elastic mechanical properties inputs required by CDP

Masonry component	Mass density (kg/m^3)	Young's modulus (GPa)	Poisson's ratio
Concrete Block	2000	16.5	0.2
Mortar Type M	2200	20	0.2
Nano-silica mix	2293	24	0.23

Table 5-2: Plasticity parameters used in the model

Parameters	All masonry components
Dilation angle ψ	36
Eccentricity	0.1
fbo/fco	1.16
K	0.67
Viscosity parameter	0

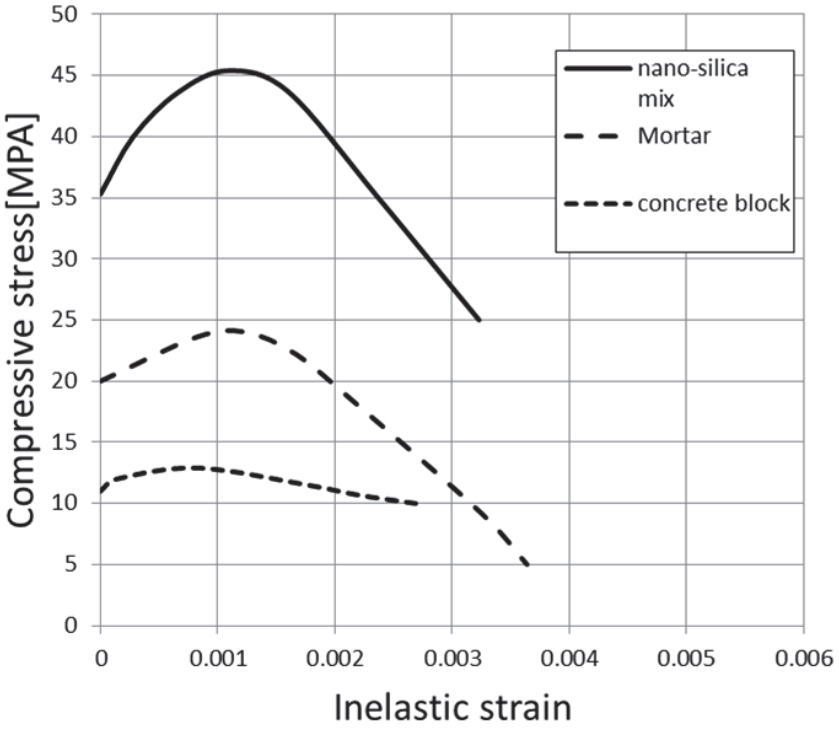

Figure 5-1: Uniaxial compression stress vs. inelastic strain

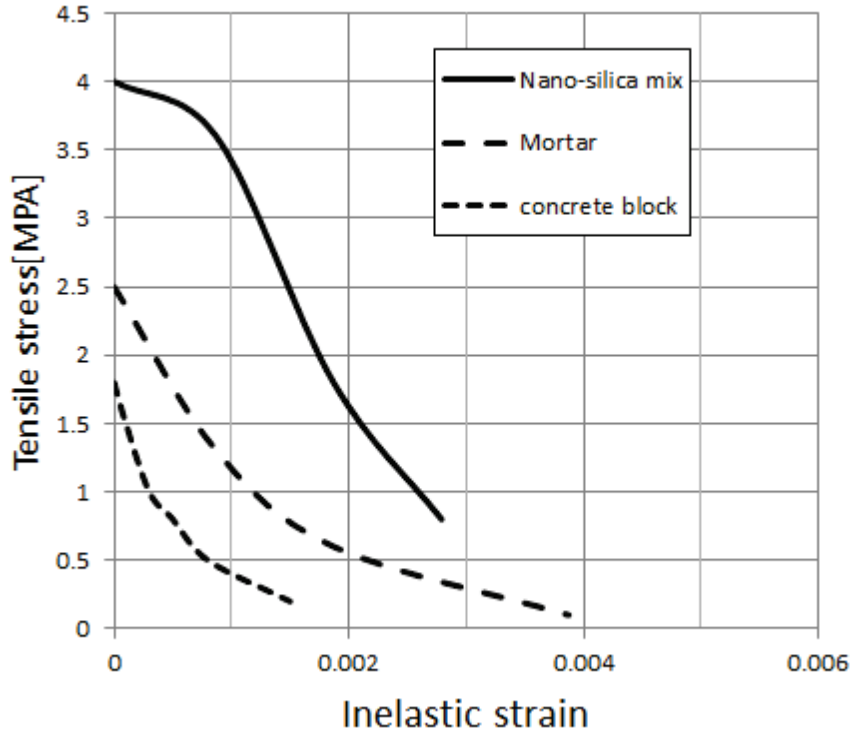

Figure 5-2: Tensile stress vs. inelastic strain

Regarding the boundary conditions, the displacements in all direction were set to be zero in the bottom of prism or the wall to make the wall fixed from the bottom like in the experimental test.

The load was employed as a pressure on the top of the prism or the wall (on the steel plate) to satisfy the load condition. Dynamic explicit were selected to be the procedure of the analysis. Because quasi-static situation is involved, Dynamic Explicit was the best option to be utilized, according to Al-Gohi et al. (2013).

All parts were meshed with a global size of 10 because it's the finest mesh available in ABAQUS. Regarding the contact property between the blocks and the mortar, the option called "hard contact" in the normal behavior was chosen to get normal pressure movement between blocks and mortar. Also, tangential behavior with a coefficient of 0.7 was used with the option called "penalty" to ensure no relative movements between blocks and mortar.

5.3 Finite Element Simulation of Masonry Prisms

5.3.1 The Control Specimen

For the control prism, an axial stress had been applied first to the wall similar to the one used in the experiment (8.5 MPa). The load-displacement curve of the model and its experimental counterpart are shown in Figure 5-3. Also, the failure mode with cracks propagation was captured with good accuracy; Figure 5-4 shows how the cracks propagate in the control specimen.

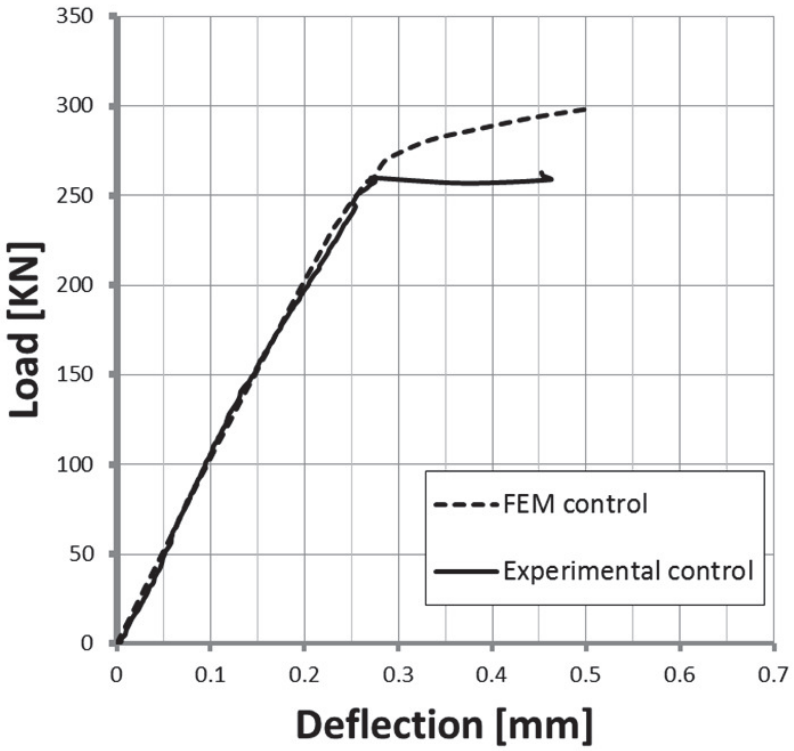

Figure 5-3: Load-deflection curve (Experimental and FEM) for the control specimen

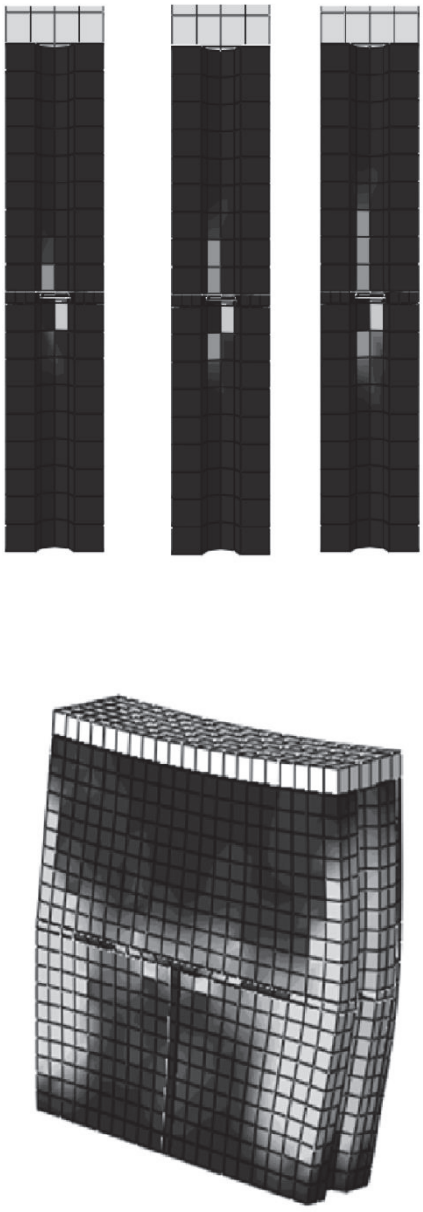

Figure 5-4: Failure mode of the control Prism in ABAQUS

5.3.2 The One-side Plastered Prism (10 mm thickness)

For the one-side plastered prism, an axial stress was applied first to the wall similar to the one used in the experiment (8.5 MPa). The Load-displacement curve of the model and its experimental counterpart are shown in Figure 5-5. Also, the failure mode with cracks propagation was captured with good accuracy; Figure 5-6 shows how the cracks propagate in the one-side plastered specimen.

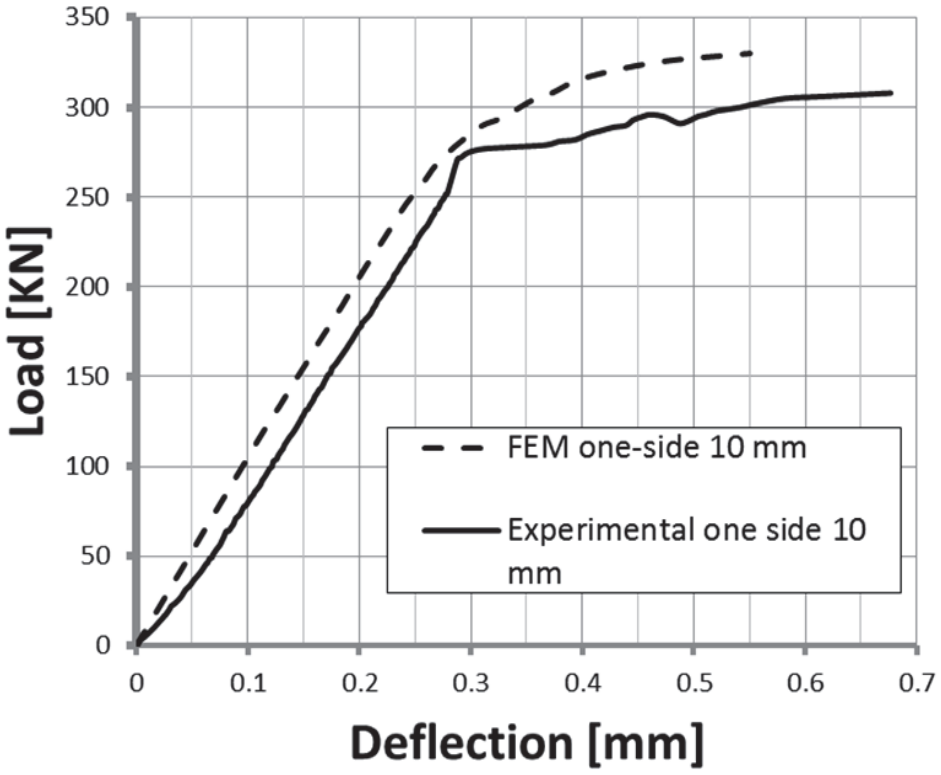

Figure 5-5: Load-deflection curve (Experimental and FEM) for the one-side plastered specimen

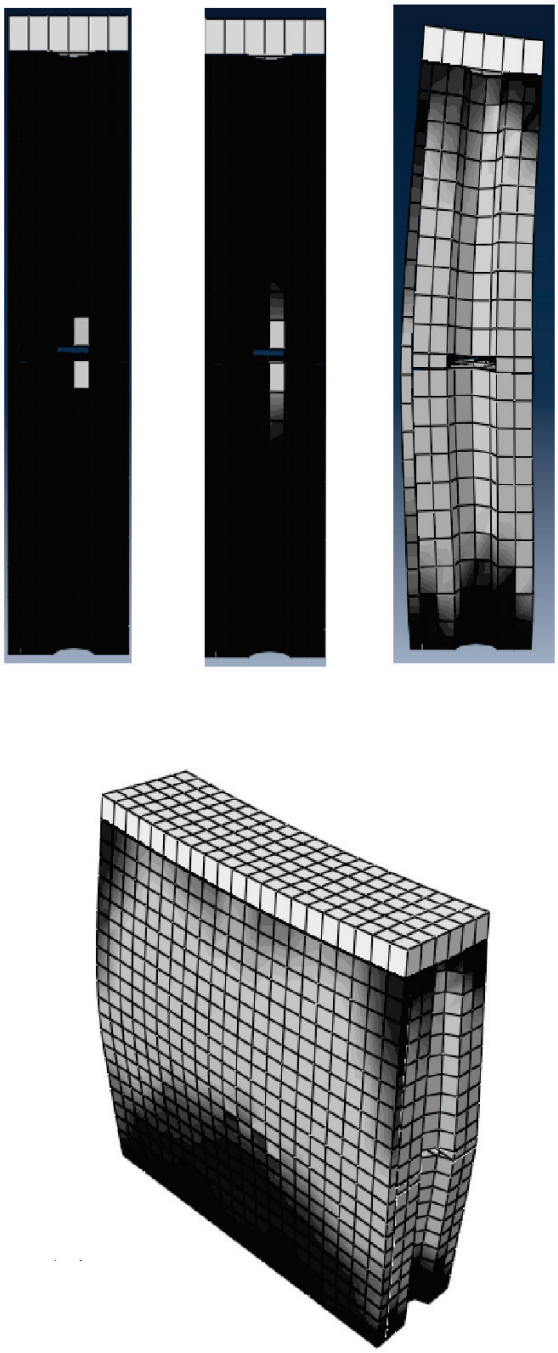

Figure 5-6: Failure mode of one-side (10 mm thickness) Prism in ABAQUS

5.3.3 The Two-side Plastered Prism (10 mm thickness)

For the tow-side plastered prism, an axial stress was applied first to the wall similar to the one used on in the experiment (10 MPa). The Load-displacement curve of the model and its experimental counterpart are shown in Figure 5-7. Also, the failure mode with cracks propagation was captured with good accuracy; Figure 5-8 shows how the cracks propagate in the two-side plastered specimen (10 mm thickness).

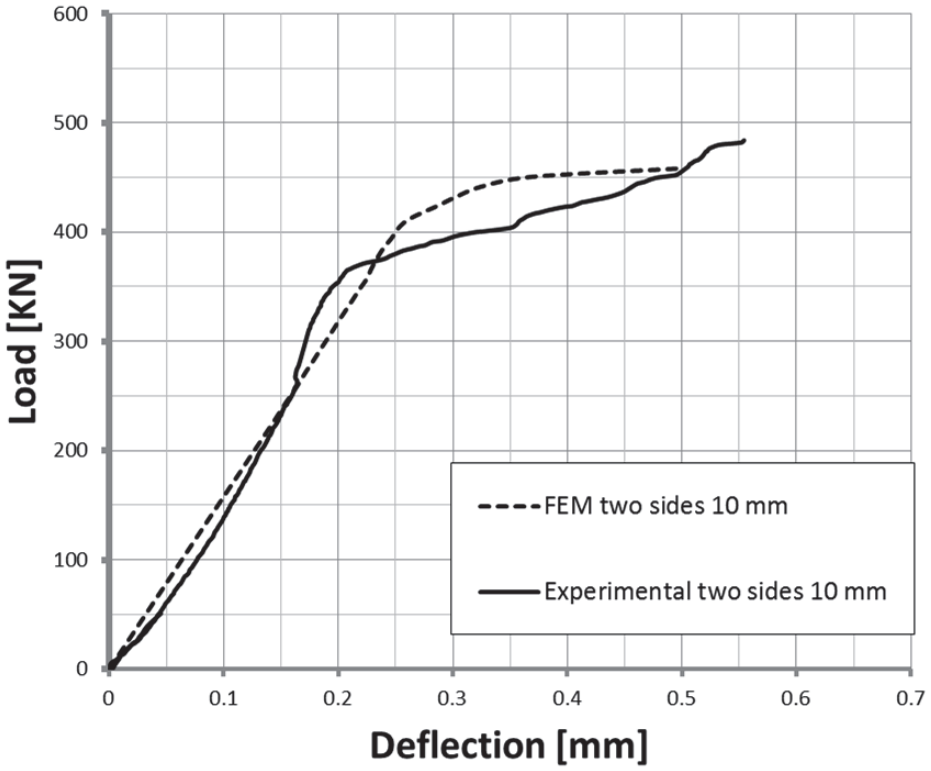

Figure 5-7: Load-deflection curve (Experimental and FEM) for the two-side (10mm thickness) specimen

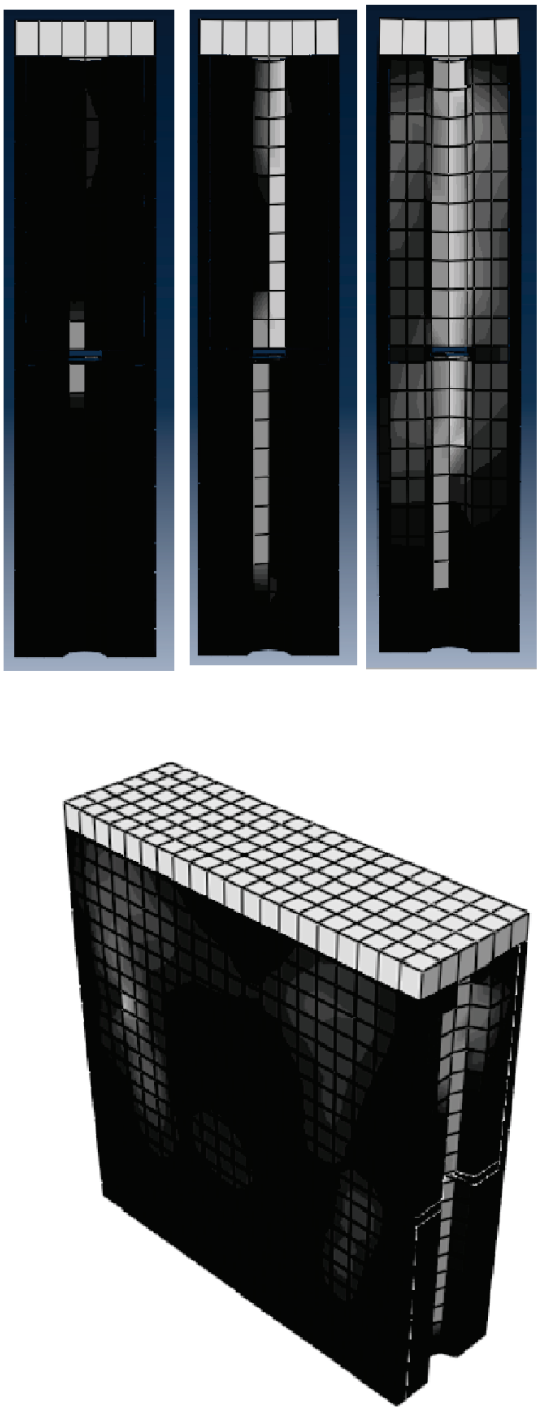

Figure 5-8: Failure mode of two-side (10 mm thickness) prism in ABAQUS

5.3.4 The Two-side Plastered Prism (20 mm thickness)

For the two-side prism, an axial stress was applied first to the wall similar to the one used in the experiment (12 MPa). The load-displacement curve of the model and its experimental counterpart are shown in Figure 5-9. Also the failure mode with cracks propagation was captured with good accuracy; Figure 5-10 shows how the cracks propagate in the two-side plastered specimen (20 mm thickness).

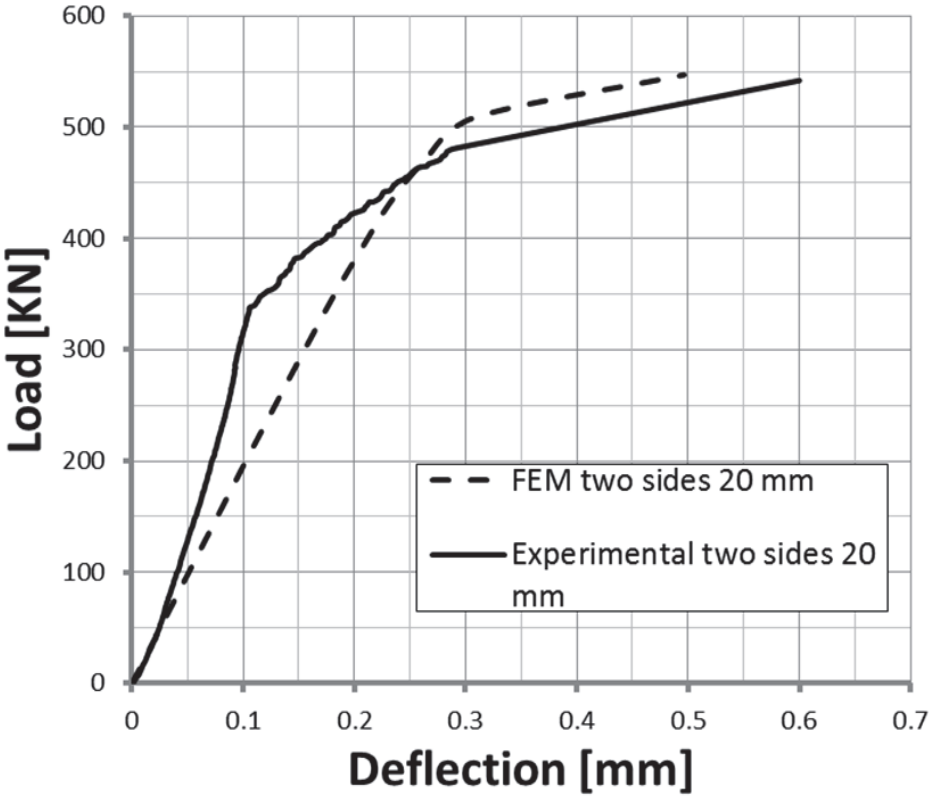

Figure 5-9: Load-deflection curve (Experimental and FEM) for the two-sides (20 mm thickness) specimen

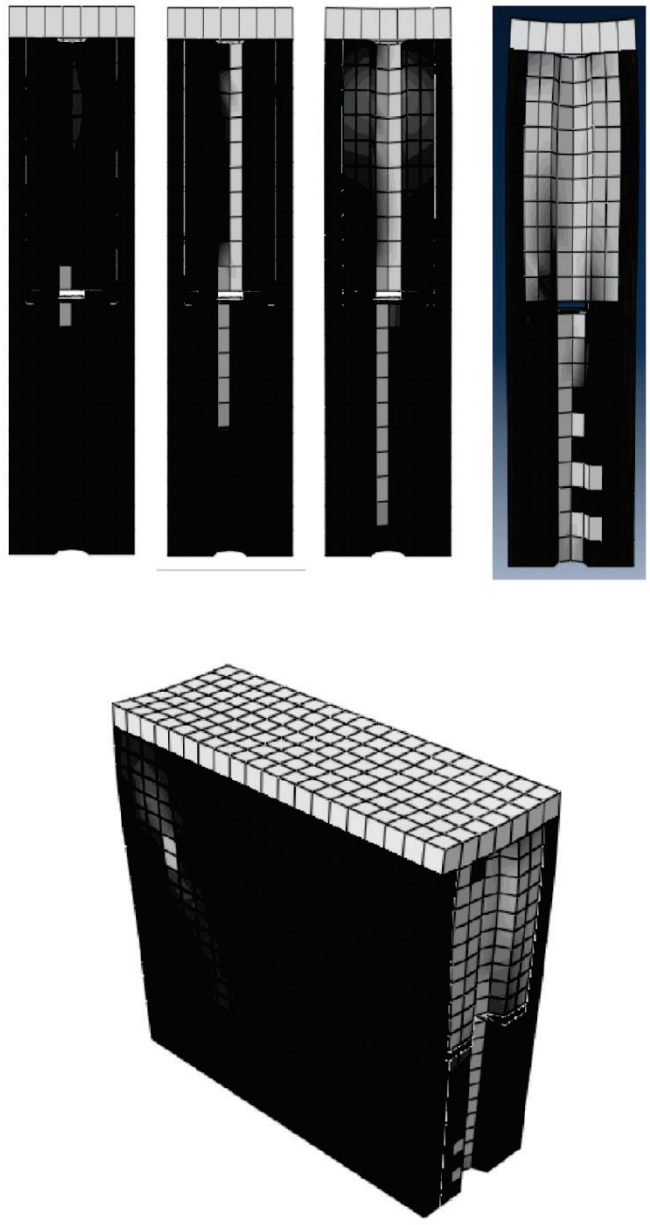

Figure 5-10: Failure mode of two-side (20 mm thickness) prism in ABAQUS

5.4 Finite Element Simulation of Masonry Walls

5.4.1 Reference Wall

For control wall, an axial stress was applied first to the wall similar to the one that used in the experiment (4.2 MPa). The lateral loading was a displacement-control type (analogous to the experimental test). The maximum displacement which was specified in the simulation was 4 mm (in the experimental test, the maximum displacement was 1.9 mm). The numerical simulation result was compared to the experimental one. Comparison between the envelopes of experimental cyclic test and numerical cyclic simulation is shown is Fig. 5-11.

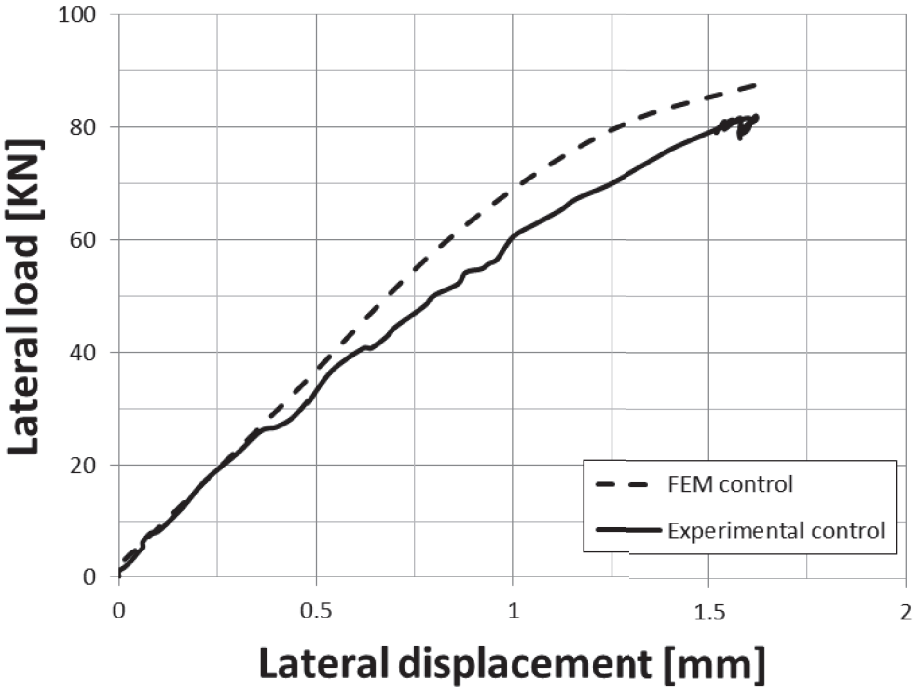

Figure 5-11: Envelopes of experimental cyclic test and numerical cyclic simulation

Figure 5-12 shows lateral load vs. displacement diagram from numerical simulation, while Figure 5-13 shows the failure mode and cracks pattern developed in the wall which are associated with the tensile damage (the tensile damage is defined as the ratio of the cracking strain to the total strain). As it shown in Figure 5-13, the tensile damage in the reference wall took place in the middle of almost every full block, while in the experimental reference wall these middle cracks in full block also took place but in more diagonal way (see Figure 3-12).

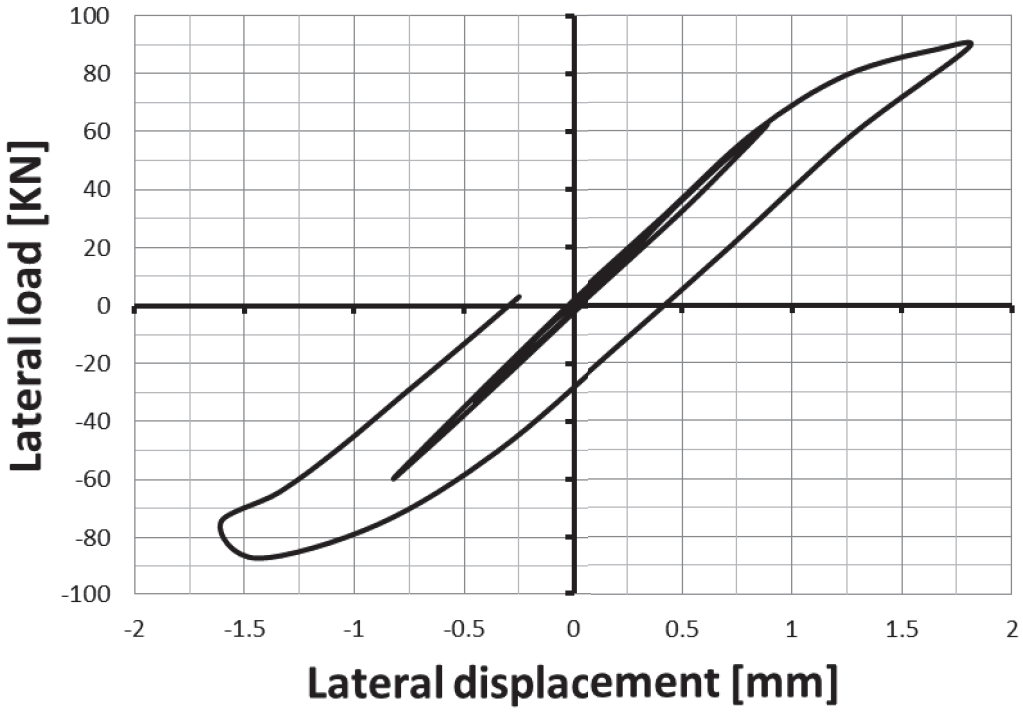

Figure 5-12: Lateral load vs. displacement diagram from numerical simulation

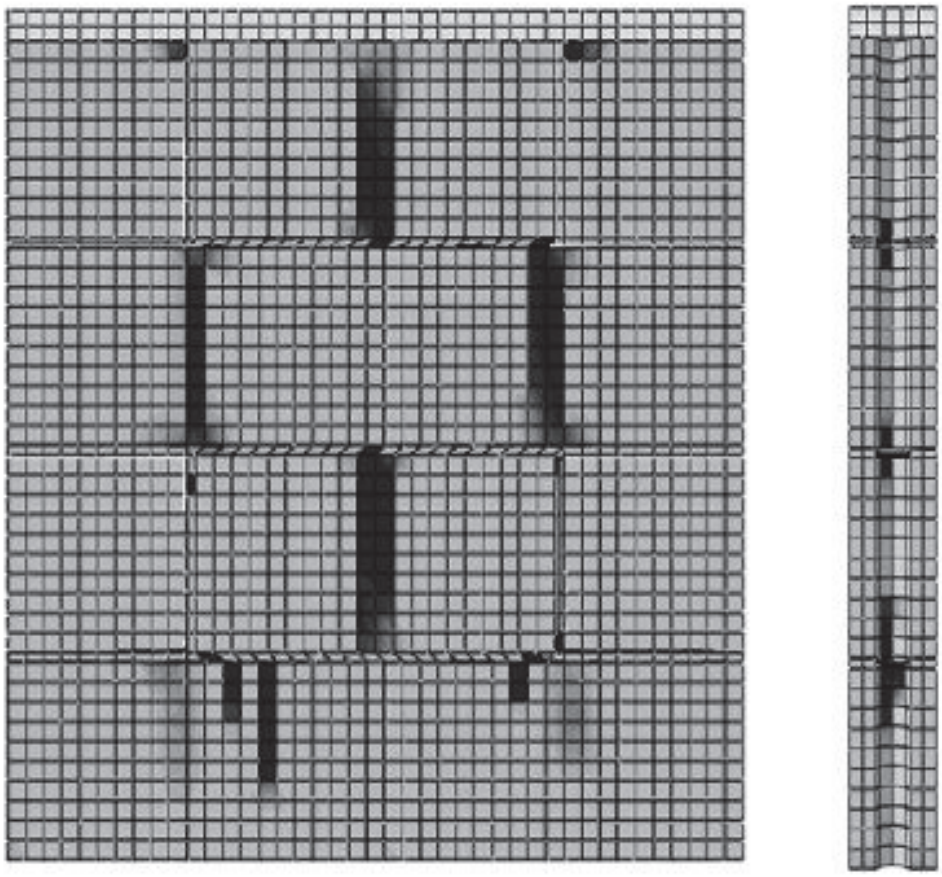

Figure 5-13: Failure mode and cracks pattern developed in wall (tensile damage)

5.4.2 One-side Plastered Wall (10 mm thickness)

For the second wall, an axial stress was applied first to the wall similar to the one used in the experiment (4.6 MPa). The lateral loading was a displacement-control type (analogous to the experimental test). The maximum displacement which was specified in the simulation was 4.0 mm (in the experimental test, the maximum displacement was 1.9 mm). The numerical simulation result was compared to the experimental one. Comparison between the envelopes of experimental cyclic test and numerical cyclic simulation is shown is Figure 5-14.

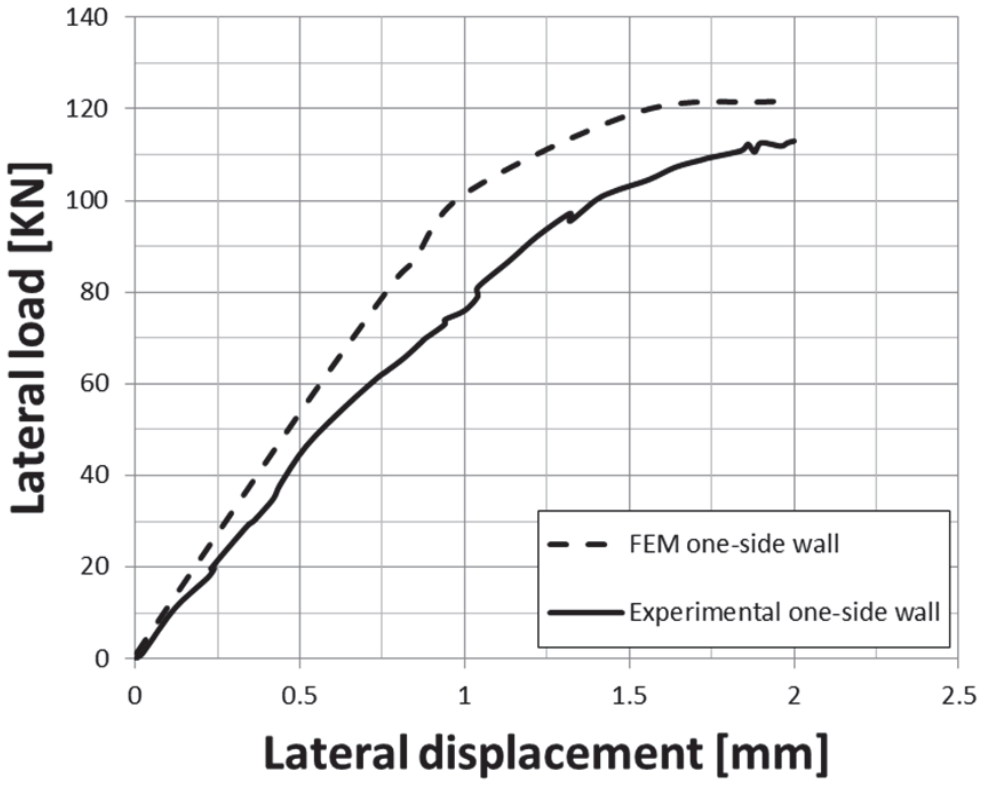

Figure 5-14: Envelopes of experimental cyclic test and numerical cyclic simulation

Figure 5-15 shows lateral load vs. displacement diagram from numerical simulation, while Figure 5-16 shows the failure mode and cracks pattern developed in wall which are associated with the tensile damage (the tensile damage is defined as the ratio of the cracking strain to the total strain). As it shown in Figure 5-16, the tensile damage is similar to the experimental wall (see Figure 3-13); the damage is diagonal from the top middle of the wall towards the bottom-compressed corner.

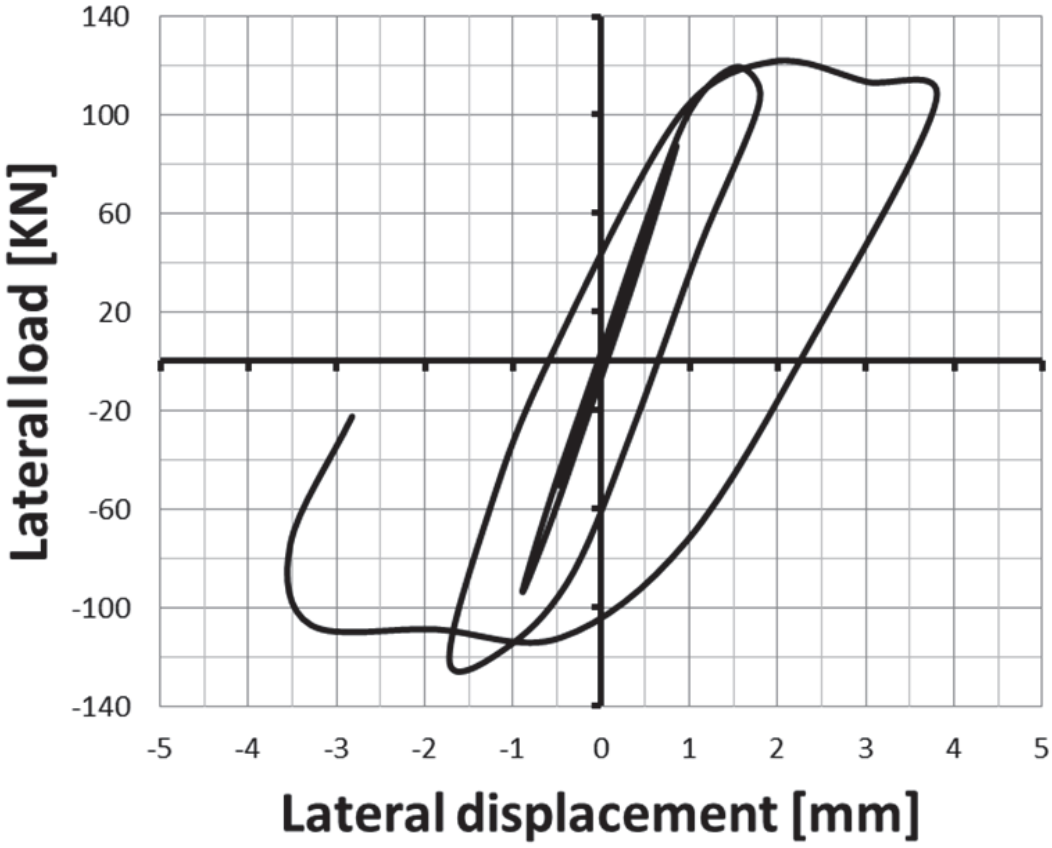

Figure 5-15: Lateral load vs. displacement diagram from numerical simulation

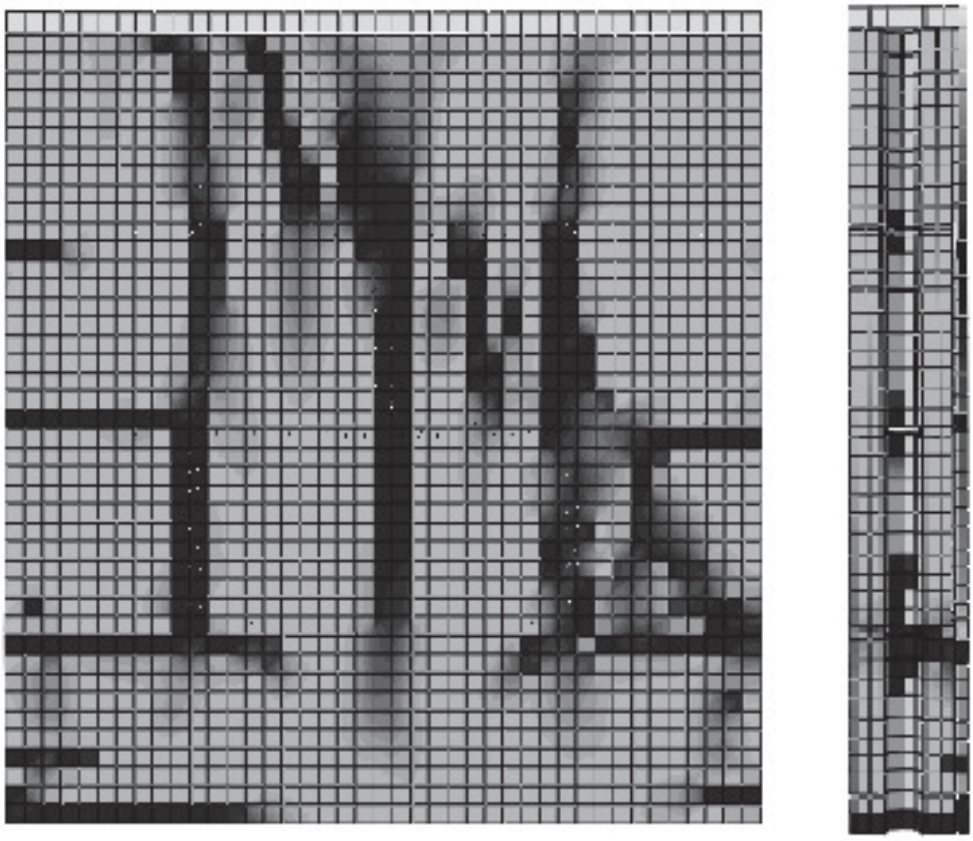

Figure 5-16: Failure mode and cracks pattern developed in wall (tensile damage)

5.4.3 Two-side Plastered Wall (10 mm thickness)

For the third specimen, an axial stress was applied first to the wall which is similar to the one used in the experiment (5.2 MPa). The lateral loading was a displacement-control type (analogous to the experimental test). The maximum displacement specified in the simulation was 8.0 mm (in the experimental test, the maximum displacement was 4.2 mm). The numerical simulation result was compared to the experimental one. Comparison between the envelopes of experimental cyclic test and numerical cyclic simulation is shown is Figure 5-17.

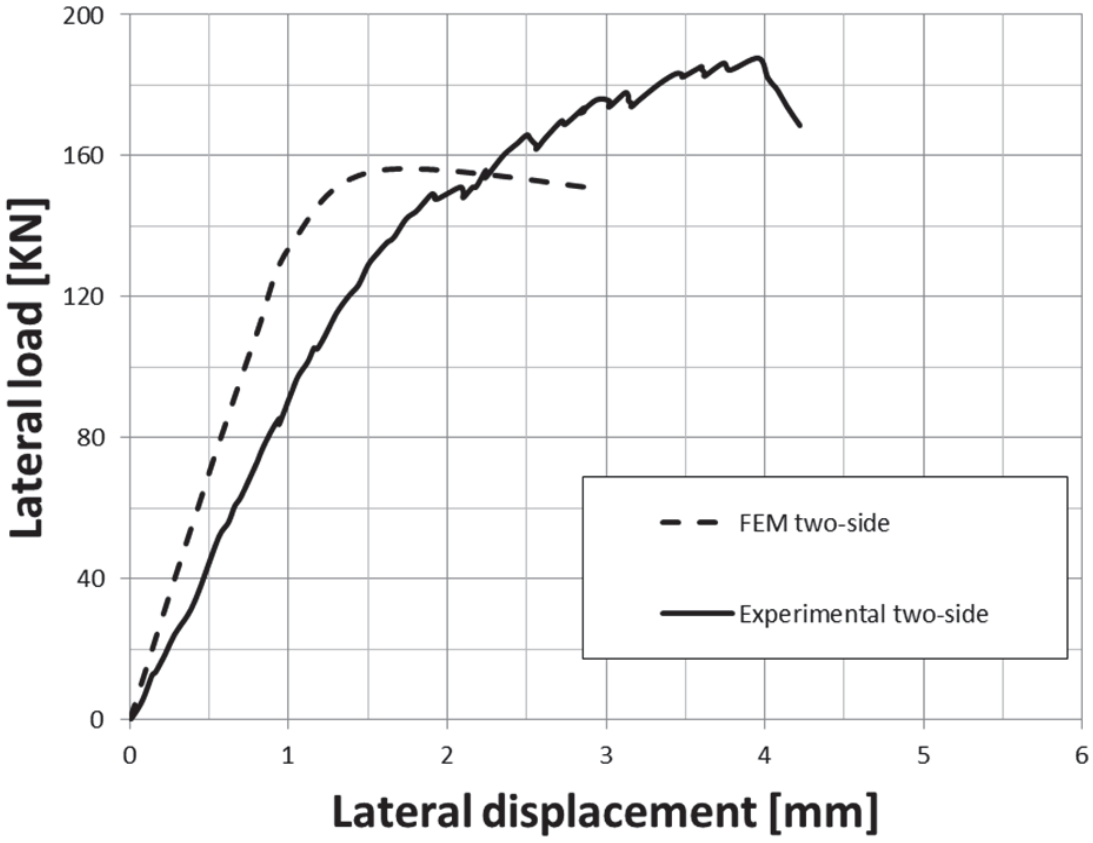

Figure 5-17: Envelopes of experimental cyclic test and numerical cyclic simulation

Figure 5-18 shows lateral load vs. displacement diagram from numerical simulation, while Figure 5-19 shows the failure mode and cracks pattern developed in which are associated with the tensile damage (the tensile damage is defined as the ratio of the cracking strain to the total strain). As it shown in Figure 5-19, the tensile damage is similar to the experimental wall (see Figure 3-15); the damage in the two-side plastered wall occurred through the top corner of the wall towards the bottom-compressed corner.

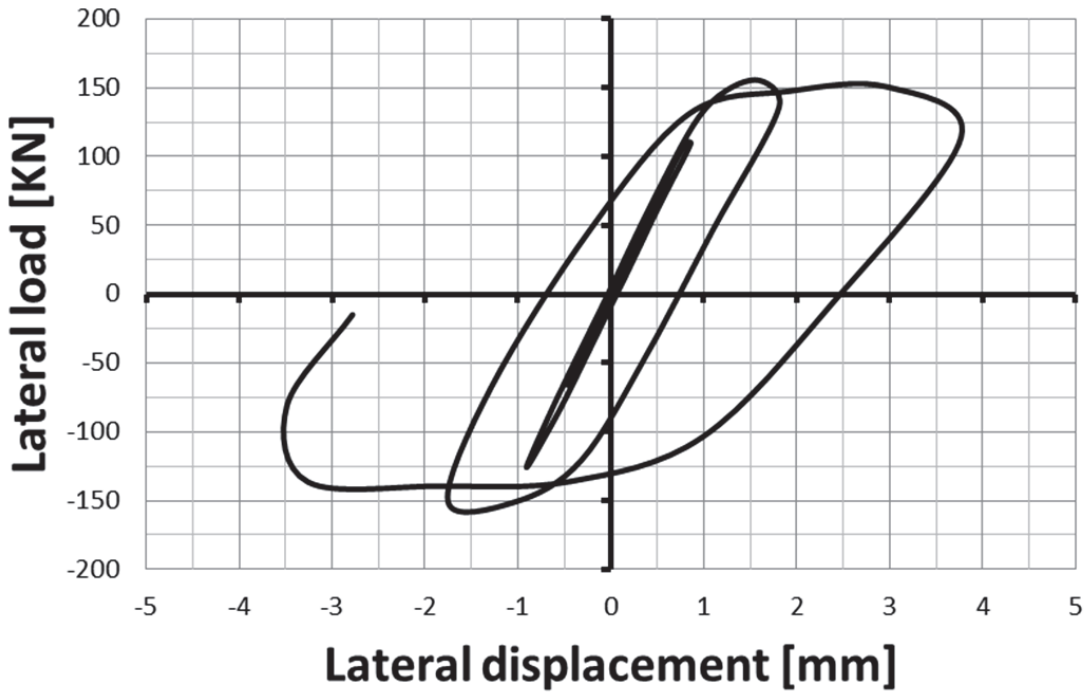

Figure 5-18: Lateral load vs. displacement diagram from numerical simulation

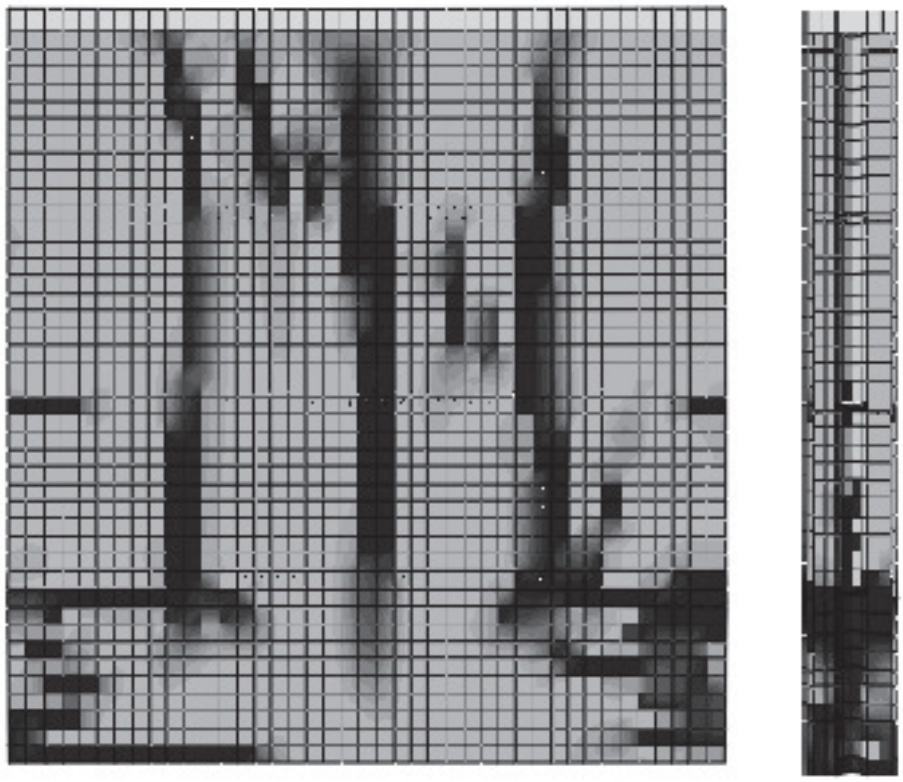

Figure 5-19: Failure mode and cracks pattern developed in wall (tensile damage)

CHAPTER 6

CONCLUSIONS AND RECOMMENDATIONS

The primary motive of this research work was to study the behavior of ordinary concrete masonry walls plastered with a high strength mortar containing nano-silica and steel fibers. In order to achieve this objective, concrete masonry walls were tested under cyclic loading. Also, prisms were tested under axial load to evaluate the compressive strength of the masonry wall, which is crucial to conduct the cyclic test for all walls.

In addition, mechanistic models were presented to estimate the capacity of the improved masonry wall using high performance mortar reinforced with steel fibers. Furthermore, finite element modeling of the walls using the CDP model in the ABAQUS was carried out to capture the lateral load-displacement response of all walls.

6.1 Experimental and Numerical Investigations on Masonry Prisms

1. The ultimate compressive strength of all concrete masonry prisms increased significantly by using a thin layer of mortar with nano-silica and steel fibers as a surface treatment. Mortar layer on both sides of the prism was very effective in increasing the compressive strength of the masonry unit; however, only one side layer was not effective.

2. All specimens developed a vertical crack in the mid-face of the web, whether they were retrofitted or not. Three modes of failure were observed during the test;

- For the reference specimen, the mid-face crack of the web caused the failure which made the top block to be crushed.
- The specimen with only one side layer was failed due to crushing of un-coated part of the prism,
- The specimen with two sides' layers was failed due to de-bonding between the plaster and the prism.

3. The initial stiffness in a range of 0.0 mm to 0.1 mm improved significantly, after the application of thin mortar layer on both sides. The masonry prism with plaster on two sides with a thickness of 10 mm and 20 mm showed an enhancement of stiffness by 30% and 200%, respectively, as compared to the control specimen.

4. The Concrete Damaged Plasticity in ABAQUS captured the behavior of the concrete masonry prisms and a good agreement was found with the experimental results in terms of ultimate compressive strength, initial stiffness and failure modes.

6.2 Experimental and Numerical Investigations on Masonry Walls

1. The thin layer of SFRHM resulted in a significant increase in the ultimate shear capacity of the concrete block masonry walls. The shear capacity of the two-side plastered wall showed a remarkable increase of about 133% as compared to the reference

wall, while the ultimate shear capacity of the one-side wall increased by 40% higher than the reference wall.

2. The initial stiffness with the range of (0-1.0 mm) of the plastered walls was considerably increased with this SFRHM thin layer. Compared to the reference wall, the two-side plastered wall developed a 52 % increase in the initial stiffness, whereas the one-side plastered wall developed a 25 % increase in the initial stiffness.

3. The two-side plastered wall showed a large deflection before it totally collapsed, demonstrating a significant enhancement in the ductile behavior of the wall. The improvement in the ductile behavior can be attributed to the incorporation of the steel fibers in the SFRHM thin layer.

4. Analytical computational based on the tensile strength of brick and the plaster to estimate the shear capacity of the SFRHM showed good agreement with the experimental results.

5. Finite element modeling of walls using concrete damaged plasticity model introduced in ABAQUS software captured the experimental behavior, showing a good agreement in terms of load-displacement response, ultimate shear capacity, stiffness and the failure modes.

6.3 Recommendations

It can be seen that there are several topics that have to be investigated as future work. Some of these topics can be summarized as follows:

• Additional monotonic and cyclic tests should be conducted with different aspect of walls ratio and plastering thickness.

• Additional cyclic tests should be conducted with different level of axial load for understanding the full behavior of shear and axial stress interaction and hysteretic response of such walls.

• Out-of-plane behavior of concrete masonry walls should be characterized experimentally and numerically.

• Behavior of wall with opening (a gap or void in the wall) should be studied experimentally and numerically.

• Study the effect of SFRHM on other types of bricks such as clay because they have different type of contact with SFRHM.

References

[1] S. Bhattacharya, S. Nayak, and S. C. Dutta, "A critical review of retrofitting methods for unreinforced masonry structures," *Int. J. Disaster Risk Reduct.*, vol. 7, pp. 51–67, 2014.

[2] M. Elgawady, P. Lestuzzi, and M. Badoux, "A Review of Conventional Seismic Retrofitting Techniques for Urm," in *13th International brick and block masonry conference, Amsterdam*, 2004, vol. 10, no. 10, pp. 1–10.

[3] T. Li, N. Galati, J. G. Tumialan, and A. Nanni, "Analysis of Unreinforced Masonry Concrete Walls Strengthened With Glass Fiber Reinforced Polymer Bars.pdf," *ACI Struct. J.*, no. 102, pp. 569–577, 2005.

[4] S. Haruehansapong, T. Pulngern, and S. Chucheepsakul, "Effect of the particle size of nanosilica on the compressive strength and the optimum replacement content of cement mortar containing nano-SiO2," *Constr. Build. Mater.*, vol. 50, pp. 471–477, 2014.

[5] B. B. Mukharjee and S. V. Barai, "Assessment of the influence of Nano-Silica on the behavior of mortar using factorial design of experiments," *Constr. Build. Mater.*, vol. 68, pp. 416–425, 2014.

[6] Y. Wang, V. C. Li, and S. Backer, "Tensile properties of synthetic fiber reinforced mortar," *Cem. Concr. Compos.*, vol. 12, pp. 29–40, 1990.

[7] "Saudi Geologist Survey." [Online]. Available: www.sgs.org.sa, 2006.

[8] P. Montes and A. Fernandez, "Behaviour of a hemispherical dome subjected to wind loading," *J. Wind Eng. Ind. Aerodyn.*, vol. 89, no. 10, pp. 911–924, 2001.

[9] S. Sheppard, Peter and Tercelj, "The effect of repair and strengthening methods for masonry walls," *7th World Conf. Earthq. Eng.*, vol. 6, pp. 255–262, 1980.

[10] J. Abrams, D., and Lynch, "Flexural behavior of retrofitted masonry piers," *r Risk Mitig. Reg. Moderate Seism. USA*, 2001.

[11] G. M. Calvi and G. Magenes, "Experimental Results on Unreinforced Masonry Shear Walls Damaged and Repaired," *Proc. 10th Int. Brick Mason. Conf. Vol. 2*, pp. 509–518, 1994.

[12] S. Lissel and N. G. Shrive, "Construction of diaphragm walls post-tensioned with carbon fiber reinforced polymer tendons," *9th NAMC*, pp. 192–203, 2003.

[13] N. G. Shrive, "The use of fibre reinforced polymers to improve seismic resistance of masonry," *Constr. Build. Mater.*, vol. 20, no. 4, pp. 269–277, 2006.

[14] M. Elgawady, P. Lestuzzi, and M. Badoux, "Aseismic retrofitting of unreinforced masonry walls using FRP," *Compos. Part B Eng.*, vol. 37, no. 2–3, pp. 148–162, 2005.

[15] A. Mosallam and S. Banerjee, "Enhancement in in-plane shear capacity of unreinforced masonry (URM) walls strengthened with fiber reinforced polymer composites," *Compos. Part B Eng.*, vol. 42, no. 6, pp. 1657–1670, 2011.

[16] S. Chuang, Y. Zhuge, T. Wong, and L. Peters, "Seismic retrofitting of unreinforced masonry walls by FRP strips," *Pacific Conf. Earthq. Eng.*, pp. 1–8,

2003.

[17] G. Vasconcelos and P. B. Lourenço, "In-Plane Experimental Behavior of Stone Masonry Walls under Cyclic Loading," *J. Struct. Eng.*, vol. 135, no. October, pp. 1269–1277, 2009.

[18] C. G. Papanicolaou, T. C. Triantafillou, M. Papathanasiou, and K. Karlos, "Textile reinforced mortar (TRM) versus FRP as strengthening material of URM walls: out-of-plane cyclic loading," *Mater. Struct.*, vol. 41, no. 1, pp. 143–157, 2007.

[19] L. Facconi, A. Conforti, F. Minelli, and G. a. Plizzari, "Improving shear strength of unreinforced masonry walls by nano-reinforced fibrous mortar coating," *Mater. Struct.*, pp. 2557–2574, 2014.

[20] T. Sevil, M. Baran, T. Bilir, and E. Canbay, "Use of steel fiber reinforced mortar for seismic strengthening," *Constr. Build. Mater.*, vol. 25, no. 2, pp. 892–899, 2011.

[21] S. Churilov and E. Dumova-Jovanoska, "In-plane shear behaviour of unreinforced and jacketed brick masonry walls," *Soil Dyn. Earthq. Eng.*, vol. 50, pp. 85–105, 2013.

[22] BS EN 1996-1-1, "Eurocode 6: Design of masonry structures - Part 1-1: General rules for reinforced and unreinforced masonry structures," vol. 2, no. 2005, p. 123, 2005.

[23] CSA Standard S304.1-04, *Design of masonry structures, Canadian Standards Association, Canada*. 2004.

[24] T. Regulations, “M a c e d o n i a,” vol. 1982, pp. 1–30, 2008.

[25] M. Tomaževič, *Earthquake-resistant Design of Masonry Buildings*. 1999.

[26] FEDRA, “version2/03, User Manual, Runet software & expert systems.” .

[27] P. S. Song and S. Hwang, “Mechanical properties of high-strength steel fiber-reinforced concrete,” *Constr. Build. Mater.*, vol. 18, no. 9, pp. 669–673, 2004.

[28] M. Nili and V. Afroughsabet, “Combined effect of silica fume and steel fibers on the impact resistance and mechanical properties of concrete,” *Int. J. Impact Eng.*, vol. 37, no. 8, pp. 879–886, 2010.

[29] M. Elgawady, P. Lestuzzi, and M. Badoux, “Retrofitting of masonry walls using shotcrete,” in *2006 NZSEE Conference*, 2006, no. 45, pp. 45–54.

[30] H. Basaran, A. Demir, and M. Bagci, “The behavior of masonry walls with reinforced plaster mortar,” *Adv. Mater. Sci. Eng.*, vol. 2013, 2013.

[31] F. L. D. E. Oliveira and J. B. D. E. Hanai, “Axial compression behavior of concrete masonry wallettes strengthened with cement mortar overlays Comportamento à compressão axial de pequenas,” *IBRACON Struct. Mater. J.*, vol. 1, no. 2, pp. 158–170, 2008.

[32] American Society for Testing and Materials, *ASTM C1314-12 Standard Test Method for Compressive Strength of Masonry Prisms*. 2015, pp. 1–10.

[33] G. Magenes and G. M. Calvi, “In-plane seismic response of brick masonry walls,” *Earthq. Eng. Struct. Dyn.*, vol. 26, no. 11, pp. 1091–1112, 1997.

[34] N. Gattesco, C. Amadio, and C. Bedon, “Experimental and numerical study on the shear behavior of stone masonry walls strengthened with GFRP reinforced mortar coating and steel-cord reinforced repointing,” *Eng. Struct.*, vol. 90, pp. 143–157, 2015.

Vitae

Name	: Ahmed Awad Saeed Sadoon
Nationality	: Sudanese
Date of Birth	: 7/10/1988
Email	: ahmed.awad.sadoon@gmail.com
Address	: House No. 362, Block 8, Omdurman, Khartoum, Sudan
Academic Background	: M.S in Civil Engineering, King Fahd University of Petroleum and Minerals (KFUPM), Dhahran, Saudi Arabia. B.S in Civil Engineering, University of Khartoum, Khartoum, Sudan.